A STUDY OF MULTILAYER PRINTED TRANSMISSION LINES AND ANTENNAS

By

Xian Hua Yang

A Thesis

Submitted to the Faculty of Graduate Studies

In Partial Fulfillment of the Requirement for the Degree of

Doctor of Philosophy in Electrical Engineering

University of Manitoba

Department of Electrical and Computer Engineering

Winnipeg, Manitoba

Canada

January 1994

ISBN 0-315-99078-3

Name Xianhua Yang

Dissertation Abstracts International is arranged by broad, general subject categories. Please select the one subject which most nearly describes the content of your dissertation. Enter the corresponding four-digit code in the spaces provided.

Electronics and Electrical Engineering

SUBJECT TERM

0544

SUBJECT CODE

U·M·I

Subject Categories

THE HUMANITIES AND SOCIAL SCIENCES

COMMUNICATIONS AND THE ARTS

Architecture 0729
Art History 0377
Cinema 0900
Dance 0378
Fine Arts 0357
Information Science 0723
Journalism 0391
Library Science 0399
Mass Communications 0708
Music 0413
Speech Communication 0459
Theater 0465

EDUCATION

General 0515
Administration 0514
Adult and Continuing 0516
Agricultural 0517
Art 0273
Bilingual and Multicultural 0282
Business 0688
Community College 0275
Curriculum and Instruction 0727
Early Childhood 0518
Elementary 0524
Finance 0277
Guidance and Counseling 0519
Health 0680
Higher 0745
History of 0520
Home Economics 0278
Industrial 0521
Language and Literature 0279
Mathematics 0280
Music 0522
Philosophy of 0998
Physical 0523
Psychology 0525
Reading 0535
Religious 0527
Sciences 0714
Secondary 0533
Social Sciences 0534
Sociology of 0340
Special 0529
Teacher Training 0530
Technology 0710
Tests and Measurements 0288
Vocational 0747

LANGUAGE, LITERATURE AND LINGUISTICS

Language
- General 0679
- Ancient 0289
- Linguistics 0290
- Modern 0291

Literature
- General 0401
- Classical 0294
- Comparative 0295
- Medieval 0297
- Modern 0298
- African 0316
- American 0591
- Asian 0305
- Canadian (English) 0352
- Canadian (French) 0355
- English 0593
- Germanic 0311
- Latin American 0312
- Middle Eastern 0315
- Romance 0313
- Slavic and East European 0314

PHILOSOPHY, RELIGION AND THEOLOGY

Philosophy 0422
Religion
- General 0318
- Biblical Studies 0321
- Clergy 0319
- History of 0320
- Philosophy of 0322

Theology 0469

SOCIAL SCIENCES

American Studies 0323
Anthropology
- Archaeology 0324
- Cultural 0326
- Physical 0327

Business Administration
- General 0310
- Accounting 0272
- Banking 0770
- Management 0454
- Marketing 0338

Canadian Studies 0385
Economics
- General 0501
- Agricultural 0503
- Commerce-Business 0505
- Finance 0508
- History 0509
- Labor 0510
- Theory 0511

Folklore 0358
Geography 0366
Gerontology 0351
History
- General 0578
- Ancient 0579
- Medieval 0581
- Modern 0582
- Black 0328
- African 0331
- Asia, Australia and Oceania 0332
- Canadian 0334
- European 0335
- Latin American 0336
- Middle Eastern 0333
- United States 0337

History of Science 0585
Law 0398
Political Science
- General 0615
- International Law and Relations 0616
- Public Administration 0617

Recreation 0814
Social Work 0452
Sociology
- General 0626
- Criminology and Penology 0627
- Demography 0938
- Ethnic and Racial Studies 0631
- Individual and Family Studies 0628
- Industrial and Labor Relations 0629
- Public and Social Welfare 0630
- Social Structure and Development 0700
- Theory and Methods 0344

Transportation 0709
Urban and Regional Planning 0999
Women's Studies 0453

THE SCIENCES AND ENGINEERING

BIOLOGICAL SCIENCES

Agriculture
- General 0473
- Agronomy 0285
- Animal Culture and Nutrition 0475
- Animal Pathology 0476
- Food Science and Technology 0359
- Forestry and Wildlife 0478
- Plant Culture 0479
- Plant Pathology 0480
- Plant Physiology 0817
- Range Management 0777
- Wood Technology 0746

Biology
- General 0306
- Anatomy 0287
- Biostatistics 0308
- Botany 0309
- Cell 0379
- Ecology 0329
- Entomology 0353
- Genetics 0369
- Limnology 0793
- Microbiology 0410
- Molecular 0307
- Neuroscience 0317
- Oceanography 0416
- Physiology 0433
- Radiation 0821
- Veterinary Science 0778
- Zoology 0472

Biophysics
- General 0786
- Medical 0760

EARTH SCIENCES

Biogeochemistry 0425
Geochemistry 0996
Geodesy 0370
Geology 0372
Geophysics 0373
Hydrology 0388
Mineralogy 0411
Paleobotany 0345
Paleoecology 0426
Paleontology 0418
Paleozoology 0985
Palynology 0427
Physical Geography 0368
Physical Oceanography 0415

HEALTH AND ENVIRONMENTAL SCIENCES

Environmental Sciences 0768
Health Sciences
- General 0566
- Audiology 0300
- Chemotherapy 0992
- Dentistry 0567
- Education 0350
- Hospital Management 0769
- Human Development 0758
- Immunology 0982
- Medicine and Surgery 0564
- Mental Health 0347
- Nursing 0569
- Nutrition 0570
- Obstetrics and Gynecology 0380
- Occupational Health and Therapy 0354
- Ophthalmology 0381
- Pathology 0571
- Pharmacology 0419
- Pharmacy 0572
- Physical Therapy 0382
- Public Health 0573
- Radiology 0574
- Recreation 0575
- Speech Pathology 0460
- Toxicology 0383

Home Economics 0386

PHYSICAL SCIENCES

Pure Sciences

Chemistry
- General 0485
- Agricultural 0749
- Analytical 0486
- Biochemistry 0487
- Inorganic 0488
- Nuclear 0738
- Organic 0490
- Pharmaceutical 0491
- Physical 0494
- Polymer 0495
- Radiation 0754

Mathematics 0405
Physics
- General 0605
- Acoustics 0986
- Astronomy and Astrophysics 0606
- Atmospheric Science 0608
- Atomic 0748
- Electronics and Electricity 0607
- Elementary Particles and High Energy 0798
- Fluid and Plasma 0759
- Molecular 0609
- Nuclear 0610
- Optics 0752
- Radiation 0756
- Solid State 0611

Statistics 0463

Applied Sciences

Applied Mechanics 0346
Computer Science 0984
Engineering
- General 0537
- Aerospace 0538
- Agricultural 0539
- Automotive 0540
- Biomedical 0541
- Chemical 0542
- Civil 0543
- Electronics and Electrical 0544
- Heat and Thermodynamics 0348
- Hydraulic 0545
- Industrial 0546
- Marine 0547
- Materials Science 0794
- Mechanical 0548
- Metallurgy 0743
- Mining 0551
- Nuclear 0552
- Packaging 0549
- Petroleum 0765
- Sanitary and Municipal 0554
- System Science 0790

Geotechnology 0428
Operations Research 0796
Plastics Technology 0795
Textile Technology 0994

PSYCHOLOGY

General 0621
Behavioral 0384
Clinical 0622
Developmental 0620
Experimental 0623
Industrial 0624
Personality 0625
Physiological 0989
Psychobiology 0349
Psychometrics 0632
Social 0451

A STUDY OF MULTILAYER PRINTED TRANSMISSION LINES AND ANTENNAS

BY

XIANHUA YANG

A Thesis submitted to the Faculty of Graduate Studies of the University of Manitoba in partial fulfillment of the requirements for the degree of

DOCTOR OF PHILOSOPHY

To My Parents

ABSTRACT

This thesis develops full wave analysis techniques for multilayer printed transmission lines and antennas and investigates bandwidth enhancement techniques for printed antennas. Initially, general solutions in space and spectral domains for the electromagnetic boundary value problem of multilayer dielectrics are presented in the form of vectorial auxiliary potential functions to form the theoretical basis for the entire thesis. Then, a space domain full wave technique is developed for open printed transmission lines, which can give full wave results for structures of finite width dielectrics. Numerical examples on single and coupled microstrip lines of finite width dielectrics are presented.

For the spectral domain solution, initially, a network approach is developed to evaluate spectral domain Green's functions of arbitrarily directed electric/magnetic currents in multilayer dielectric structures. It reduces a very lengthy derivation process into a simple and systematic procedure. Results for single layer grounded dielectrics supporting both electric and magnetic currents are presented to validate the approach.

A unified spectral domain full wave technique is then presented for printed antennas with multilayer dielectrics. It can treat different feeding structures and radiating elements of arbitrary shape geometries. New formulations for quick evaluation of far field radiation patterns are also developed.

As an application example, aperture coupled microstrip antennas of various coupling apertures and radiating elements are analyzed. Results are presented to discuss the effects of structural parameters.

Several techniques are proposed to enhance bandwidth performance of printed antennas. Subarrays of coplanar or stacked parasitic elements can widen bandwidth and increase directivity. Slotted patch can achieve dual–frequency operations with only a single patch and single feed. Techniques for achieving multi–frequency operations are also presented.

Finally, a concluding remark is presented to outline the future work in this area.

ACKNOWLEDGEMENT

My greatest appreciation and most sincere gratitude are due to my advisor, Dr. L. Shafai, for giving me an opportunity to study with him. His constant academic guidance, life advice, financial support, and patience in correcting my English composition during last three years were essential for completion of my study and writing this thesis. He was always there when I need help. His profound physical insight into the problems helped me building a little bit of mine. I will never forget the time he spent to help me analyze the problems, fabricate antenna samples, and do measurement.

I would like to thank Dr. A. Sebak for many good advices, helpful discussions and pleasant cooperations. Sincere thanks are also due to Professor E. Bridges for his advices in microwave engineering and my work as teaching assistant. I also benefited from many academic and nonacademic discussions with Dr. H. Moheb, Dr. H. Legay, Mr. J. Roy, Dr. Y. Lin, and a good number of other friends.

I am grateful to all members of my advisory committee and examination committee for their time, suggestions and comments.

I would also like to take this opportunity to thank the Faculty of Graduate Studies for Graduate Student Fellowship, Dr. S. Onyshko and the Department of Electrical and Computer Engineering and the Faculty of Engineering for Graduate Student Conference Travel's Award, Dr. P. N. Shivakumar and the Institute of Industrial Mathematical Science for a conference sponsorship.

I dedicated this thesis to my parents to acknowledge their continuous encouragement, love, support, and understanding. I am also indebted to my younger sister and brother who took over most of my duties in the family.

Last but not least, I would like to thank my wife for her support and understanding of my neglects, especially during the period of preparation of this thesis.

Table of Contents

Figure Captions

Chapter 1 INTRODUCTION

1.1 Motivation and Objective of the Thesis

The technology of microwave and monolithic integrated circuits has experienced impressive advances in recent years. It has enabled implementation of many new devices and numerous printed circuit systems have been developed for various applications. However, once fabricated, It is generally difficult, if not impossible, to adjust the performance of monolithic integrated circuits. Their design must be accurate which is usually handled analytically using the CAD techniques. Since the effectiveness and accuracy of a CAD tool is largely based on the analysis techniques implemented in the computer program, an accurate and fast analysis process is very important to the successful design and fabrication of microwave and monolithic integrated circuit systems.

Printed transmission lines and antennas are two basic passive components in microwave and monolithic integrated circuits, and there have been constant efforts for developing effective and accurate analysis techniques for them. Most studies on printed transmission lines involve enclosed structures, or open structures with dielectrics extending to infinity in two dimensions. Publications addressing finite dielectric widths are very limited and address only some quasi–static problems of open planar transmission lines of finite wide dielectrics. In addition, existing work on printed antennas are mainly on structures with single or two layers. However, in practical applications, the open planar transmission lines have only finite wide dielectrics and increasing number of dielectric layers are used in

printed antennas to enhance their performances or fulfill different requirements. A realization of such kinds of needs for both multilayer planar transmission lines and printed antennas initiated the theoretical part of research in this thesis.

On the other hand, research on performance enhancement technique has always been very active due to limitations in electrical performance of printed antennas, such as the narrow bandwidth, and low directivity of the element. In this research, several performance enhancement techniques are developed to widen the bandwidth and/or increase directivity of microstrip antennas.

1.2 Printed Transmission Lines

Printed transmission lines are composed of several conducting plates and either enclosed or open dielectric layers. They cannot support the TEM wave modes due to the presence of inhomogeneous dielectrics. The basic printed transmission line is the microstrip line as shown in Fig.1.1. There are also some other kind of structures, such as the slot line, coplanar waveguide, and fin–line in the enclosed structure.

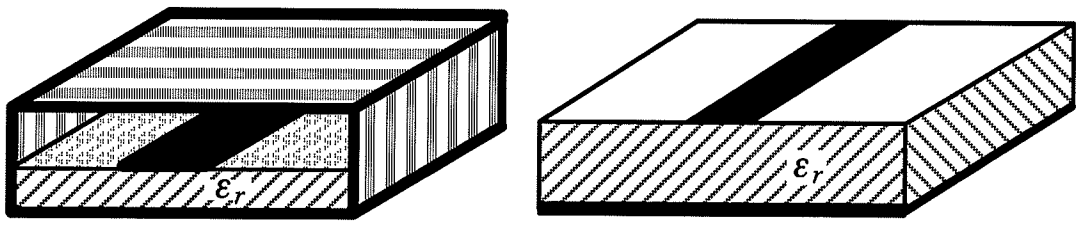

(a) enclosed structure (b) open structure

Fig.1.1. Enclosed and open microstrip lines

1.3 Printed Antennas

The concept of microstrip radiators was first proposed in 1953[1], almost at the same time as the microstrip lines. But, practical antennas were not developed until early 1970's[2],[3] when they are used as conformal antennas on missiles and aircrafts, where the conformal antennas were needed. Since then, research on microstrip antennas has been growing rapidly with thousands of papers being published in this area and progress made both theoretically and experimentally. Several books and a special issue of IEEE transaction were published in early 1980's[4]–[6] and a handbook[7] on microstrip antennas was also written which includes most of the developments by international community of printed antenna specialists before 1990.

1.3.1 Basic performance and features

The basic configuration of a microstrip antenna is shown in Fig.1.2a. It is composed of three parts, the dielectric substrate with a ground plane, printed radiating elements which may be conductors printed on the dielectric or slots on the ground plane, and the feeding structure which may be coaxial probe or printed transmission lines. It radiates a relatively broad beam broadside to the plane of the substrate as shown in Fig.1.2b.

It is obvious from Fig.1.2a that microstrip antennas have features of low–profile, low–weight, low–cost, easy of integration into arrays or with microwave integrated circuits, and conformal to curved surfaces. They are therefore, utilized both in civilian and military applications. However, as compared with other microwave antennas, microstrip antennas have a number of major electrical weakness, such as narrow bandwidth, spurious feed radiation, poor polarization purity and limited power capacity. And, these disadvantages have

restricted their applications. Consequently, in the past few years, much research work, both theoretically and experimentally, have been done to overcome these disadvantages of microstrip antennas.

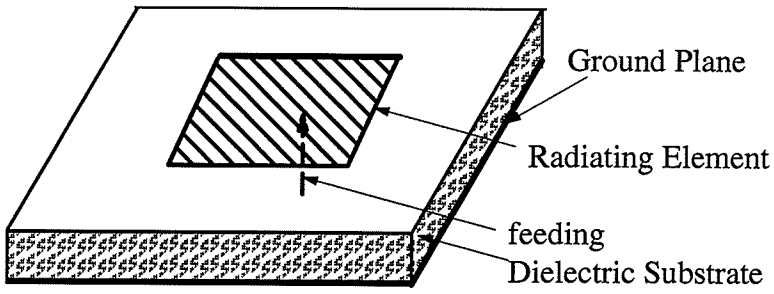

(a) basic configuration

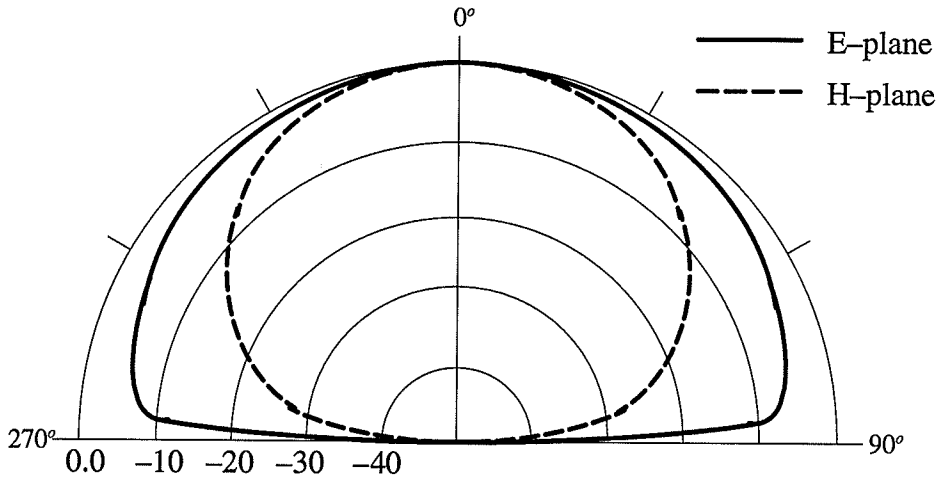

(b) typical radiation pattern

Fig.1.2. A microstrip antenna and its radiation pattern

1.3.2 Various radiating elements

The radiating element in a printed antenna can be a printed conducting patch or printed slot with various shapes. Some typical, but not all, shapes of printed antennas are shown in Fig.1.3. They are also many modifications to these basic shapes which can be found in [7].

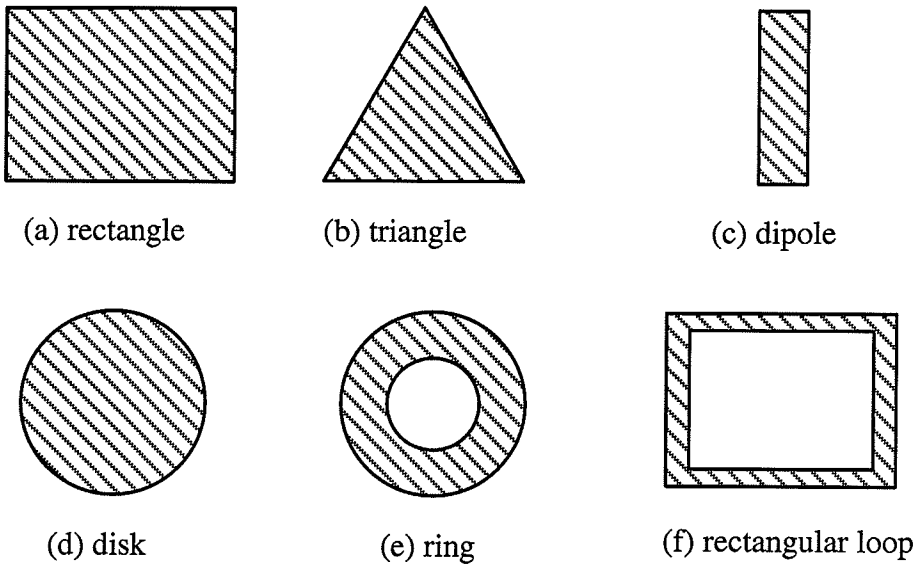

Fig.1.3. Some basic radiating elements of printed antennas

1.3.3 Multilayer dielectric structures

Conventionally, printed antennas are fabricated in one or two dielectric layers. Recently, more and more multilayer dielectric structures are used to achieve high performance antennas or to fulfil structural requirements. For example, a number of microstrip antenna disadvantages can be overcome by stacking several antennas of different sizes to form multi–resonance structures. By using multilayer dielectric structures, the antennas and feeding structures can be stacked to save space of the entire system.

1.3.4 Various feeding techniques

Printed antennas can be fed either directly by connecting them with feedlines, including the coaxial probe feeding and microstrip line feeding, or, through electromagnetically coupled feedlines, including the gap coupled microstrip line feeding, proximity coupled microstrip line feeding, and aperture coupled microstrip line feeding(Fig.1.4). These techniques can be used individually or simultaneously in an array, and each one has advantages and disadvantages. Features of these feeding techniques are summarized below.

(1) Coaxial probe feeding

In the coaxial probe feeding(Fig.1.4a)[6], the probe is soldered directly to the patch, or using some modifications, such as the capacitance gap[8] or ring[9] between the probe and the patch. The input impedance can be adjusted by changing the position of the probe. This coaxial cable lies behind the ground plane and do not contribute to the radiation. Only the vertical probe itself may produce spurious radiation. However, this structure suffers from the complexity of mechanical connections, especially in a large array, and the asymmetry of the feed may cause higher cross polarizations and sidelobe levels.

(2) Direct connected microstrip line feeding

In this structure(Fig.1.4b), the microstrip antenna is connected directly to the microstrip feedline[4][5]. This is a very simple structure for integration of the antenna and feedline. The input impedance can be adjusted by changing the feeding position. But, the feedline will produce spurious radiation that affects the antenna polarization and sidelobes. This method also is not suitable for direct integration of radiating elements and active devices.

The circuit and antenna requirements often conflict and their mutual coupling deteriorate the performance. In a large array, it can be used in conjunction with other techniques to simplify the feeding network. The notched feeding structure[10][11] is one of its modifications. Again, the asymmetry of the feed may affect the cross polarization and sidelobe level.

(3) Gap coupled microstrip line feeding

The gap coupled microstrip line feeding(Fig.1.4c)[4],[5] may be considered as a modification to the direct microstrip line feeding. It provides isolation for the direct currents between the feedline and radiating element. Therefore, it is suitable for mounting of the active elements between the antenna and feedline. It has almost the all advantages of the direct microstrip line feed, except it suffers from some restriction on the feeding position. It also suffers from disadvantages of the direct microstrip line feeding and the feedline and gap discontinuity produces spurious radiation. The asymmetry of the feeding may deteriorate the cross polarization and sidelobe level. It is also difficult sometime to make compensation between the circuit and antenna requirements. One extension of such a feeding structure is that of using one patch to feed another patch through electromagnetic coupling which leads to a kind of subarray composed of coplanar parasitic elements.

(4) Proximity coupled microstrip line feeding

As in the previous feeding structure, the proximity coupled microstrip line feeding(Fig.1.4d)[12] also provides isolation for direct currents between the feedline and radiating elements. The feedline is fabricated on the lower dielectric and the radiating element is on the upper one which can increase its bandwidth. The input impedance can be adjusted by changing the position and/or the extension of the feedline. The different requirements of antenna and circuit can be both fulfilled quite well. It posses other advan-

tages and disadvantages similar to the gap coupled and direct connected microstrip line feeds. But the contribution from the spurious radiation of the feedline may be smaller because it is on the lower substrate. However, the twin layer structure increases the mutual coupling between elements in the array. Again, the concept of proximity coupled feeding has been extended to stacked microstrip antennas where a patch, or several patches, at an upper dielectric layer is fed by another patch on the lower dielectric layer.

(5) Aperture coupled microstrip line feeding

Microstrip radiating elements can also be fed by microstrip lines through a coupling aperture on the ground plane(Fig.1.4e)[13]. In this structure, the feedline and radiating elements are isolated somewhat by the ground plane which allows different substrates to be used in each side, suitable for both antenna and microwave integrated circuits. Also, the size and position of the coupling aperture provides more freedoms in the design. The electrically small coupling aperture ensures a very small backward radiation. However, the narrow bandwidth of the coupling aperture makes the antenna bandwidth narrower than that of other microstrip antenna types.

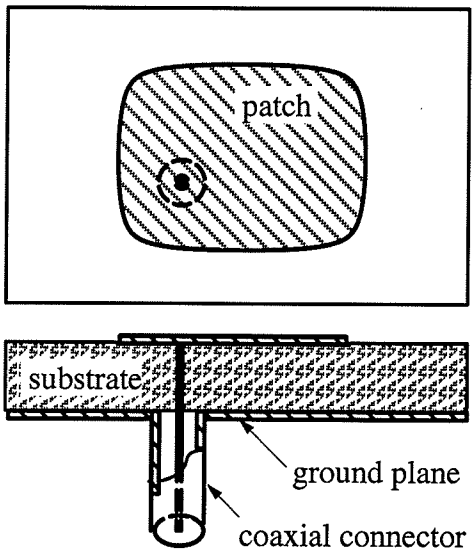

(a) coaxial probe feeding

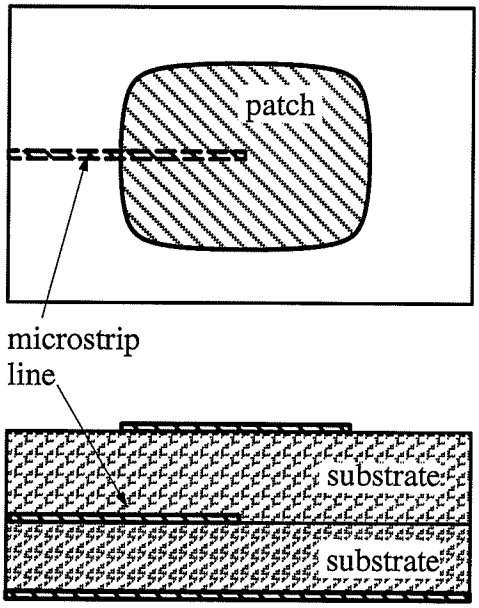

(d) proximity coupled feeding

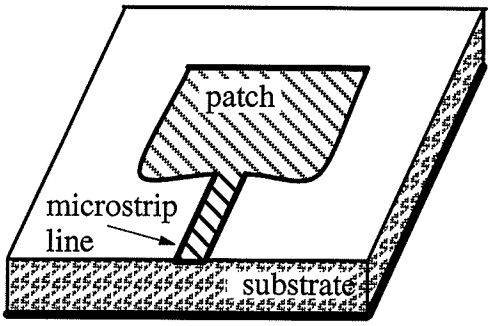

(b) direct connected feeding

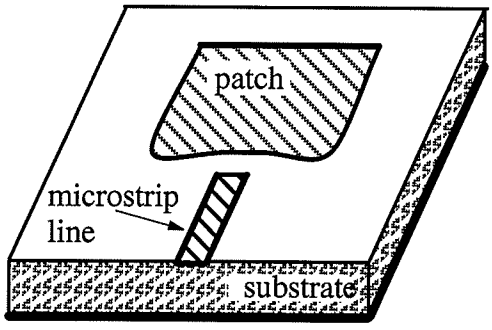

(c) gap coupled feeding

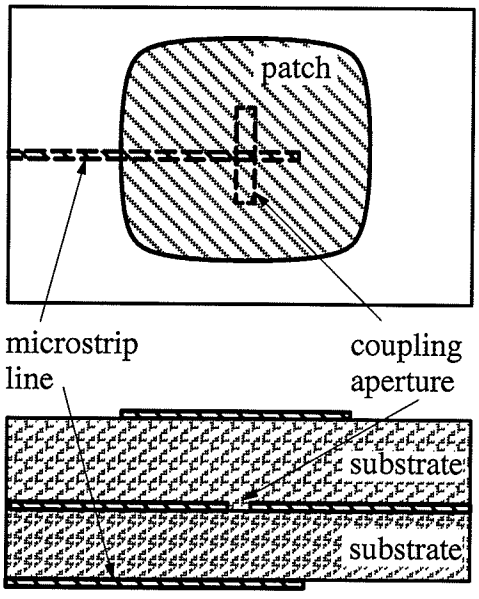

(e) aperture coupled feeding

Fig.1.4. Feeding techniques for microstrip antennas.

1.4 Arrangement of the Thesis

In Chapter 2, a unified auxiliary potential function theory is presented for the open structures with inhomogeneous dielectrics. In preparation for the analysis of microstrip lines and antennas, the problem of stratified dielectric layers is discussed in detail. Then various analysis techniques for microstrip lines and antennas are reviewed in conjunction with their advantages and disadvantages.

A space domain full wave technique is developed in Chapter 3 for the analysis of open printed transmission lines. Initially, a special form of finite difference, the method of line, is extended to the infinite region and then, the Helmholtz equations in each region are solved and boundary conditions on the interface of dielectric layers are enforced to obtain a set of linear algebraic equations. By some matrix manipulation, the wave number and electromagnetic field distributions of printed lines are obtained. This technique is especially suitable for open structures with finite width dielectrics although it can also be applied to structure with infinitely wide dielectrics. Numerical results on a single and coupled microstrip antennas with finite width dielectric and ground plane are presented.

In Chapter 4, a network approach is developed for the evaluating of spectral domain Green's functions of arbitrarily directed electric/magnetic currents in multilayer dielectric structures. By substituting the dielectric layer with an equivalent network and replacing the electric/magnetic current sources by appropriate electric current/voltage generators, the spectral domain Green's functions can be evaluated very efficiently by using a network approach. This approach is very suitable for the development of a general computer program for treating structures of arbitrary number of layers of dielectrics. An example is presented to compare with results obtained by using a field matching at the layer interface.

In Chapter 5, a unified spectral domain technique is developed to analyze printed antennas with multilayer dielectrics. By using spectral domain Green's functions, a set of spectral domain integral equations is obtained. Then, the spectral domain moment method is applied to enforce the boundary conditions. New formulations are presented for quick evaluation of far field radiation patterns. Treatment of various feeding structures are discussed, and entire domain and subsectional basis functions are employed in the analysis of structures with regular geometries. For the structure with arbitrary geometries, nodal based basis functions are also proposed and studied.

In Chapter 6, microstrip antennas fed with aperture coupling are studied in detail. The features of aperture coupled microstrip antennas are discussed with respect to the analysis results. The effect of various parameters on antenna performances are discussed, and results for several different patches fed with different coupling apertures are presented.

In Chapter 7, several techniques are proposed to enhance performance of microstrip antennas. Both wideband techniques and multiple frequency operation techniques are described.

Chapter 8 is a conclusion of the thesis. The main contributions of the thesis are summarized in this chapter and some future work in this area are outlined.

Chapter 2 THEORETICAL ANALYSIS OF OPEN MULTILAYER DIELECTRIC STRUCTURES

In a homogeneous, linear, isotropic and source free dielectric region, relationships between the components of harmonic electromagnetic fields are

$$\begin{aligned} \nabla \times \mathbf{E} &= -j\omega\mu\,\mathbf{H} & \nabla \times \mathbf{H} &= j\omega\varepsilon\,\mathbf{E} \\ \nabla \cdot \mathbf{D} &= 0 & \nabla \cdot \mathbf{B} &= 0 \end{aligned} \tag{2.1}$$

where $\varepsilon = \varepsilon_o \varepsilon_r$ and $\mu = \mu_o \mu_r$, and a time varying factor $e^{j\omega t}$ is assumed.

The solution of the electromagnetic field boundary value problem can be obtained by solving (2.1) in conjunction with the appropriate boundary conditions and excitation situations. Usually, the solution procedure can be simplified by introducing auxiliary potential functions[14][15], for which two types of vectorial potential functions are used in the literature. Both are provided here and shown that they are essentially the same. Then the electromagnetic boundary value problems for the multilayer dielectrics are discussed. In the last section, a comparative study of various analysis techniques for microstrip antenna is provided.

2.1 Auxiliary Vectorial Potential Functions

There are mainly two types of auxiliary vectorial potential functions which used in electromagnetic field boundary value problems, i.e., the vectorial electric and magnetic potentials, and the Hertzian electric and magnetic potentials.

The definitions for the vectorial electric and magnetic potential functions are[14][15]

$$\begin{aligned} \mathbf{H} &= \nabla \times \mathbf{A} \\ \mathbf{E} &= -j\omega\mu_o\mu_r\mathbf{A} + \frac{1}{j\omega\varepsilon_o\varepsilon_r}\nabla(\nabla \cdot \mathbf{A}) \end{aligned} \tag{2.2}$$

$$\begin{aligned} \mathbf{E} &= -\nabla \times \mathbf{F} \\ \mathbf{H} &= -j\omega\varepsilon_o\varepsilon_r\mathbf{F} + \frac{1}{j\omega\mu_o\mu_r}\nabla(\nabla \cdot \mathbf{F}) \end{aligned} \tag{2.3}$$

where μ_r and ε_r is the relative dielectric constant in the region.

The definitions of the Hertzian electric and magnetic potential functions are[14][15]

$$\begin{aligned} \vec{\mathbf{E}} &= \varepsilon_r^{-1}\nabla \times \nabla \times \vec{\Pi}_e \\ \vec{\mathbf{H}} &= j\omega_o\varepsilon_o\nabla \times \vec{\Pi}_e \end{aligned} \tag{2.4}$$

$$\begin{aligned} \vec{\mathbf{E}} &= -jk_o\nabla \times \vec{\Pi}_h \\ \vec{\mathbf{H}} &= \frac{1}{\eta_o}\nabla \times \nabla \times \vec{\Pi}_h \end{aligned} \tag{2.5}$$

where $k_o = \omega\sqrt{\mu_o\varepsilon_o}$ and $\eta_o = \sqrt{\mu_o/\varepsilon_o}$.

It is obvious from (2.2)–(2.5) that, these two sets of auxiliary vectorial potential functions can be transformed to each other, and either of them can be used in practical applications. As a matter of fact, in the analysis of planar transmission lines with finite width dielectrics,

the Hertzian electric and magnetic potential functions are adopted because they give simpler boundary conditions at the truncation of dielectrics. For the spectral domain analysis of printed antennas, the vectorial electric and magnetic potential functions defined in (2.2) and (2.3) are used in order to establish analogy between dielectric layers and equivalent transmission lines.

2.2 Field Theory for Stratified Dielectrics

The stratified dielectric structure can only support hybrid modes due to the complexity of the boundary conditions at dielectric interfaces. Consider a dielectric layer as shown in Fig.2.1. The vectorial electric and magnetic potential functions are assumed as

$$\mathbf{A} = \hat{\mathbf{a}}_z \, A_z(x, y, z)$$
$$\mathbf{F} = \hat{\mathbf{a}}_z \, F_z(x, y, z) \tag{2.6}$$

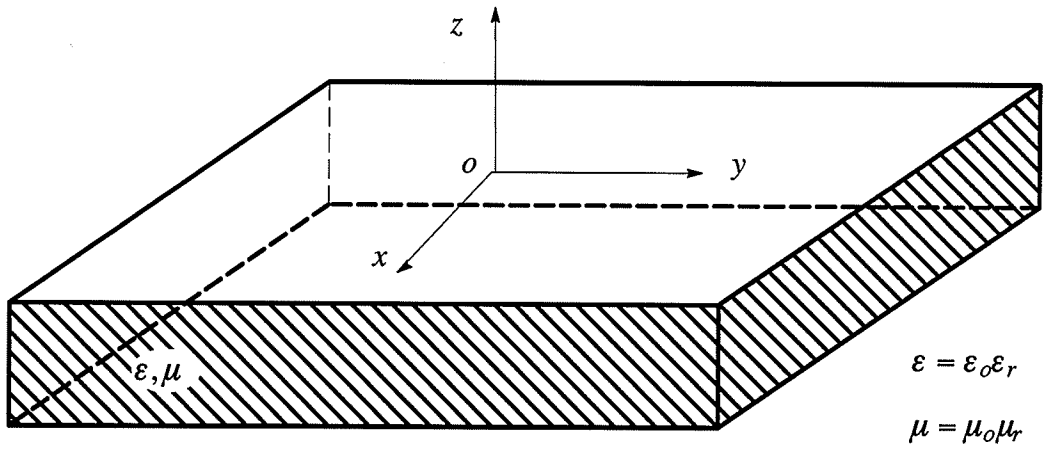

Fig.2.1. A dielectric layer

then the electromagnetic field components are

$$E_x = \frac{1}{j\omega\varepsilon}\frac{\partial^2 A_z}{\partial x \partial z} - \frac{\partial F_z}{\partial y} \qquad H_x = \frac{1}{j\omega\mu}\frac{\partial^2 F_z}{\partial x \partial z} + \frac{\partial A_z}{\partial y}$$

$$E_y = \frac{1}{j\omega\varepsilon}\frac{\partial^2 A_z}{\partial y \partial z} + \frac{\partial F_z}{\partial x} \qquad H_y = \frac{1}{j\omega\mu}\frac{\partial^2 F_z}{\partial y \partial z} - \frac{\partial A_z}{\partial x} \tag{2.7}$$

$$E_z = \frac{1}{j\omega\varepsilon}\left(\frac{\partial^2}{\partial z^2} + k^2\right)A_z \qquad H_z = \frac{1}{j\omega\mu}\left(\frac{\partial^2}{\partial z^2} + k^2\right)F_z$$

and the potential functions satisfy the following equations

$$\begin{aligned} \nabla^2 A_z + k^2 A_z &= 0 \\ \nabla^2 F_z + k^2 F_z &= 0 \end{aligned} \tag{2.8}$$

where $k^2 = \omega^2\varepsilon\mu$, $\omega^2 = 2\pi/\lambda$.

The general solutions to (2.8) can be found with some unknown coefficients and A_z and F_z are substituted into (2.7) to get the expressions for all electromagnetic field components. Those unknown coefficients in the expression of A_z and F_z can then be determined by considering the boundary conditions and exciting situations.

For dielectrics extending to infinity in two dimensions, the electromagnetic field boundary value problem can be transformed into the spectral domain by defining the following Fourier transform pair,

$$\tilde{Q}(k_x, k_y, z) = \int\int_{-\infty}^{\infty} Q(x, y, z)\, e^{-jk_x x}\, e^{-jk_y y}\, dx\, dy \tag{2.9}$$

$$Q(x, y, z) = \frac{1}{4\pi^2}\int\int_{-\infty}^{\infty} \tilde{Q}(k_x, k_y, z)\, e^{jk_x x}\, e^{jk_y y}\, dk_x dk_y \tag{2.10}$$

which results in

$$\tilde{E}_x = \frac{k_x}{\omega\varepsilon}\frac{\partial \tilde{A}_z}{\partial z} - jk_y \tilde{F}_z \qquad \tilde{H}_x = \frac{k_x}{\omega\mu}\frac{\partial \tilde{F}_z}{\partial z} + jk_y \tilde{A}_z$$

$$\tilde{E}_y = \frac{k_y}{\omega\varepsilon}\frac{\partial \tilde{A}_z}{\partial z} + jk_x \tilde{F}_z \qquad \tilde{H}_z = \frac{1}{j\omega\mu}\left(\frac{\partial^2}{\partial z^2} + k^2\right)\tilde{F}_z \tag{2.11}$$

$$\tilde{E}_z = \frac{1}{j\omega\varepsilon}\left(\frac{\partial^2}{\partial z^2} + k^2\right)\tilde{A}_z \qquad \tilde{H}_y = \frac{k_y}{\omega\mu}\frac{\partial \tilde{F}_z}{\partial z} - jk_x \tilde{A}_z$$

and

$$\begin{aligned} &\frac{\partial^2 \tilde{A}_z}{\partial z^2} + k_z^2 \tilde{A}_z = 0 \\ &\frac{\partial^2 \tilde{F}_z}{\partial z^2} + k_z^2 \tilde{F}_z = 0 \end{aligned} \tag{2.12}$$

where $k_z^2 = k^2 - k_x^2 - k_y^2$.

It is very easy to obtain the general solutions for Eq.(2.12) with unknown coefficients which can be determined in a similar way as in the space domain solution.

For a dirac–delta function excitation, analytical expressions can be obtained for the unknown coefficients of electric and magnetic potential functions. However, for a general excitation, such analytical expressions do not exist. Therefore, the numerical methods are adopted to get numerical results.

2.3 Theoretical Analysis of Printed Antennas

Many methods have been developed for the analysis of microstrip antennas. These methods can be divided into two categories of the **network models** based on the magnetic surface current sources, including the transmission line model, modal expansion cavity model and the multiport network model; and **the integral equation methods** based on the surface or volume electric and magnetic currents, including the equivalent source method, the method of Green's functions, and the spectral domain moment method. The network models are simpler and need less computation, while the integral equation methods are usually more exact but need more computation efforts. It is also difficult to treat structure with multilayer dielectrics by using the network models, while no extra effort is needed in the integral equation methods. In the following sections, a brief description of the principles, advantages and disadvantages of these methods with representative references are given.

2.3.1 Transmission line model

Microstrip patch antennas have a physical structure derived from the microstrip transmission line. Consequently, the transmission line model[16][17] is the first and most obvious choice for the analysis. In this model, the microstrip patch element is treated as a line resonator with no transverse field variations. The fields vary along its length and radiation occurs mainly from the fringing fields at the open circuited ends. The radiator may be repre-

sented as two slots. That is, the microstrip patch is expressed as a transmission line with two end loaded impedances representing the radiating slots.

The transmission line model is simple both in the analysis and design of rectangular microstrip patch antennas. However, it can only be applied to the patch elements with simple and regular configurations and to thin dielectric substrates due to the fact that it can not take into account the surface wave effects.

2.3.2 Cavity model

The cavity model[18] approximates the region between the microstrip patch and its ground plane by a thin TM_z – mode electromagnetic cavity bounded by a magnetic wall along the edges and two electric walls of the patch and ground plane. The field between the patch and the ground plane is expanded in terms of a series of cavity resonant modes or eigenfunctions along with their eigenvalues or resonant frequencies associated with the modes. The radiation effect and other losses are represented in terms of either an artificially increased substrate loss tangent or an impedance boundary condition at the walls. The fields of the antenna may be assumed to be those of the cavity and used to evaluate the radiation patterns, radiated power and input admittance at any feed point.

This model provides a clear physical explanation of the solution which is especially important to control the polarization or to explore wideband techniques for microstrip antennas. But, it can not take into account the surface wave effect and multilayer effect, and is difficult to consider the mutual coupling between elements in the array.

2.3.3 Multiport network model

As an extension of the cavity model, the multiport network model[19] treats electromagnetic fields underneath the patch and outside separately. The patch itself is modelled as a

two dimensional planar network with a multiple number of ports located all around its edges. Each port represents a small section(the section is small enough so that the fields over its length may be assumed uniform) of the edge of the patch. The fields outside the patch(the fringing fields at the edges, the surface wave fields and the radiation field) are incorporated by adding equivalent edge admittance networks, including radiating edge admittance networks and non–radiating edge admittance networks, connected to various edges of the patch. This model can take into account the junction between the feed line and the patch and can also consider the mutual coupling between two radiating edges.

This model combines the concept of network theory with microstrip antennas which makes it possible to use available network analysis and design theories and software in microstrip antenna analysis and design. But large computation time is needed to treat complex problems.

2.3.4 Equivalent source method

The equivalent source method[20] is based on the equivalence principle. Initially, the effect of the dielectric substrate is represented by equivalent electric and magnetic currents and a set of integral equations are established by satisfying all the boundary conditions of the original problem with the equivalent electric and magnetic currents being unknown. The moment method is then applied to solve these integral equations. This method is accurate in formulation by considering all boundary conditions.

This method can be applied to various structures with arbitrary patch and dielectric substrate shapes, especially with finite dielectric substrate and ground plane. When it is applied to the axial symmetric geometries, much computation time and storage can be saved by expanding the field distributions in terms of a limited number of azimuthal modes

representing the physical modes of the structure, since microstrip patch antennas are highly resonant structures. Also, solutions obtained by using this modal expansion have clear physical meanings. However, huge memory and computation are required when it is applied to structures with large dielectrics and with no axial symmetry.

2.3.5 Spatial and spectral domain moment methods

The spatial domain moment method[21],[22] and spectral domain moment methods[23] are similar with only a difference that in the first method, calculation is done in the space domain while in the second method, it is handled in the spectral domain. In both methods, integral equations with the surface electric current on the patch being unknown are established by using the boundary conditions on the surface of the patch. The effect of the ground plane and the dielectric substrates are included in the Green's functions. The surface electric current on the patch is normally determined by using the moment method in the space or spectral domain.

The spatial domain moment method also establishes relationships between problems with stratified dielectrics and problems in the free space with different Green's functions. However, it needs large computation time to evaluate Green's functions. The computation time can be saved dramatically by using complex image theory to consider the effect of dielectrics[24].

The spectral domain moment method can treat microstrip antennas easily for various dielectrics(multi–layer, anisotropic, etc.), arbitrary radiating elements and feeds. And, when it is applied to microstrip antenna arrays with infinite number of elements, the formulation and computation can be simplified significantly. However, it also has large computation and storage requirements.

Chapter 3 A SPACE DOMAIN FULL WAVE TECHNIQUE FOR OPEN PRINTED TRANSMISSION LINES

In this chapter, a space domain full wave approach is developed to analyze open printed transmission lines. The method of lines, a special type of finite difference technique used in the analysis of enclosed printed structures, is extended to the printed structures in open space. This technique can be used to analyze various open printed lines and is suitable especially for dielectric substrates with discontinuities and/or with finite ground planes where a full wave approach is not available yet. The convergence of the method is examined by numerical experiments. As application examples, the dispersion characteristics of open single and coupled microstrip lines with finite dielectric substrates are calculated and compared with the full wave results for structures with infinite width dielectric/conductor and the available quasi–static results for single microstrip line with finite dielectric in the literature. The effect of dielectric width on the characteristics is also discussed.

3.1 Outline of Analysis Technique

Open printed transmission lines are widely used in microwave and millimeter wave integrated circuits. Such transmission lines with continuous and infinite dielectric layers may be analyzed by many effective methods. Their characteristics have therefore been systematically studied[25]. However, practical structures usually have discontinuities in the dielectric layers(Fig.3.1a) or use substrates of finite width(Fig.3.1b). Their characteristics are therefore expected to be different from those without discontinuities, but unfortunately,

at present there exist only a few quasi–static results for open microstrip lines with finite dielectric substrates[26][27]. On the other hand, at high operating frequencies, the frequency dependent characteristics are needed to accurately design circuits or antennas.

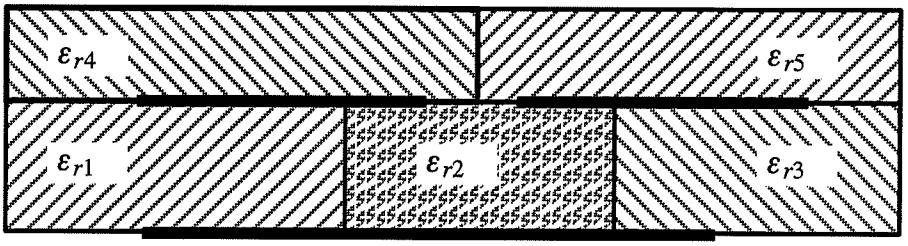

(a) with discontinuous dielectrics

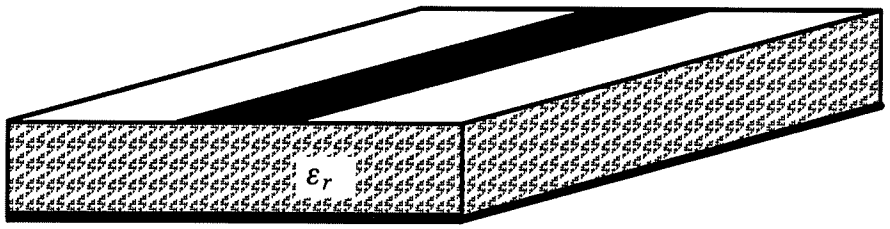

(b) with finite wide dielectric and/or ground plane

Fig.3.1. Open printed transmission lines

Traditionally, the method of lines has been used effectively in various enclosed planar or quasi–planar microwave structures[28]–[32]. In this chapter, this method is extended to open unbounded regions[33] by introducing a form of coordinate transformation. Based on this extension, a unified full wave approach[34] is presented here for the analysis of open printed transmission lines. The approach itself is general and can be used in either case with or without discontinuities in the dielectric layer. Of course, its advantage lies in its capability of giving the full wave characteristics of structures with discontinuous dielectric layers which are presently unavailable in the literature.

The procedure for application of the method of lines to the enclosed problems has been discussed in many publications[28]–[32]. In this chapter, initially, the formulation of the technique is provided briefly and its difference as compared with the conventional ones is pointed out. Then, the convergence of the method is examined carefully by numerical experiments. As application examples, the dispersion characteristics of open single and coupled microstrip lines of finite dielectric substrate widths are calculated. The results are compared with those of other full wave methods for structures with infinitely wide dielectrics and the available quasi–static results for the single microstrip lines of finite dielectric widths. Some differences are observed. This means that the full wave results for the structures with infinitely wide dielectrics can not be used directly in the case of finite dielectric case and the quasi static results for structures with finite dielectric can not be used at higher frequencies. However, similarities are found between the full wave results of structures with infinitely wide and finite dielectrics, which implies that nomograms used in the design of structures with infinitely wide dielectrics [25] may also be used for structures with finite dielectrics.

3.2 Formulations

An open printed transmission line with a single layer dielectric is shown in Fig.3.2a, which is composed of three dielectric regions($\varepsilon_{r1}, \varepsilon_{r2}, \varepsilon_{r3}$) and several conducting strips on its lower and upper interfaces while the areas above and below the layer are free space. The structure with a ground plane at the interface can be obtained by letting one of the conducting strips become infinitely wide, whereas that with a finite dielectric width is obtained by selecting $\varepsilon_{r1} = \varepsilon_{r3} = 1.0$.

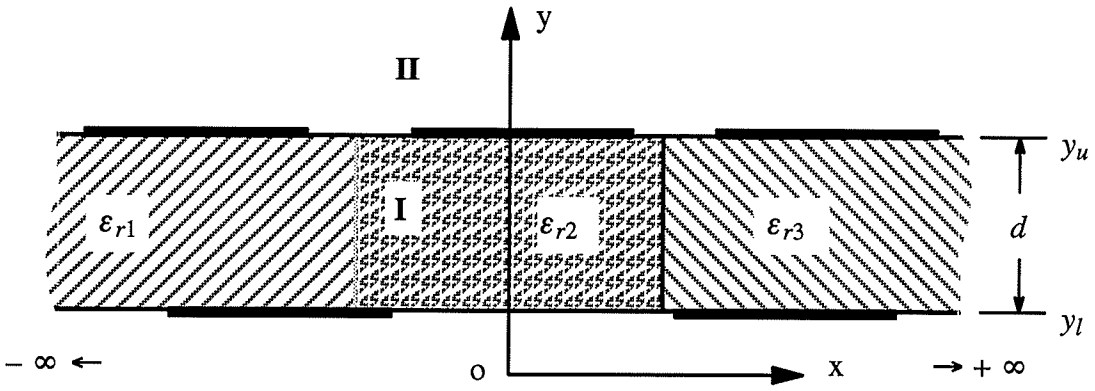

(a) original region in $x-y$ plane

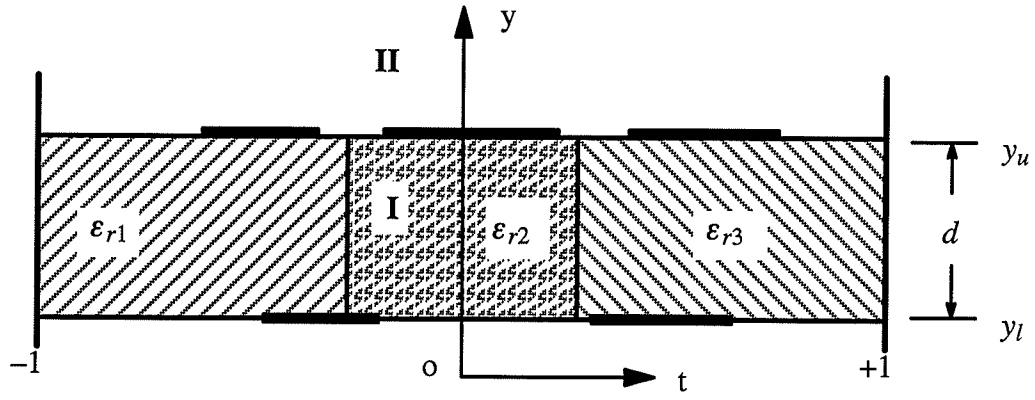

(b) mapped region in $t-y$ plane

Fig.3.2. Original and finite mapped regions of a discontinuous dielectric layer

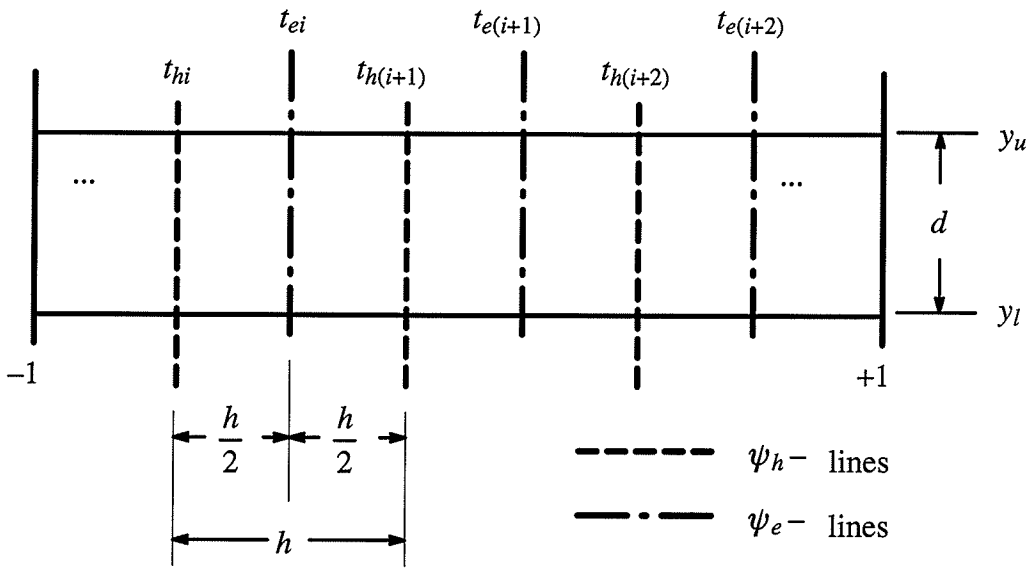

(c) discretization in $t-y$ plane

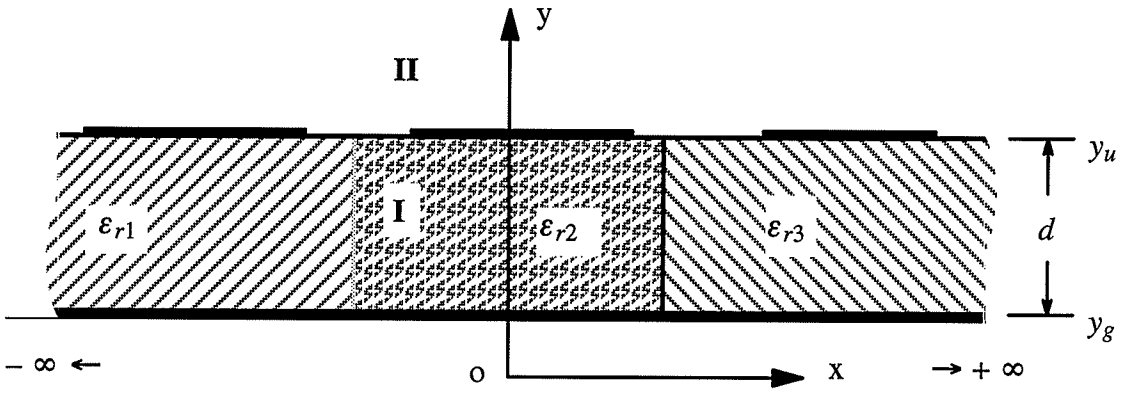

(d) perfectly conducting plane terminating

Fig.3.2 (continued)

3.2.1 Hybrid modes in the structure

As it is discussed in chapter 2, the electromagnetic fields in the structure of Fig.3.2a can be represented by hybrid modes of two types, the longitudinal section electric(LSE) and longitudinal section magnetic(LSM) modes. For completeness, fields in each layer expressed in terms of Hertzian vector potentials are written as

$$\begin{aligned} \vec{\mathbf{E}} &= \varepsilon_r^{-1}(x)\nabla \times \nabla \times \vec{\Pi}_e - jk_o \nabla \times \vec{\Pi}_h \\ \eta_o \vec{\mathbf{H}} &= jk_o \nabla \times \vec{\Pi}_e + \nabla \times \nabla \times \vec{\Pi}_h \end{aligned} \tag{3.1}$$

where $\varepsilon_r(x)$ is the relative dielectric constant in the layer which is dependent on x, $k_o = \omega\sqrt{\mu_o \varepsilon_o}$, $\eta_o = \sqrt{\mu_o/\varepsilon_o}$ and the Hertzian vector potentials $\vec{\Pi}_e$, $\vec{\Pi}_h$ have only the $\hat{\mathbf{x}}$ – components as

$$\begin{aligned} \vec{\Pi}_e &= \hat{\mathbf{x}}\, k_o^{-2}\, \psi_e\, e^{-jk_z z} \qquad \text{(LSM modes)} \\ \vec{\Pi}_h &= \hat{\mathbf{x}}\, k_o^{-2}\, \psi_h\, e^{-jk_z z} \qquad \text{(LSE modes)} \end{aligned} \tag{3.2}$$

where the dependence $e^{j\omega t}$ has been assumed, k_z is the propagation constant of the line, and the scalar potentials ψ_e, ψ_h must satisfy the following Helmholtz equations:

$$\begin{aligned} \varepsilon_r(x)\frac{\partial}{\partial x}\left(\varepsilon_r^{-1}(x)\frac{\partial^2 \psi_e}{\partial x^2}\right) + \frac{\partial^2 \psi_e}{\partial y^2} + \left(\varepsilon_r(x)k_0^2 - k_z^2\right)\psi_e = 0 \\ \frac{\partial^2 \psi_h}{\partial x^2} + \frac{\partial^2 \psi_h}{\partial y^2} + \left(\varepsilon_r(x)k_0^2 - k_z^2\right)\psi_h = 0 \end{aligned} \tag{3.3}$$

Therefore, the propagation constant k_z of the line may be obtained by solving (3.3) in combination with the appropriate boundary conditions of the structure.

3.2.2 Coordinate transformation between open and closed regions

In the structures of Fig.3.2, some of the boundaries are located at infinity. Usually in most solution methods, a boundary at infinity is substituted by a finite artificial boundary and then the problem is solved inside this finite artificial boundary, instead of its real open boundary. However, even when the artificial boundary is made large enough, there are still differences between the results obtained using the artificial boundary and the real problem. On the other hand, when the artificial boundary is made too large, the area becomes very large and introduces difficulties in application of numerical computation.

In the application of the method of lines, one needs to discretize the region only in one direction and the fields in the other direction may be expressed in explicit forms[28][29]. Therefore, when applying the method of lines to analyze the open problem as shown in Fig.3.2a, one needs to treat the unbounded region only in the $\hat{\mathbf{x}}-$ direction. In [33], the coordinate transformation was used to map the unbounded open region into a half–bounded region and then the method of lines was used to analyze the open microstrip line. This technique is adopted here for the analysis of problems with discontinuous dielectric layers.

There are a number of mapping functions that can be used to map the unbounded open regions(Fig.3.2a) into a half–bounded region(Fig.3.2b). In this paper, the following algebraic function is used(Assuming that the coordinate system in Fig.3.2a is x, y, z and that in Fig.3.2b is t, y, z)

$$k_o x = \frac{t}{1-|t|} s \qquad x \in (-\infty, +\infty), t \in (-1, +1) \tag{3.4}$$

where s is a constant that determines the shape of the mapping function which should be chosen carefully in the numerical processing. Then all the partial derivatives with respect to x in (3.3) may be expressed with respect to t as follows

$$\begin{aligned} \frac{\partial \psi_u}{\partial x} &= k_0 p(t) \frac{\partial \psi_u}{\partial t} \\ \frac{\partial^2 \psi_u}{\partial x^2} &= k_0 p(t) \frac{\partial}{\partial t}\left(k_o p(t) \frac{\partial \psi_u}{\partial t} \right) \end{aligned} \tag{3.5}$$

where subscript $u = e, h$ and

$$p(t) = \frac{dt}{d(k_o x)} \tag{3.6}$$

By such a coordinate transformation, the original open structure of Fig.3.2a is mapped into the half–bounded structure of Fig.3.2b, where the boundary along the $\hat{\mathbf{x}}-$ direction is closed and the boundary along the $\hat{\mathbf{y}}-$ direction is kept open.

3.2.3 Discretization in the transformed region

To solve the problem in the mapped half–bounded region of Fig.3.2b, one needs to discretize the $t-$ variable in the partial differential equations which are obtained by substituting (3.5) into (3.3). In this mapped region, the method of lines may be used in a similar way

as it is used in a closed region with a difference that in the present case the region in the $\hat{\mathbf{y}}-$ direction is open.

Initially, two sets of N straight lines parallel to the $y-$ axis are laid into the cross section as shown in Fig.3.2c. Then, the potentials ψ_e, ψ_h in the differential equations are replaced by their discrete values at these two sets of lines. For clarity, the lines corresponding to the potential ψ_e are named as "ψ_e- lines" while those of the potential ψ_h as "ψ_h- lines". The ψ_e- lines are placed at $t = t_{e1}, t_{e2}, \cdots, t_{eN}$ and the ψ_h- lines are at $t = t_{h1}, t_{h2}, \cdots, t_{hN}$. The distance between the two adjacent ψ_e- lines or ψ_h- lines is $h = 2/(N+0.5)$, i.e., $t_{e(i+1)} - t_{ei} = t_{h(i+1)} - t_{hi} = h$. Thus, the distance between the two adjacent ψ_e-, ψ_h- lines is $h/2$, i.e., $t_{e(i+1)} - t_{h(i+1)} = t_{h(i+1)} - t_{ei} = h/2$.

In addition to the above general rule for the placement of ψ_e- and ψ_h- lines, there are two other points that should be noted regarding certain special boundaries perpendicular to the $\hat{\mathbf{t}}-$ direction:

(1). At the electric wall perpendicular to the $\hat{\mathbf{t}}-$ direction, the tangential electric fields must be zero which results in setting $\psi_h = 0$ and $\frac{\partial \psi_e}{\partial t} = 0$. Therefore, a ψ_h- line is placed at the electric wall to fulfill these boundary conditions. Similarly, at the magnetic wall perpendicular to the $\hat{\mathbf{t}}-$ direction, the tangential magnetic fields should be zero which results in setting $\psi_e = 0$ and $\frac{\partial \psi_h}{\partial t} = 0$, and therefore, a ψ_e- line must be placed at the magnetic wall to fulfill these boundary conditions.

(2). When there is a discontinuity of the dielectric constant along the $\hat{\mathbf{t}}-$ direction, the boundary condition at the discontinuity interface which is perpendicular to the $\hat{\mathbf{t}}-$ direction must be fulfilled. For this purpose, a ψ_h- line is placed at the discontinuity interface between the two dielectrics, and the value of $\varepsilon_r(t)$ in the permittivity matrix $[\varepsilon_{rh}]$ at this line is assumed as the average of its values at two adjacent dielectrics.

The derivatives of ψ_e , ψ_h with respect to t , in the mapped region, are replaced by their values at the ψ_e- or ψ_h- lines through the following central finite difference scheme

$$\left(\frac{\partial A}{\partial t}\right)_i = \frac{A_{i+1/2} - A_{i-1/2}}{h} \tag{3.7}$$

where A represents either ψ_u or $\frac{\partial \psi_u}{\partial t}$, subscript i implies the position at $t = t_{ui}$, $i \pm 1/2$ for $t = t_{ui} \pm h/2$ and $u = e, h$.

Therefore, according to (3.5) and (3.7), one has

$$\begin{aligned}\left(\frac{\partial A}{\partial x}\right)_i &= \left(k_o p(t) \frac{\partial A}{\partial t}\right)_i \\ &= k_o p(t_{ui}) \frac{A_{i+1/2} - A_{i-1/2}}{h}\end{aligned} \tag{3.8}$$

and can therefore express the derivatives in (3.3) in terms of a finite difference matrix as

$$\frac{\partial \psi_h}{\partial x} \Rightarrow k_o\ h^{-1}\ [\mathbf{D}_e]\ [\Psi_h]$$

$$\frac{\partial \psi_e}{\partial x} \Rightarrow k_o\ h^{-1}\ [\mathbf{D}_h]\ [\Psi_e]$$

$$\frac{\partial^2 \psi_h}{\partial x^2} \Rightarrow k_o^2\ h^{-2}\ [\mathbf{D}_h]\ [\mathbf{D}_e]\ [\Psi_h] \tag{3.9}$$

$$\varepsilon_r^{-1}(x)\frac{\partial \psi_e}{\partial x} \Rightarrow k_o\ h^{-1}\ [\varepsilon_{rh}]^{-1}\ [\mathbf{D}_h]\ [\Psi_e]$$

$$\varepsilon_r(x)\frac{\partial}{\partial x}\left(\varepsilon_r^{-1}(x)\frac{\partial \psi_e}{\partial x}\right) \Rightarrow k_o^2\ h^{-2}\ [\varepsilon_{re}]\ [\mathbf{D}_e]\ [\varepsilon_{rh}]^{-1}\ [\mathbf{D}_h]\ [\Psi_e]$$

where $[\Psi_e]$ and $[\Psi_h]$ are $N \times 1$ matrices representing the set of the values of ψ_e and ψ_h at the ψ_e- and ψ_h- lines respectively, i.e.

$$\begin{aligned} [\Psi_e] &= [\psi_e(t_{e1}), \psi_e(t_{e2}), \ldots, \psi_e(t_{eN})]^T \\ [\Psi_h] &= [\psi_h(t_{h1}), \psi_h(t_{h2}), \ldots, \psi_h(t_{hN})]^T \end{aligned} \tag{3.10}$$

and $[\varepsilon_{re}]$ and $[\varepsilon_{rh}]$ are $N \times N$ diagonal matrices with the diagonal elements representing the set of the values of ε_r at the ψ_e- and ψ_h- lines as

$$\begin{aligned} [\varepsilon_{re}] &= \mathbf{diag}\ (\varepsilon_r(t_{e1}), \varepsilon_r(t_{e2}), \ldots, \varepsilon_r(t_{eN})) \\ [\varepsilon_{rh}] &= \mathbf{diag}\ (\varepsilon_r(t_{h1}), \varepsilon_r(t_{h2}), \ldots, \varepsilon_r(t_{hN})) \end{aligned} \tag{3.11}$$

while $[\mathbf{D}_e]$ and $[\mathbf{D}_h]$ are $N \times N$ matrices given by

$$[\mathbf{D}_e] = \begin{bmatrix} -p(t_{e1}) & p(t_{e2}) & 0 & \cdots & 0 & 0 \\ 0 & -p(t_{e2}) & p(t_{e2}) & \cdots & 0 & 0 \\ 0 & 0 & -p(t_{e3}) & \cdots & 0 & 0 \\ \vdots & \vdots & \vdots & \vdots & \vdots & \vdots \\ \cdot & \cdot & \cdot & \cdots & -p(t_{e(N-1)}) & p(t_{e(N-1)}) \\ 0 & 0 & 0 & \cdots & 0 & -p(t_{eN}) \end{bmatrix}$$

$$[\mathbf{D}_h] = \begin{bmatrix} p(t_{h1}) & 0 & 0 & \cdots & 0 & 0 \\ -p(t_{h2}) & p(t_{h2}) & 0 & \cdots & 0 & 0 \\ 0 & -p(t_{h3}) & p(t_{h3}) & \cdots & 0 & 0 \\ \vdots & \vdots & \vdots & \vdots & \vdots & \vdots \\ \cdot & \cdot & \cdot & \cdots & p(t_{h(N-1)}) & 0 \\ 0 & 0 & 0 & \cdots & -p(t_{hN}) & -p(t_{hN}) \end{bmatrix} \tag{3.12}$$

Substituting (3.9) into (3.3), one can obtain the following matrix equations for $[\Psi_e]$ and $[\Psi_h]$:

$$\frac{d^2}{dy^2}\,[\Psi_{e,h}] - k_o^2\, h^{-2}\,[\mathbf{Q}_{e,h}]\,[\Psi_{e,h}] - k_z^2\,[\Psi_{e,h}] = [\,0\,] \tag{3.13}$$

where $[\mathbf{Q}_e]$ and $[\mathbf{Q}_h]$ are $N \times N$ unsymmetrical trigonal matrices

$$\begin{aligned} [\mathbf{Q}_e] &= -\left([\varepsilon_{re}]h^2 + [\varepsilon_{re}][\mathbf{D}_e][\varepsilon_{rh}]^{-1}[\mathbf{D}_h]\right) \\ [\mathbf{Q}_h] &= -\left([\varepsilon_{rh}]h^2 + [\mathbf{D}_h][\mathbf{D}_e]\right) \end{aligned} \tag{3.14}$$

Since $[\mathbf{Q}_e]$ and $[\mathbf{Q}_h]$ are unsymmetrical trigonal matrices, it is difficult to write the explicit solution of (3.13). Therefore, one needs to implement certain transformations in (3.13) to obtain the explicit solution form.

It is known that[35] $[\mathbf{Q}_e]$ and $[\mathbf{Q}_h]$ can be transformed into the following diagonal forms

$$[\mathbf{T}_{e,h}]^{-1}\ [\mathbf{Q}_{e,h}]\ [\mathbf{T}_{e,h}]\ =\ [\Lambda_{e,h}] \tag{3.15}$$

where $[\Lambda_e], [\Lambda_h]$ are $N \times N$ diagonal eigenvalue matrices of $[\mathbf{Q}_e], [\mathbf{Q}_h]$

$$[\Lambda_{e,h}]\ =\ \mathbf{diag}\ (\lambda_{ei,hi}) \qquad\qquad (\ i = 1, 2, \cdots, N\ ) \tag{3.16}$$

and their diagonal elements λ_{ei} and λ_{hi} are the $i-$ th eigenvalues of $[\mathbf{Q}_e]$ and $[\mathbf{Q}_h]$ respectively. $[\mathbf{T}_e]$ and $[\mathbf{T}_h]$ are, of course, the corresponding eigenvector matrices of $[\mathbf{Q}_e]$ and $[\mathbf{Q}_h]$.

Therefore, $[\Psi_e]$ and $[\Psi_h]$ can be expressed by their transformed matrices $[\tilde{\Psi}_e]$ and $[\tilde{\Psi}_h]$ as

$$[\Psi_{e,h}]\ =\ [\mathbf{T}_{e,h}]\ [\tilde{\Psi}_{e,h}] \tag{3.17}$$

Substituting them into (3.12), one obtains:

$$\frac{d^2}{dy^2}\ [\tilde{\Psi}_{e,h}] - k_o^2\ [\mathbf{K}_{e,h}]\ [\tilde{\Psi}_{e,h}]\ =\ [\ 0\ ] \tag{3.18}$$

where $[\mathbf{K}_e]$ and $[\mathbf{K}_h]$ are $N \times N$ diagonal matrices

$$[\mathbf{K}_{e,h}] = \mathbf{diag}\ (k^2_{ei,hi}\ ) \tag{3.19}$$

and their diagonal elements are determined by

$$k_{ei,hi} = \sqrt{\varepsilon_{eff} + h^{-2}\lambda_{ei,hi}} \tag{3.20}$$

and $\varepsilon_{eff} = k_z^2/k_o^2$ is the effective dielectric constant to be determined.

3.2.4 Solutions in one layer

For a single layer, (3.18) can also be expressed in the following single variable form

$$\frac{d^2}{dy^2}\ \tilde{\psi}_{ei,hi} - k_o^2\ k^2_{ei,hi}\ \tilde{\psi}_{ei,hi} = 0 \tag{3.21}$$

and its general solutions are given by

$$\tilde{\psi}_{\ ei,hi} = a_{ei,hi}\ e^{k_{ei,hi}\,k_o y} + b_{ei,hi}\ e^{-k_{ei,hi}\,k_o y} \tag{3.22}$$

where $a_{ei,hi}$ and $b_{ei,hi}$ are the coefficients to be determined by the boundary conditions.

The general solutions of (3.22) may be written as a relationship between $[\tilde{\Psi}_e]$ and $[\tilde{\Psi}_h]$ and their normal derivatives in the upper and lower interfaces of the same layer. For example, for the layer I as shown in Fig.3.2, with the lower interface at $y = y_l$ and the upper interface at $y = y_u$, the transfer relations are

$$\begin{bmatrix} \frac{d}{dy}\left[\tilde{\Psi}_{e,h}\right]_{y_l} \\ \frac{d}{dy}\left[\tilde{\Psi}_{e,h}\right]_{y_u} \end{bmatrix} = k_o \begin{bmatrix} -\gamma_{e,h} & \alpha_{e,h} \\ -\alpha_{e,h} & \gamma_{e,h} \end{bmatrix} \begin{bmatrix} \left[\tilde{\Psi}_{e,h}\right]_{y_l} \\ \left[\tilde{\Psi}_{e,h}\right]_{y_u} \end{bmatrix} \tag{3.23}$$

where

$$\begin{aligned} [\gamma_{e,h}] &= \mathbf{diag}\left\{ k_{ei,hi} / \tanh\left(k_o k_{ei,hi}\, d\right) \right\} \\ [\alpha_{e,h}] &= \mathbf{diag}\left\{ k_{ei,hi} / \sinh\left(k_o k_{ei,hi}\, d\right) \right\} \end{aligned} \tag{3.24}$$

and $d = y_u - y_l$ is the thickness of the dielectric layer.

In particular, when one of the interfaces at $y = y_g$ is a perfectly conducting surface, as in Fig.3.2d, one has

$$\begin{aligned} [\mathbf{T}_e][\tilde{\Psi}_e]_{y_g} = [0] \quad &\Rightarrow \quad [\tilde{\Psi}_e]_{y_g} = [0] \\ [\mathbf{T}_e]\frac{d}{dy}[\tilde{\Psi}_h]_{y_g} = [0] \quad &\Rightarrow \quad \frac{d}{dy}[\tilde{\Psi}_h]_{y_g} = [0] \end{aligned} \tag{3.25}$$

and, when one of the interfaces approaches infinity, i.e. $y \to \infty$, one obtains

$$\begin{aligned} [\mathbf{T}_e][\tilde{\Psi}_e]_{y\to\infty} = [0] \quad &\Rightarrow \quad [\tilde{\Psi}_e]_{y\to\infty} = [0] \\ [\mathbf{T}_h][\tilde{\Psi}_h]_{y\to\infty} = [0] \quad &\Rightarrow \quad [\tilde{\Psi}_h]_{y\to\infty} = [0] \end{aligned} \tag{3.26}$$

3.2.5 The electromagnetic field components

According to (3.1), (3.2) and (3.9), all electromagnetic field components in the layer can be expressed by $[\Psi_e]$ and $[\Psi_h]$ as

$$
\begin{aligned}
[\mathbf{E}_x] &= -h^{-2}[\varepsilon_{re}]^{-1}\ [\mathbf{Q}_e][\Psi_e] \\
[\mathbf{E}_y] &= h^{-1}[\varepsilon_{re}]^{-1}[\mathbf{D}_e][\mathbf{G}_e][\Psi_e] - \sqrt{\varepsilon_{eff}}[\Psi_h] \\
[\mathbf{E}_z] &= -j\left\{h^{-1}\sqrt{\varepsilon_{eff}}[\varepsilon_{rh}]^{-1}[\mathbf{D}_h][\Psi_e] - [\mathbf{G}_h][\Psi_h]\right\} \\
[\mathbf{H}_x] &= -\eta_o^{-1}\ h^{-2}[\mathbf{Q}_h][\Psi_h] \\
[\mathbf{H}_y] &= \eta_o^{-1}\left\{h^{-1}[\mathbf{D}_h][\mathbf{G}_h][\Psi_h] + \sqrt{\varepsilon_{eff}}[\Psi_e]\right\} \\
[\mathbf{H}_z] &= -j\eta_o^{-1}\left\{h^{-1}\sqrt{\varepsilon_{eff}}[\mathbf{D}_e][\Psi_h] + [\mathbf{G}_e][\Psi_e]\right\}
\end{aligned}
\tag{3.27}
$$

where

$$
[\mathbf{G}_{e,h}] = [\mathbf{T}_{e,h}][\gamma_{e,h}][\mathbf{T}_{e,h}]^{-1} \tag{3.28}
$$

3.2.6 Matching of the boundary conditions at the interface

So far, all the electromagnetic field components have been expressed in terms of $[\Psi_e]$ and $[\Psi_h]$. These terms, $[\Psi_e]$ and $[\Psi_h]$ have general solutions as shown in (3.22) with coefficients and the effective dielectric constant in k_{ei} and k_{hi} as unknowns. The unknown coefficients in (3.22) may be eliminated by fulfilling the boundary conditions at the interfaces between the dielectric layers.

Substituting the electromagnetic field components from (3.27) into the boundary condition equations at each interface and after some mathematical manipulations, one can obtain a set of simultaneous equations for the relationship between the strip electric current and the electric field components at the interface with the strip at $y = y_s$,

$$
\begin{aligned}
[\mathbf{E}_x]_{y_s} &= j\eta_o h^{-1}[\mathbf{Z}_{xx}][\mathbf{J}_x] + \eta_o h^{-1}[\mathbf{Z}_{xz}][\mathbf{J}_z] \\
[\mathbf{E}_z]_{y_s} &= \eta_o[\mathbf{Z}_{zx}][\mathbf{J}_x] + j\eta_o[\mathbf{Z}_{zz}][\mathbf{J}_z]
\end{aligned}
\tag{3.29}
$$

where $[\mathbf{J}_x]$ and $[\mathbf{J}_z]$ are $N \times 1$ matrices of the transverse and longitudinal electric currents on the strip, and $[\mathbf{Z}_{xx}]$, $[\mathbf{Z}_{xz}]$, $[\mathbf{Z}_{zx}]$, and $[\mathbf{Z}_{zz}]$ are $N \times N$ matrices dependent only on the effective dielectric constants ε_{eff}.

For the structure shown in Fig.3.2d, where the dielectric is terminated by a perfect conductor in one side, the $[\mathbf{Z}_{xx}]$, $[\mathbf{Z}_{xz}]$, $[\mathbf{Z}_{zx}]$, and $[\mathbf{Z}_{zz}]$ matrices can be expressed as follows:

$$
\begin{aligned}
[\mathbf{Z}_{xx}] &= -h^{-1}[\varepsilon_{re}^{I}]^{-1}[\mathbf{Q}_e^{I}][\mathbf{P}]^{-1} \\
[\mathbf{Z}_{xz}] &= \sqrt{\varepsilon_{eff}}[\varepsilon_{re}^{I}]^{-1}[\mathbf{Q}_e^{I}][\mathbf{P}]^{-1}[\mathbf{S}][\mathbf{Q}_h^{II}]^{-1} \\
[\mathbf{Z}_{zx}] &= h^{-1}\sqrt{\varepsilon_{eff}}[\mathbf{W}] \\
[\mathbf{Z}_{zz}] &= \left\{h^2[\mathbf{G}_h^{I}][\Delta]^{-1} + \varepsilon_{eff}[\mathbf{W}][\mathbf{S}]\right\}[\mathbf{Q}_h^{II}]^{-1}
\end{aligned}
\tag{3.30}
$$

with

$$
\begin{aligned}
[\mathbf{W}] &= \left([\varepsilon_{re}^{I}]^{-1}[\mathbf{D}_e] - [\mathbf{G}_h^{I}][\Delta]^{-1}[\Omega]\right)[\mathbf{P}]^{-1} \\
[\mathbf{S}] &= [\mathbf{D}_h]\left\{[\mathbf{I}] + ([\mathbf{I}] - [\Theta_h])[\Delta]^{-1}\right\} \\
[\mathbf{P}] &= h^{-2}\varepsilon_{eff}[\mathbf{D}_h]([\mathbf{I}] - [\Theta_h])[\Delta]^{-1}[\Omega] + [\mathbf{G}_e^{I}] - [\mathbf{G}_e^{II}][\Theta_e] \\
[\Delta] &= [\Theta_h] - [\mathbf{G}_h^{II}]^{-1}[\mathbf{G}_h^{I}]
\end{aligned}
\tag{3.31}
$$

and

$$
\begin{aligned}
[\Omega] &= [\mathbf{G}_h^{II}]^{-1}\left\{[\mathbf{D}_e][\Theta_e] - [\varepsilon_{rh}]^{-1}[\mathbf{D}_e]\right\} \\
[\Theta_e] &= [\mathbf{Q}_e^{II}]^{-1}[\varepsilon_{re}^{I}]^{-1}[\mathbf{Q}_e^{I}] \\
[\Theta_h] &= [\mathbf{Q}_h^{II}]^{-1}[\mathbf{Q}_h^{I}]
\end{aligned}
\tag{3.32}
$$

where the superscript I and II represent the values in layer I and layer II as indicated in Fig.3.2d.

Since the electric currents J_x and J_z are nonzero only at the surface of the metallic strip, where E_x and E_z must be zero, one can obtain the following reduced homogeneous equations from (3.29):

$$
\begin{aligned}
[\mathbf{E}_x]_{strip} &= j\eta_o h^{-1}[\mathbf{Z}_{xx}^{11}][\mathbf{J}_x]_{strip} + \eta_o h^{-1}[\mathbf{Z}_{xz}^{11}][\mathbf{J}_z]_{strip} = [0] \\
[\mathbf{E}_z]_{strip} &= \eta_o[\mathbf{Z}_{zx}^{11}][\mathbf{J}_x]_{strip} + j\eta_o[\mathbf{Z}_{zz}^{11}][\mathbf{J}_z]_{strip} = [0]
\end{aligned}
\tag{3.33}
$$

The Equations of (3.33) must have nontrivial solutions, since the electric currents on the strips can not be all zero. Thus, the effective dielectric constant $\varepsilon_{eff} = k_z^2/k_o^2$ can be obtained through an iterating procedure from the determinant of the coefficient matrix of (3.33), i.e.

$$
\det\left\{[\mathbf{Z}_{zz}^{11}] + [\mathbf{Z}_{zx}^{11}][\mathbf{Z}_{xx}^{11}]^{-1}[\mathbf{Z}_{xz}^{11}]\right\} = 0 \tag{3.34}
$$

Once the effective dielectric constant $\varepsilon_{eff} = k_z^2/k_o^2$ is obtained, all the electric field components and other characteristics of the transmission lines, such as the characteristic impedance of the line, can be obtained via a computation of the transmission power[29][30].

3.3 Convergence of the Method

The convergence of the method is examined by the analysis of a single microstrip line with a finite width dielectric substrate, as shown in Fig.3.3. In Fig.3.3a, the convergence curves for the effective dielectric constants are provided as a function of N (the number of lines in half space), for different values of M (the number of lines in half of the dielectric substrate). The structure is a conducting strip with constant conducting and dielectric substrate widths. It shows that the method convergences by increasing N. But, the rate of convergence depends on the value of M. When M is small, the results converge slowly and the final values depend on the value of M (For instance, the final value for $M = 8$ and 24 are different by about 2%). This indicates that the selected value of M must be large enough to insure the solution accuracy. In addition, for adequately large values of M, the convergence with N becomes very rapid. For example, for $M \geq 16$, the numerical results for the effective dielectric constant vary only within a range of approximately 0.1% , when $N \geq 40$. This is due to the fact that the field lines are concentrated in the dielectric region and therefore, more attention must be paid to their accurate computation.

The dependence of the convergence on M could be seen more clearly in Fig.3.3b where another set of curves are plotted to show the convergence of the effective dielectric constant versus M. It shows that when M is adequately large($M \geq 20$ in this example) the results become almost independent of M. For structures with wider dielectric substrates as shown in Fig.3.3c and Fig.3.3d, field lines are spread in the dielectric region and therefore larger M values are needed to obtain a convergent result. Otherwise, these results show similar convergence properties as before. In this case, the numerical results for the effective dielectric constant vary only within a range of approximately 0.1% when $N \geq 50$ and $M \geq 20$ (Fig.3.3c). Again for $M \geq 30$ in Fig.3.3d, they remain almost independent of M, but values of N are larger than those in Fig.3.3b.

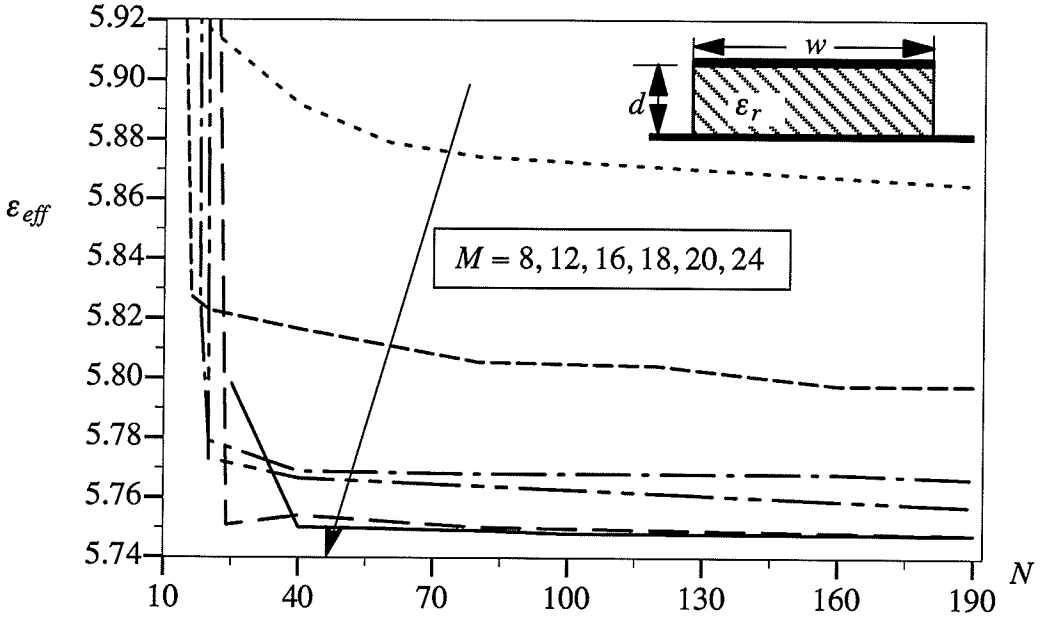

(a) convergence with respect to N

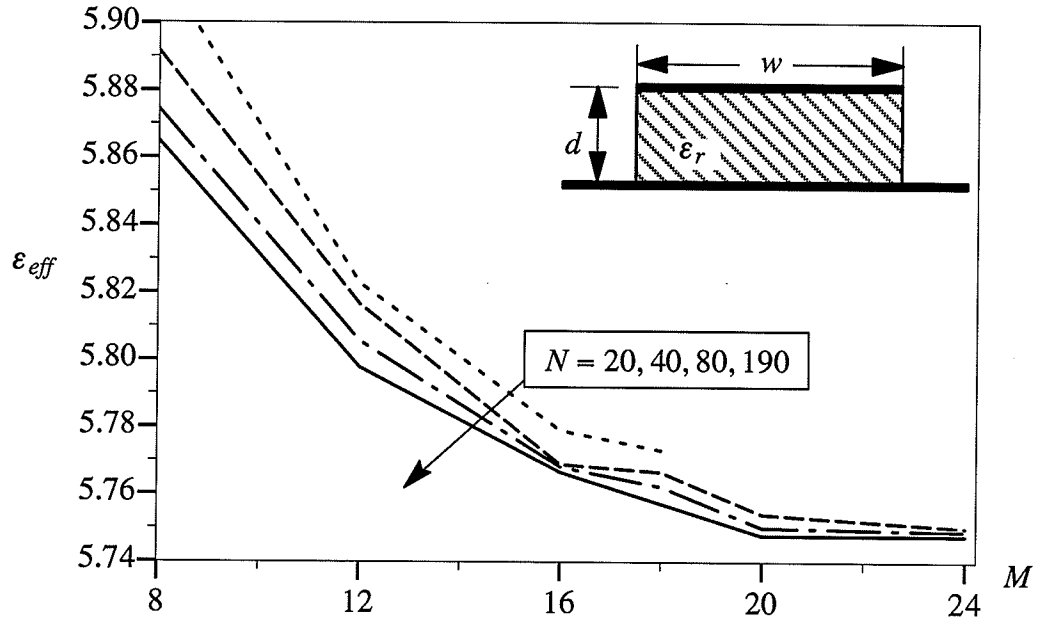

(b) convergence with respect to M

Fig.3.3. Testing for the convergence of the method. (N -- number of lines in half space, M -- number of lines in half of dielectric substrate) ($\varepsilon_r = 9.7$, $d/\lambda_o = 0.1$, $w/d = 1.0$)

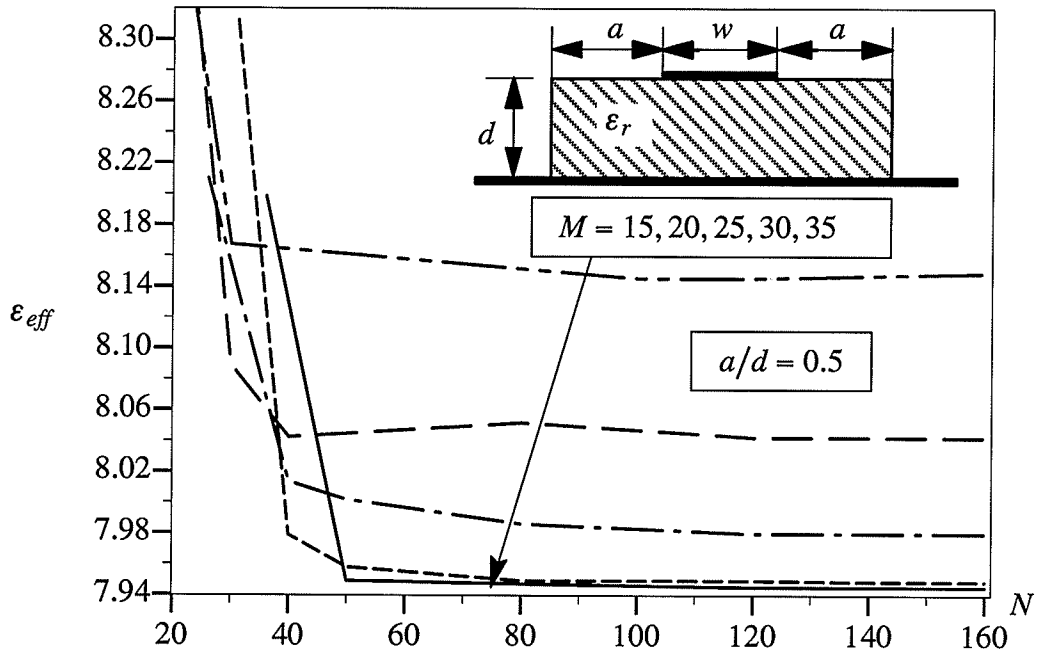

(c) convergence with respect to N

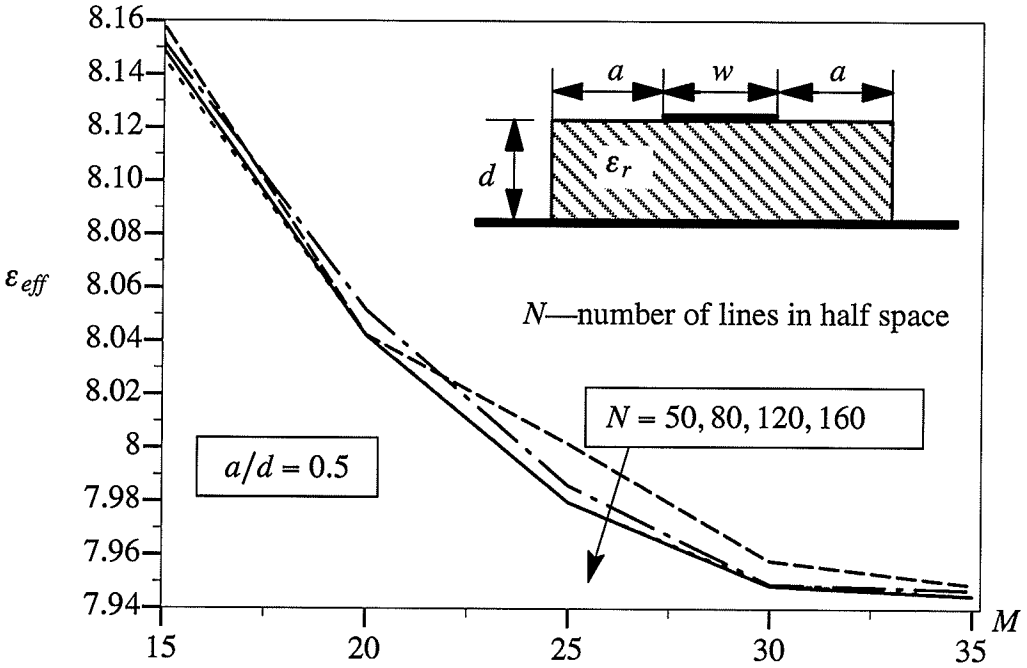

(d) convergence with respect to M

Fig.3.3 (continued)

All numerical experiments made above are for the case of $\varepsilon_r = 9.7$. For other dielectric substrates, the rate of convergence depends on their dielectric constant. When the relative dielectric constant becomes smaller, the rate of convergence also decreases. Because in this case, the fringing field is not as concentrated as the higher dielectric constant case.

3.4 Numerical Results of Single and Coupled Microstrip Lines

The method presented above can be used to analyze open planar structures with continuous or discontinuous dielectric layers and/or with a finite ground plane width. As an example, an open microstrip line with an infinitely wide dielectric and ground plane is analyzed and compared with results of spectral domain full wave methods[36] in Fig.3.4. Their good agreement indicates the validity of this technique.

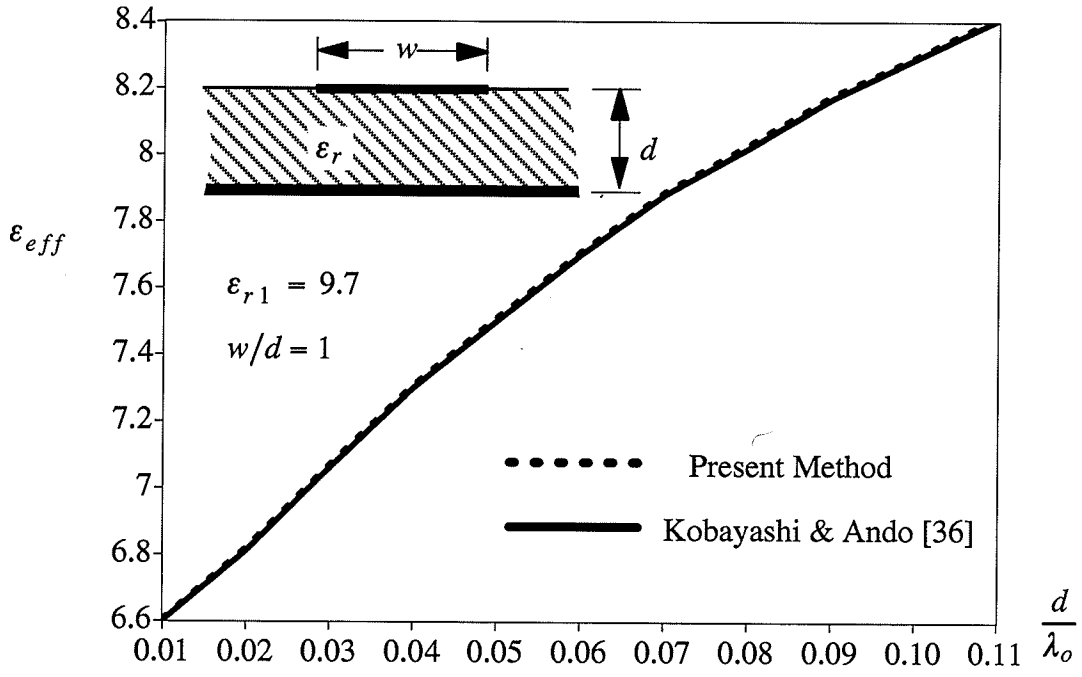

Fig.3.4. Results for an open microstrip line with infinitely width dielectric

The technique is then applied to analyze the open single and coupled microstrip lines of finite width dielectric substrate. Since similar full wave analysis results for open planar waveguides of finite dielectric substrates are not available, the results obtained here can only be compared with available quasi–static results[26] and with the full wave results of the structures with infinitely wide dielectric substrates. In Fig.3.5, the dispersions of the effective dielectric constant calculated by the present method are compared with the quasi–static results[26]. The latter method gives results independent of frequency. As it is expected, the difference between the full wave and the quasi–static results is small when the operating frequency is small. As the frequency increases, their difference increases rapidly and the quasi–static solutions can no longer be used to obtain meaningful results. This figure also shows that, the difference between the quasi–static and full wave results is dependent on the size of the dielectric substrate. For small substrate widths, their difference is small, especially at low frequencies where the quasi–static results approach the full wave ones. However, this is no longer true for wider dielectric substrates where differences also exist at low frequencies.

In Fig.3.6, the effects of finite dielectric substrate widths on the dispersion characteristics of open microstrip lines are considered where the effective dielectric constant versus the ratio a/d are shown for different values of d/λ_o . It shows that by increasing the dielectric width, the effective dielectric constant also increases and approaches its upper bound value for a structure with an infinite dielectric substrate. It is interesting to note that, although the results are dependent strongly on d/λ_o , their rate of change with a/d is almost independent of d/λ_o . They increase rapidly for $a/d < 0.4$, but their rate of change decreases thereafter. There is a definite turning point around $a/d = 0.4$, which shows that most of the fringing fields are concentrated within the region of $a/d < 0.4$. It is evident that the size of this region is dependent almost entirely on a/d.

Fig.3.7 Shows the dispersion characteristics of the above geometry for different dimensions of the structure. Again, the results increase monotonically with frequency, or, by increasing the substrate thickness.

In Fig.3.8, the dispersion characteristics of the odd and even modes for a few selected line dimensions of the open coupled microstrip lines with finite width dielectric substrate are shown. In this case, the static results for structures with a finite dielectric substrate are not available in the literature. The results obtained by this technique are then compared with the full wave results of structures with an infinitely wide dielectric substrate[37] and show differences between them. This means that the characteristics of infinitely wide dielectric substrates can not be used, in some cases, for accurate design of lines with finite dielectrics.

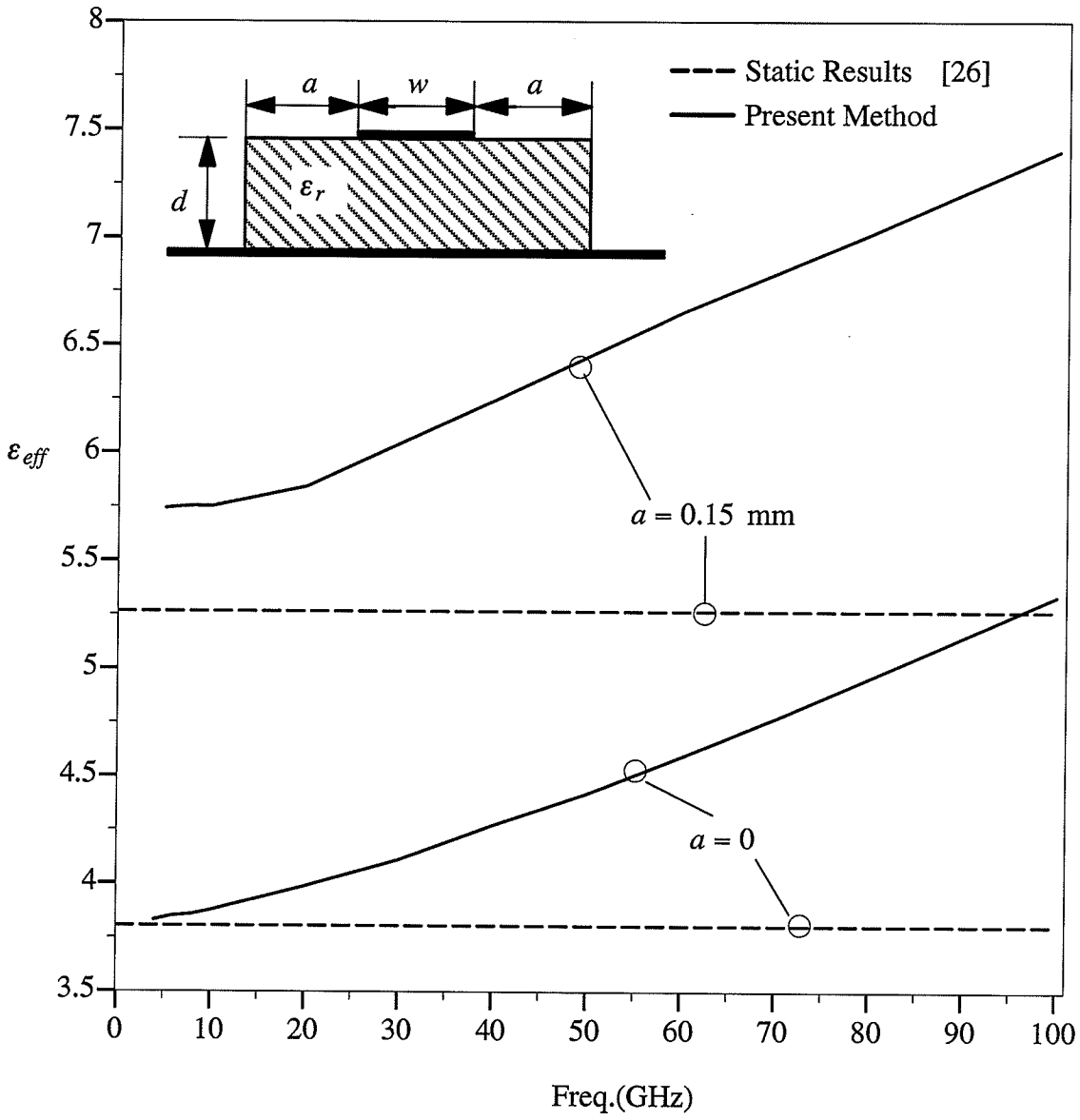

Fig.3.5. Comparison between the quasi–static and full wave results.
($\varepsilon_r = 9.0$, $d = 0.3$ mm , $w = 0.3$ mm)

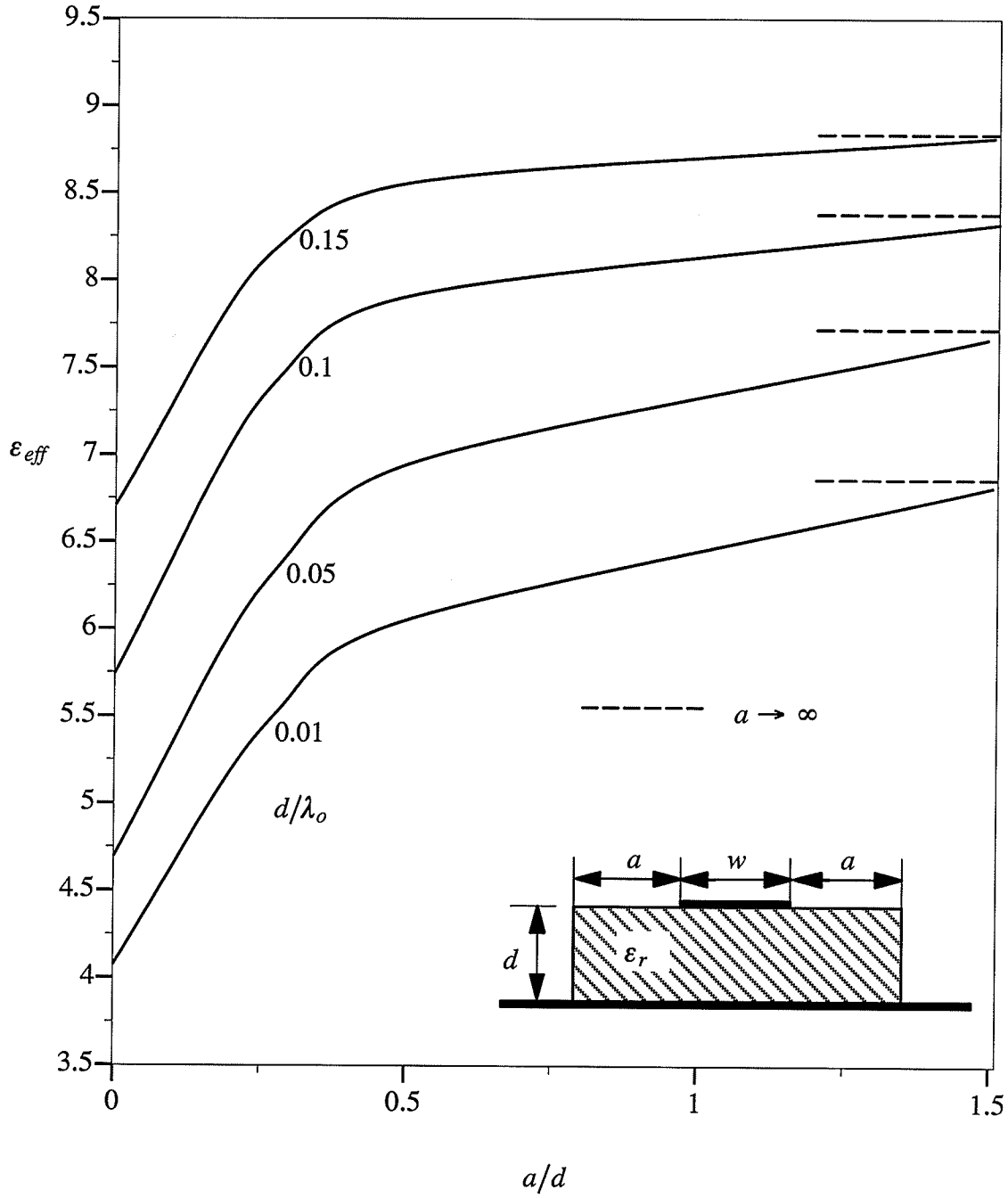

Fig.3.6. Effects of the dielectric width on the characteristics of microstrip lines. ($\varepsilon_r = 9.7$, $w/d = 1.0$)

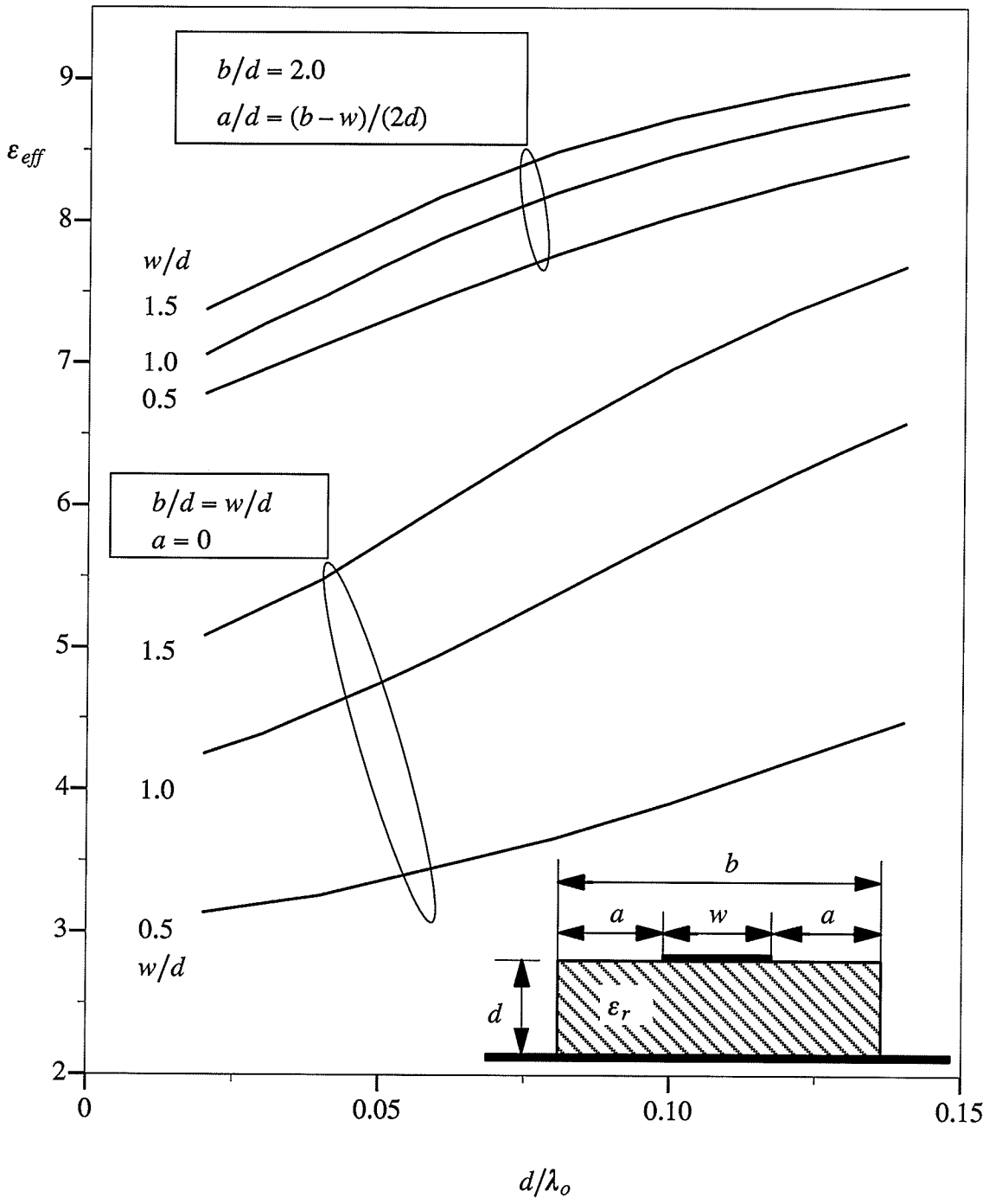

Fig.3.7. Dispersions of microstrip line of different dielectric widths($\varepsilon_r = 9.7$).

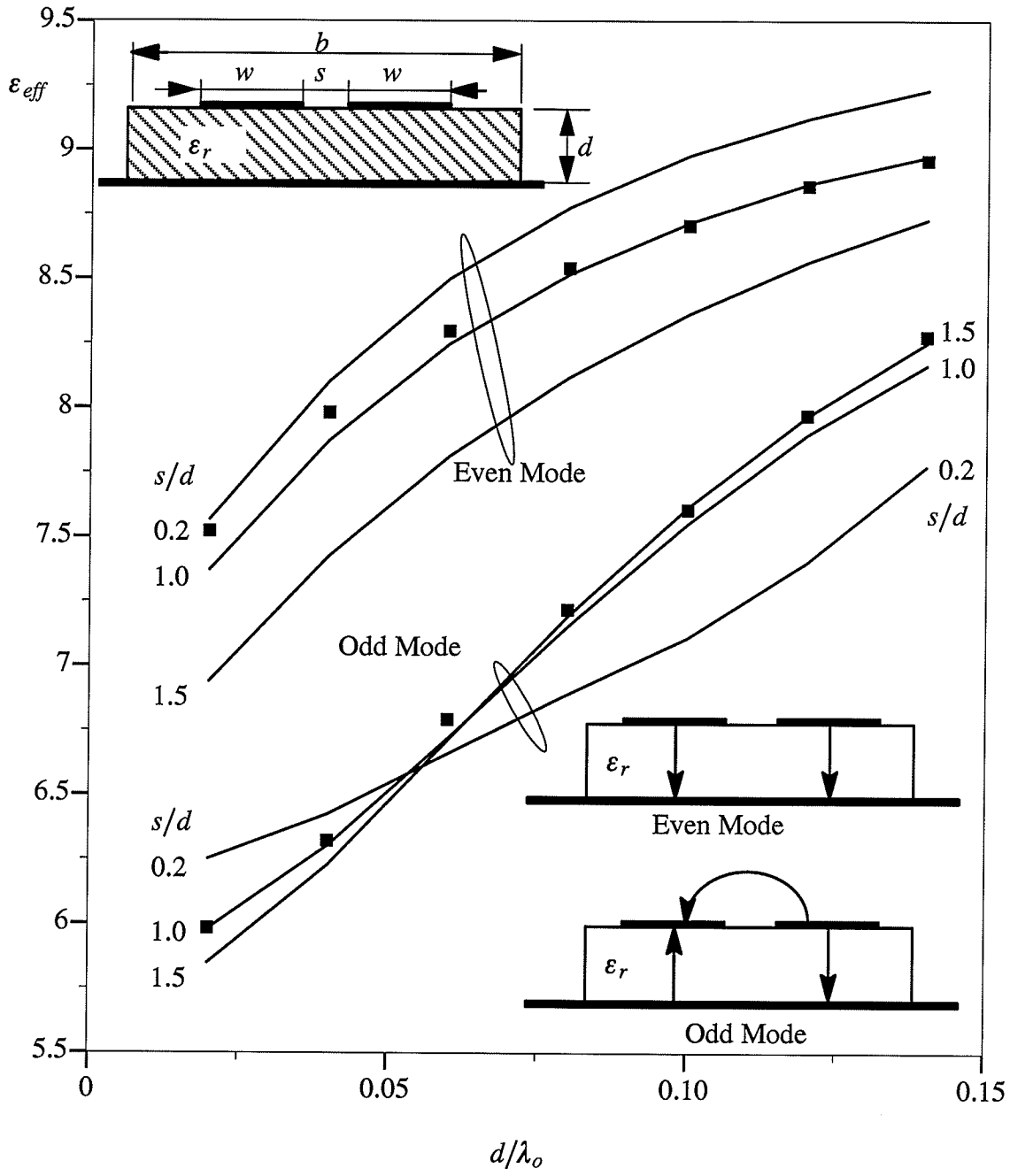

■ Results of [37] for infinitely wide dielectric with $s/d = 1.0$

——— Results for finite dielectric

$\varepsilon_r = 9.7, \quad w/d = 1.0, \quad b/d = 4.0$.

Fig.3.8. Dispersions of open coupled microstrip lines of finite dielectric widths.

3.5 Conclusions

Based on an extended method of lines, a unified full wave approach for the analysis of open planar or quasi planar waveguides was presented. It is general and can be applied to structures with continuous or discontinuous dielectric layers. However, its advantages are more obvious when it is used in the latter case, where a full wave approach is not available yet. The convergence of the method was examined by analyzing open microstrip lines of finite dielectric substrate widths. As application examples, both open single and coupled microstrip lines with various substrate widths were analyzed and their dispersion characteristics were provided. The results were compared with available full wave and quasi–static results. The effects of the dielectric width and thickness on the characteristics of structures were also discussed.

Chapter 4 A NETWORK APPROACH FOR THE EVALUATION OF SPECTRAL DOMAIN GREEN'S FUNCTIONS

As it was pointed out, one important step in the spectral domain moment method is to evaluate the spectral domain Green's functions. The most direct way to do so is to expand electromagnetic wave modes in each dielectric layer, and then match the boundary conditions at each interface[38][39]. For a single layer dielectric, this is not very complicated. However, for multi–layer dielectric structures, this leads to a very lengthy derivation process. There have been some efforts towards the simplification of this process. In [40], an immitance approach is proposed to derive spectral domain Green's functions for planar electric currents in printed transmission lines of two dimensional problems. In [41], a set of formulations are derived to evaluate Green's functions by an iteration process. In [42], a dyadic spectral domain Green's function for single layer grounded dielectrics was derived for electric currents and a corresponding network displayed for this structure. However, the Green's function was still derived from the Maxwell's equations and boundary conditions.

In this chapter, a network approach is developed to evaluate spectral domain Green's functions for arbitrarily directed electric or magnetic currents in multilayer dielectrics. Each dielectric layer is substituted with a two port network while the multilayer structure is replaced by a ladder connection of those two port networks for individual layers. The arbitrary directed electric or magnetic currents are decomposed into horizontal and vertical components with respect to dielectric interfaces, and the horizontal components are further divided into two orthogonal components. Each current component is replaced by an electric current or voltage generator in the network. The spectral domain Green's functions are

equivalent to network parameters. Therefore, the complicated procedure to evaluate the spectral domain Green's function for a multilayer dielectric structure can be obtained in a simple and systematic way. The approach is presented in detail in the following section and applied to an example to compare with results obtained by the field matching approach.

4.1 Decomposition of Modes in the Spectral Domain

The hybrid modes in a dielectric layer can be expressed by vector electric and magnetic potential functions in the spectral domain as

$$\tilde{E}_x = \frac{k_x}{\omega\varepsilon_o\varepsilon_r}\frac{\partial\tilde{A}_z}{\partial z} - jk_y\tilde{F}_z \qquad \tilde{H}_x = \frac{k_x}{\omega\mu_o\mu_r}\frac{\partial\tilde{F}_z}{\partial z} + jk_y\tilde{A}_z$$

$$\tilde{E}_y = \frac{k_y}{\omega\varepsilon_o\varepsilon_r}\frac{\partial\tilde{A}_z}{\partial z} + jk_x\tilde{F}_z \qquad \tilde{H}_y = \frac{k_y}{\omega\mu_o\mu_r}\frac{\partial\tilde{F}_z}{\partial z} - jk_x\tilde{A}_z \tag{4.1}$$

$$\tilde{E}_z = \frac{1}{j\omega\varepsilon_o\varepsilon_r}\left(\frac{\partial^2}{\partial z^2} + k_o^2\varepsilon_r\mu_r\right)\tilde{A}_z \qquad \tilde{H}_z = \frac{1}{j\omega\mu_o\mu_r}\left(\frac{\partial^2}{\partial z^2} + k_o^2\varepsilon_r\mu_r\right)\tilde{F}_z$$

Consider the definition of inverse Fourier Transform

$$Q(x,y,z) = \frac{1}{4\pi^2}\int\int_{-\infty}^{\infty}\tilde{Q}(k_x,k_y,z)\,e^{jk_x x}\,e^{jk_y y}\,dk_x dk_y \tag{4.2}$$

Eq.(4.2) shows that the propagating electromagnetic waves in the space domain is a super-position of inhomogeneous waves in the spectral domain. Each plane wave propagates in the direction given by the angle $\phi = \pi + \cos^{-1}\left(k_x/\sqrt{k_x^2+k_y^2}\right)$ measured from the x axis.

Therefore, one may define a new coordinate system (u, v, z) from the original coordinate system (x,y,z) by using the following coordinate transformation as shown in Fig.4.1.

$$\begin{cases} u = x\cos\phi + y\sin\phi \\ v = -x\sin\phi + y\cos\phi \end{cases} \tag{4.3}$$

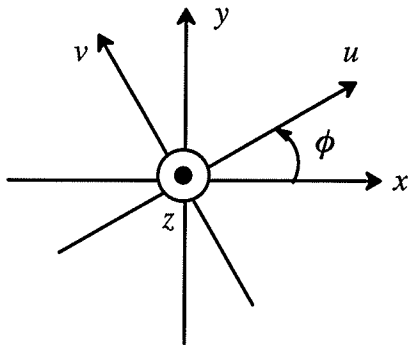

$$\phi = \pi + \cos^{-1}\left(k_x/\sqrt{k_x^2+k_y^2}\right)$$

$$\sin\phi = -\frac{k_y}{\beta} \qquad \cos\phi = -\frac{k_x}{\beta}$$

$$\beta = \sqrt{k_x^2+k_y^2}$$

Fig.4.1. Transformation between two coordinate systems

Then, the spectral domain electromagnetic field in the system (x,y,z) given in (4.1) can be transformed into the new coordinate system (u,v,z) by relation (4.3), which is decomposed into two orthogonal modes, *TM* to z and *TE* to z, as follows(Fig.4.2)

TM_z :

$$\tilde{E}_u = -\frac{\beta}{\omega\varepsilon_o\varepsilon_r}\frac{\partial\tilde{A}_z}{\partial z}$$

$$\tilde{H}_v = j\beta\tilde{A}_z \tag{4.4}$$

$$\tilde{E}_z = \frac{1}{j\omega\varepsilon_o\varepsilon_r}\left(\frac{\partial^2}{\partial z^2} + k_o^2\varepsilon_r\mu_r\right)\tilde{A}_z$$

$$\tilde{E}_v = -j\beta\tilde{F}_z$$

$$TE_z: \qquad \tilde{H}_u = -\frac{\beta}{\omega\mu_o\mu_r}\frac{\partial\tilde{F}_z}{\partial z} \tag{4.5}$$

$$\tilde{H}_z = \frac{1}{j\omega\mu_o\mu_r}\left(\frac{\partial^2}{\partial z^2} + k_o^2\varepsilon_r\mu_r\right)\tilde{F}_z$$

By considering relations $\frac{\partial^2\tilde{A}_z}{\partial z^2} = -k_z^2\tilde{A}_z$ and $k_z^2 = k_o^2\varepsilon_r\mu_r - \beta^2$, (4.4) and (4.5) become

$$TM_z: \quad \tilde{E}_u = -\frac{\beta}{\omega\varepsilon_o\varepsilon_r}\frac{\partial\tilde{A}_z}{\partial z}, \qquad \tilde{H}_v = j\beta\tilde{A}_z, \qquad \tilde{E}_z = \frac{\beta^2}{j\omega\varepsilon_o\varepsilon_r}\tilde{A}_z \tag{4.6}$$

$$TE_z: \quad -\tilde{E}_v = j\beta\tilde{F}_z, \qquad \tilde{H}_u = -\frac{\beta}{\omega\mu_o\mu_r}\frac{\partial\tilde{F}_z}{\partial z}, \qquad \tilde{H}_z = \frac{\beta^2}{j\omega\mu_o\mu_r}\tilde{F}_z \tag{4.7}$$

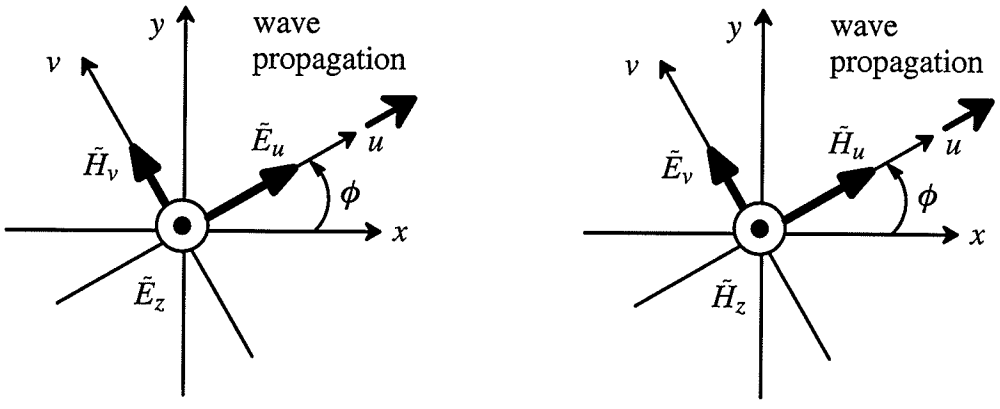

(a) *TM* to *z* (b) *TE* to *z*

Fig.4.2. Orthogonal modes in a new coordinate system

4.2 Equivalent Transmission Lines for Dielectric Layers

4.2.1 Equivalent transmission line for a single dielectric layer

It is very easy to find from (4.6) and (4.7) that electromagnetic field components of each mode satisfy the transmission line equation in a source free region, i.e.,

$$TM_z: \quad \frac{\partial}{\partial z}\tilde{E}_u = -j\frac{k_z^2}{\omega\varepsilon_o\varepsilon_r}H_v \quad , \qquad \frac{\partial}{\partial z}\tilde{H}_v = -j\omega\varepsilon_o\varepsilon_r E_u \tag{4.8}$$

$$TE_z: \quad \frac{\partial}{\partial z}\left(-\tilde{E}_v\right) = -j\omega\mu_o\mu_r\tilde{H}_u \quad , \qquad \frac{\partial}{\partial z}\tilde{H}_u = -j\frac{k_z^2}{\omega\mu_o\mu_r}\left(-\tilde{E}_v\right) \tag{4.9}$$

which means that the $\tilde{E}_{u(v)}$ transverse electric field and the $\tilde{H}_{u(v)}$ magnetic field are equivalent to the voltage and current in the equivalent transmission lines as shown in Fig.4.3,

$$\begin{aligned} &\tilde{E}_u \leftrightarrow V_e \quad , \qquad \tilde{H}_v \leftrightarrow I_e \quad ; \\ &-\tilde{E}_v \leftrightarrow V_h \quad , \qquad \tilde{H}_u \leftrightarrow I_h \quad . \end{aligned} \tag{4.10}$$

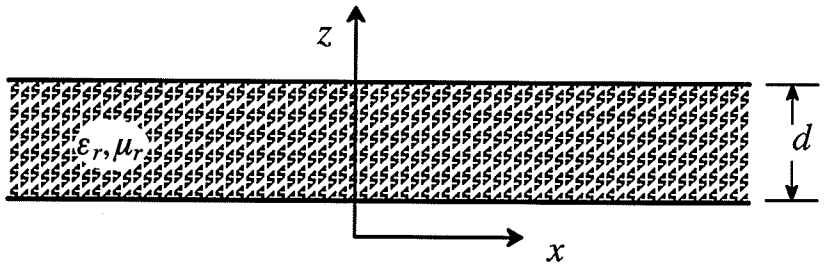

(a) dielectric layer

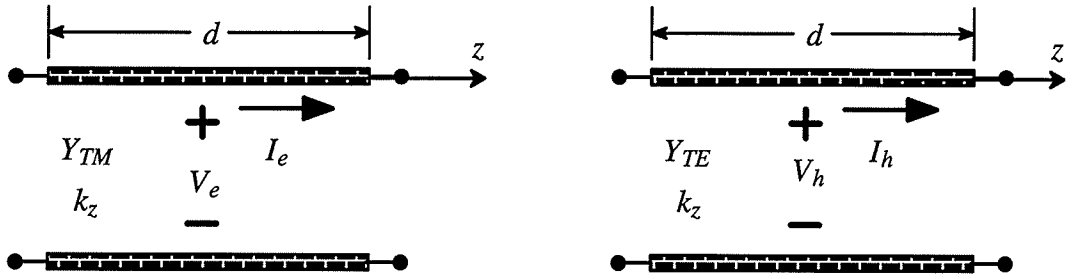

(b) *TM* to z mode

(c) *TE* to z mode

Fig.4.3. Equivalent transmission lines for a single dielectric layer

The propagation constant for these two equivalent transmission lines is $k_z = \sqrt{k_o^2 \varepsilon_r \mu_r - \beta^2}$ while their characteristic admittances are different

$$Y_{TM} = \frac{I_e^+}{V_e^+} = \frac{\tilde{H}_v}{\tilde{E}_u} = \frac{\omega \varepsilon_o \varepsilon_r}{k_z}$$

$$Y_{TE} = \frac{I_h^+}{V_h^+} = \frac{\tilde{H}_u}{-\tilde{E}_v} = \frac{k_z}{\omega \mu_o \mu_r} \tag{4.11}$$

where $\frac{\partial}{\partial z}\tilde{A}_z = -jk_z\tilde{A}_z$, and $\frac{\partial}{\partial z}\tilde{F}_z = -jk_z\tilde{F}_z$ are assumed because only one direction for the propagating wave should be considered to evaluate the characteristic admittance.

Fig.4.3 also shows that the two modes in a dielectric layer can be replaced by a single equivalent transmission line with different parameters.

According to the equivalence between the field and circuit parameters, a short circuit(Fig.4.4) can be used to model a perfect conductor terminated dielectric layer, and a dielectric extending to infinity can be modelled by a matched impedance load.(Fig.4.5).

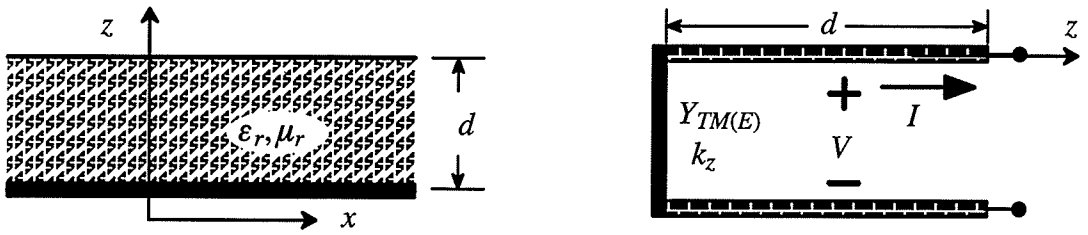

(a) dielectric layer (b) short circuit equivalence

Fig.4.4. Equivalent circuits for a dielectric terminated by a conductor

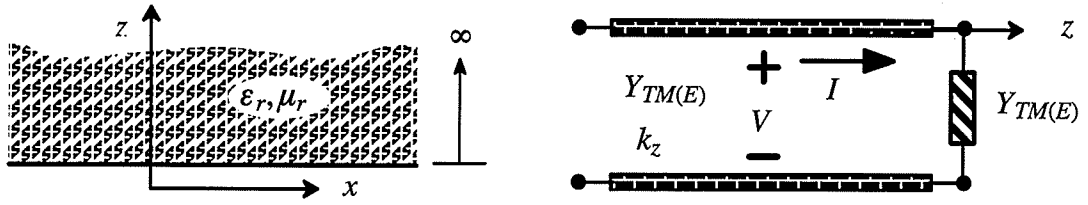

(a) dielectric layer (b) matched load equivalence

Fig.4.5. Equivalent circuits for a dielectric extending to infinity

4.2.2 Equivalent network for multilayer dielectrics

In multilayer dielectric systems, each layer can be modelled by two equivalent transmission lines with their own parameters for two different modes, while the whole system can be modelled by two different cascaded ladder transmission lines for two modes as shown in Fig.4.6b. Then the *ABCD* matrix for the whole network can be easily obtained by simply multiplying that of each section

$$\begin{bmatrix} A & B \\ C & D \end{bmatrix}_{TM(E)} = \prod_{i=1}^{N} \begin{bmatrix} \cos(k_{z\,i}\, d_i) & j \sin(k_{z\,i}\, d_i) / Y_{TM(E)1} \\ j Y_{TM(E)1} \sin(k_{z\,i}\, d_i) & \cos(k_{z\,i}\, d_i) \end{bmatrix} \tag{4.12}$$

which is equivalent to a two port Π network as shown in Fig.4.6c (see equation (A.6)). If the top or the bottom layer is terminated or open to infinity, it is then simplified to a single one port network with one admittance.

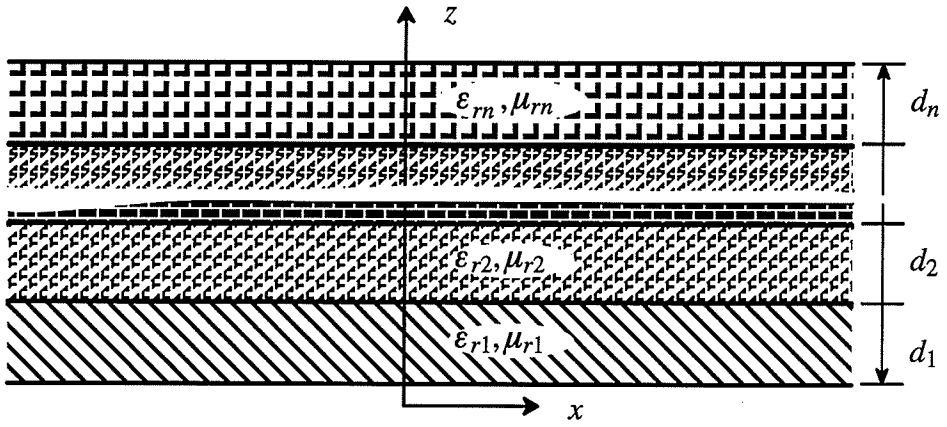

(a) multilayer dielectrics

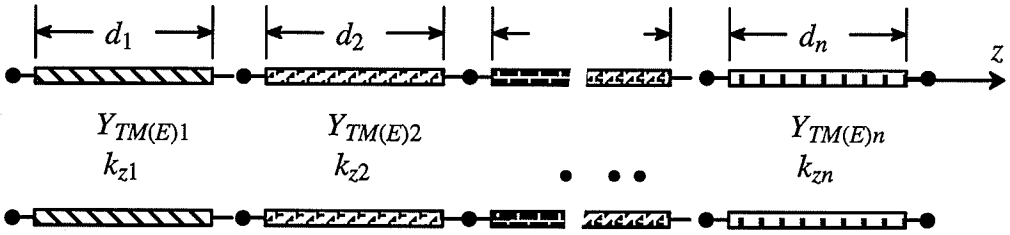

(b) equivalent ladder network

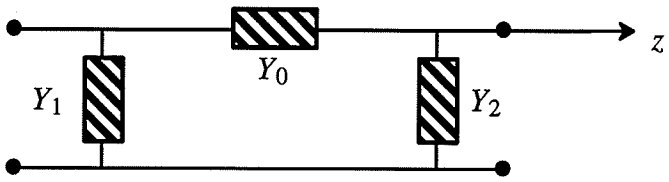

(c) equivalent Π network

Fig.4.6. Equivalent network for multilayer dielectrics.

4.3 Equivalent Networks for Sources

An arbitrary directed electric or magnetic current $\tilde{\mathbf{J}}/\tilde{\mathbf{M}}$ as shown in Fig.4.7 can be decomposed into two components in the transformed coordinate system (u, v, z), one is the horizontal component $\tilde{J}_h/\tilde{M}_h$ lying in the uov plane which can be further divided into two orthogonal components $\tilde{J}_u/\tilde{M}_u$ and $\tilde{J}_v/\tilde{M}_v$, the other is the vertical component $\tilde{J}_z/\tilde{M}_z$ in the z direction. Then the electromagnetic fields produced by this arbitrary directed electric/magnetic currents is the superposition of those fields produced by three components. Its Green's function can also be expressed in a dynamic form as

$$\begin{aligned}\tilde{\vec{\mathbf{G}}} = {} & \hat{\mathbf{u}}(\hat{\mathbf{u}}\tilde{G}_{uu} + \hat{\mathbf{v}}\tilde{G}_{vu} + \hat{\mathbf{z}}\tilde{G}_{zu}) + \hat{\mathbf{v}}(\hat{\mathbf{u}}\tilde{G}_{uv} + \hat{\mathbf{v}}\tilde{G}_{vv} + \hat{\mathbf{z}}\tilde{G}_{zv}) \\ & + \hat{\mathbf{z}}(\hat{\mathbf{u}}\tilde{G}_{uz} + \hat{\mathbf{v}}\tilde{G}_{vz} + \hat{\mathbf{z}}\tilde{G}_{zz})\end{aligned} \tag{4.13}$$

So the dyadic Green's function can be obtained by evaluating each scalar one.

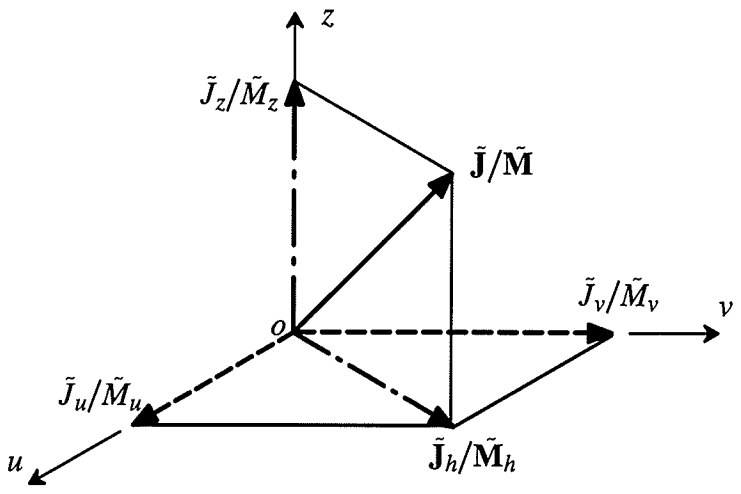

Fig.4.7. Decomposition of an arbitrary directed electric/magnetic current

4.3.1 Horizontal components

Eqs.(4.6) and (4.7) imply that a u directed electric current will only excite a TM to z mode, and a v directed electric current will produce only a TE to z mode. While for the magnetic current, a u directed component will only excite a TE to z mode and a v directed component will produce only a TM to z mode. Therefore, the equivalent circuits of horizontal current components shown in Fig.4.8a can be derived by using the boundary conditions at the interface and the equivalent network as shown in Fig.4.8b.

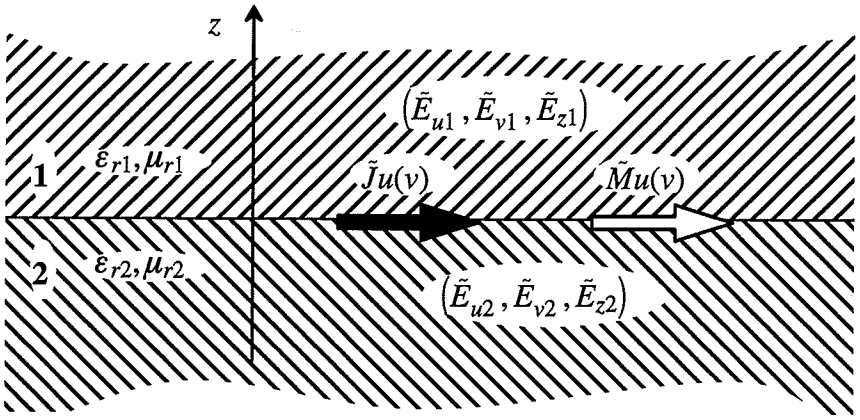

(a) horizontal electric/magnetic current components

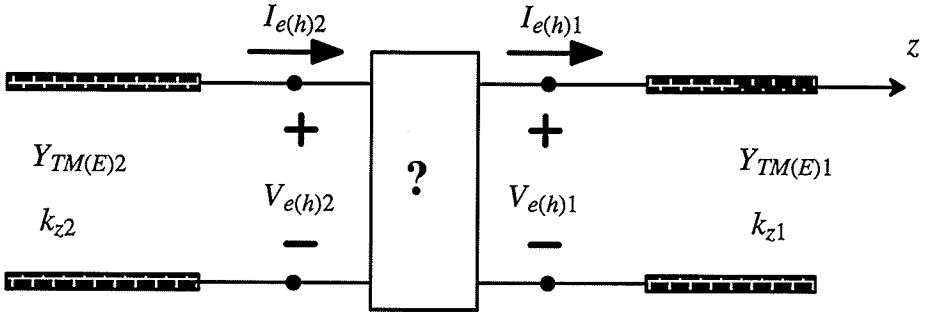

(b) equivalent network for current

Fig.4.8. Network modelling of horizontal current components

Take the electric cuurent component $\tilde{J}_u$ as an example, which will produce a TM_z mode. The following relation can be derived from the boundary condition at the interface as in Fig.4.8

$$\tilde{H}_{v1} - \tilde{H}_{v2} = -\tilde{J}_u \tag{4.14}$$

Replacing field components with their equivalent circuit parameters given in (4.10) yields

$$I_{e1} - I_{e2} = -\tilde{J}_u \tag{4.15}$$

which means that the u directed current component at the interface is equivalent to an electric current generator in the equivalent network.

Similarly, the electric cuurent component $\tilde{J}_v$ can also be modelled by an electric current generator in the TE_z equivalent network. And equivalent magnetic current components $\tilde{M}_u$, $\tilde{M}_v$ can be modelled by electric voltage generator. The equivalent electric current or voltage generators for electric and equivalent magnetic current components are shown in Fig.4.9. The mathematical formulations are

$$\begin{aligned} I_{ge} &= -\tilde{J}_u \quad , \qquad I_{gh} = \tilde{J}_v \quad ; \\ V_{ge} &= -\tilde{M}_v \quad , \qquad V_{gh} = -\tilde{M}_u \quad . \end{aligned} \tag{4.16}$$

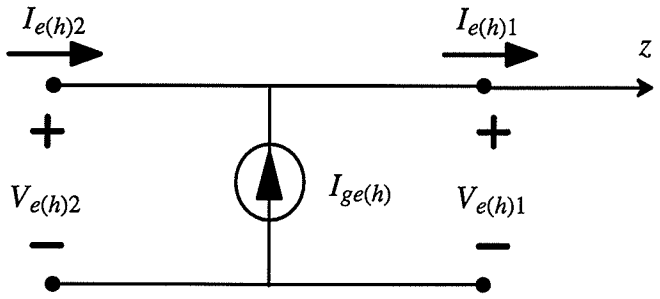

(a) equivalent electric current generator for horizontal electric currents

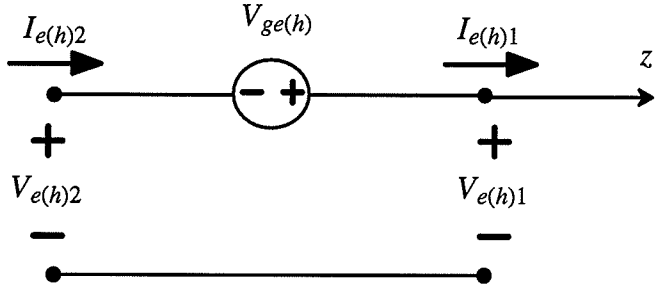

(b) equivalent electric voltage generator for horizontal magnetic currents

Fig.4.9. Equivalent sources for horizontal current components

4.3.2 Vertical components

The equivalent network for vertical current components in Fig.4.10a can also be obtained according to the equivalence between the electromagnetic field components and the network current and voltage. A vertical electric current will only excite a TM to z mode as

$$\frac{\partial^2 \tilde{A}_z}{\partial z^2} + k_z^2 \tilde{A}_z = -\tilde{J}_z \tag{4.17}$$

and $\tilde{J}_z = \delta(z - z_o)\exp(-jk_x x_o - jk_y y_o)$.

It is easy to obtain the following relations from (4.17) and (4.4)

$$\frac{\partial \tilde{E}_u}{\partial z} = -j\frac{k_z^2}{\omega\varepsilon_o\varepsilon_r}\tilde{H}_v + \frac{\beta}{\omega\varepsilon_o\varepsilon_r}\tilde{J}_z$$
$$\tilde{E}_u = -\frac{1}{j\omega\varepsilon_o\varepsilon_r}\frac{\partial \tilde{H}_v}{\partial z} \tag{4.18}$$

Considering the equivalence relation in (4.10), one has

$$-\frac{\partial V_e}{\partial z} = j\frac{k_z^2}{\omega\varepsilon_o\varepsilon_r}\tilde{I}_e - \frac{\beta}{\omega\varepsilon_o\varepsilon_r}\tilde{J}_z$$
$$-\frac{\partial I_e}{\partial z} = j\omega\varepsilon_o\varepsilon_r V_e \tag{4.19}$$

Eq.(4.19) is the governing equation for a transmission line with an electric voltage generator. Therefore, a vertical electric current in the dielectric is equivalent to the voltage generator as shown in Fig.4.10b.

Similarly, a vertical magnetic current in the dielectric excites only TE to z mode, which results in the following governing equation for a transmission line with an electric current generator and is equivalent to the voltage generator as shown in Fig.4.10c.

$$-\frac{\partial V_h}{\partial z} = j\omega\mu_o\mu_r I_h$$
$$-\frac{\partial I_h}{\partial z} = j\frac{k_z^2}{\omega\mu_o\mu_r}\tilde{V}_h - \frac{\beta}{\omega\mu_o\mu_r}\tilde{M}_z \tag{4.20}$$

The equivalence relations between the voltage generator and the vertical electric current, and the electric current generator and the magnetic current are

$$V_{ge} = \frac{\beta}{\omega \varepsilon_o \varepsilon_r} \tilde{J}_z \quad , \qquad I_{gh} = \frac{\beta}{\omega \mu_o \mu_r} \tilde{M}_z \quad . \tag{4.21}$$

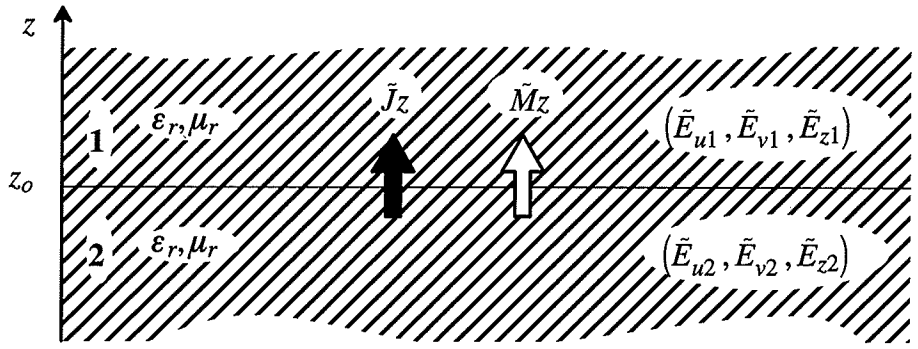

(a) a vertical electric/magnetic component

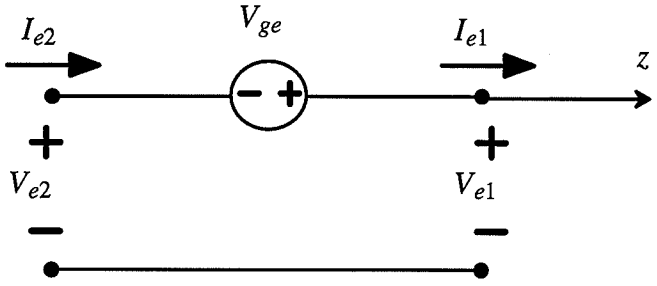

(b) equivalent electric voltage generator for a vertical electric current component

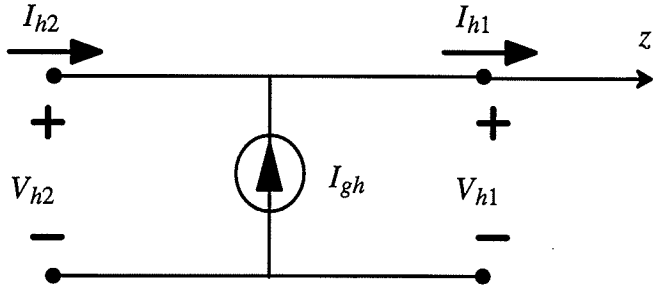

(c) equivalent electric current generator for a vertical magnetic current component

Fig.4.10. Equivalent sources for vertical current components

4.4 Network Approach Evaluation of Green's Functions

Now that the multilayer dielectrics are substituted with equivalent transmission lines and all electric and equivalent magnetic current components are replaced by the electric voltage and current generators, the spectral domain Green's functions can be evaluated by calculating the appropriate network parameters in the network.

In a practical multilayer dielectric structure, the electric or magnetic current sources may be placed at a layer interface or inside one single dielectric layer. Generally, there is no difference between these two situations, because in the second case, one may divide this single layer into two layers with the same dielectric parameters and a general formulation can also be obtained with the current position as a varying parameter.

The procedure to evaluate these network parameters is as follows. First, the cascaded network between the source point and field point is replaced by a two port Π network as discussed in section 4.2, and the circuit beyond source point and field point is then equivalent to a single admittance. The electric/magnetic current components are equivalent to electric current/voltage generator as discussed in section 4.3. The problem is equivalent to the network problem as shown in Fig.4.11a or Fig.4.11b, depending on the current types. Generally, it is easy to find the electric voltage and current at the field point. For the network of Fig.4.11a, one has

$$\begin{cases} V_1 = Y_s \, Z_1 \, V_s \\ I_1 = Y_s \, Y_T \, Z_1 \, V_s \end{cases} \tag{4.22}$$

which for the network of Fig.4.11b, they become

$$\begin{cases} V_1 = Z_1 \, I_s \\ I_1 = Y_T \, Z_1 \, I_s \end{cases} \tag{4.23}$$

where $Z_1 = Y_o / \left[(Y_1 + Y_s)(Y_o + Y_2 + Y_T) + Y_o (Y_2 + Y_T) \right]$.

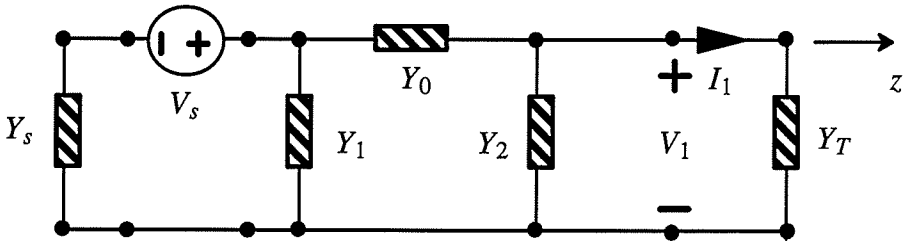

(a) Network with electric voltage generator

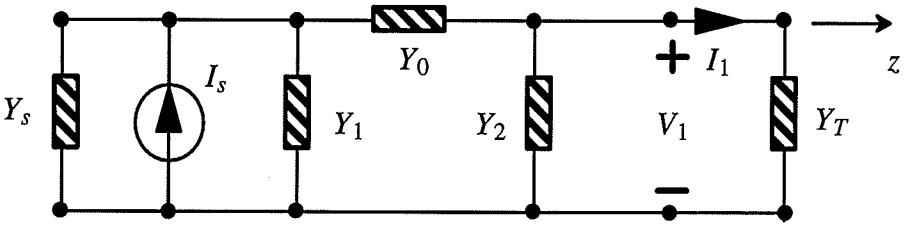

(b) Network with electric current generator

Fig.4.11. Network approach for the evaluation of Green's functions

As it is shown in eq.(4.10), the electric voltage (V_1) and current (I_1) at the field point are equivalent to the electric field ($\tilde{E}_u$, $\tilde{E}_v$) and magnetic fields ($\tilde{H}_u$, $\tilde{H}_v$), respectively, in the transformed coordinates (u, v, z). From (4.16) and (4.21), it is known that the electric current generator (I_s) and voltage generator (V_s) are equivalent to the electric current or magnetic current, respectively. Therefore, the spectral domain Green's functions in the transformed coordinates (u, v, z) can be obtained by eq.(4.22) or (4.23).

Finally, the Green's functions in the (x, y, z) coordinate system can be obtained from those in (u, v, z) coordinate system using the coordinate transformation (4.3), i.e.,

$$\begin{cases} \tilde{E}_x = \tilde{E}_u \cos\phi + \tilde{E}_v \sin\phi \\ \tilde{E}_y = -\tilde{E}_u \sin\phi + \tilde{E}_v \cos\phi \end{cases} \tag{4.24}$$

When a part or the entire network is resonating, the electric current or voltage in the network has singularities, which corresponds to the surface wave modes in a multilayer dielectric structure. It is easy to determine the condition of singularities from the equivalent network, which is another advantage of the network approach. The reason for these singularities is that there is no loss in the network. Therefore, singularities can be avoided by considering a lossy network, which is equivalent to lossy dielectrics in the real world.

4.5 An Example

A single layer grounded dielectric with both electric and magnetic currents is shown in Fig.4.12a. As shown in Fig.4.12b, the dielectric layer is replaced by its equivalent transmission line and the free space area is equivalent to an admittance, and all electric and magnetic current components are replaced by appropriate electric current and voltage generators. It should be noted that different parameters should be used for different modes, i.e.,

$$Y_{TM1} = \frac{\omega\varepsilon_o\varepsilon_r}{k_{z1}}, \quad Y_{TM2} = \frac{\omega\varepsilon_o}{k_{z2}}, \quad Y_{TE1} = \frac{k_{z1}}{\omega\mu_o}, \quad Y_{TE2} = \frac{k_{z2}}{\omega\mu_o}, \quad k_{z1} = \sqrt{k_o^2\varepsilon_r - \beta^2},$$

$$k_{z2} = \sqrt{k_o^2 - \beta^2}.$$

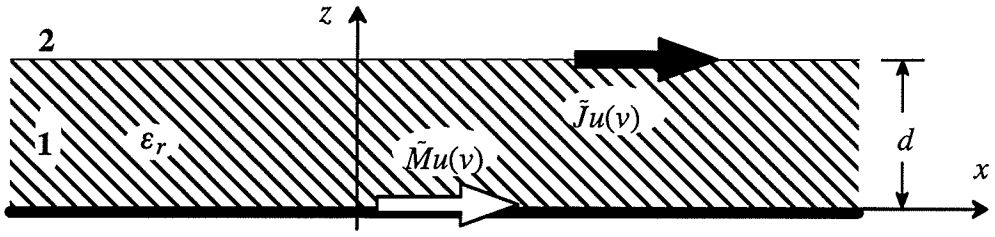

(a) electric or equivalent magnetic currents at dielectric interface

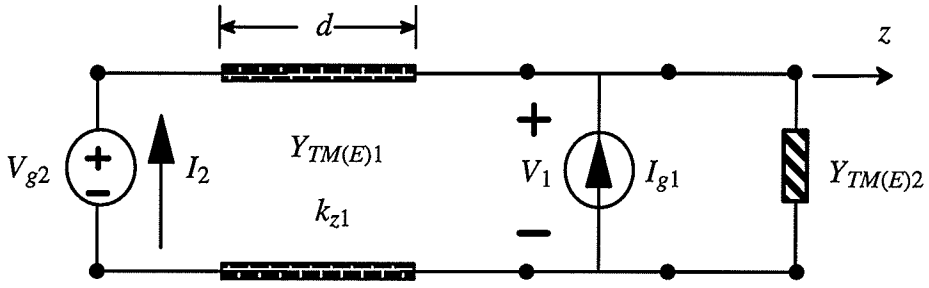

(b) equivalent transmission lines

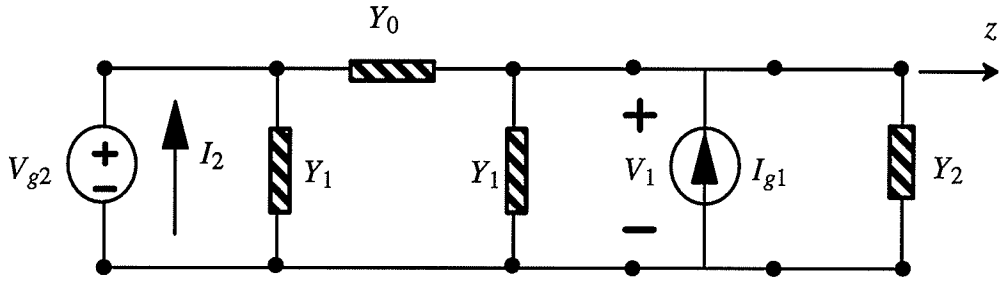

(b) equivalent network

Fig.4.12. A single layer grounded dielectric with electric and magnetic currents and its equivalent networks

The equivalent transmission lines is further replaced by the equivalent network shown in Fig.4.12c where the transmission line section of length d is replaced by a two port Π network. The $ABCD$ matrix of the transmission line section is

$$\begin{bmatrix} A & B \\ C & D \end{bmatrix}_{TM(E)1} = \begin{bmatrix} \cos(k_{z1}d) & j\sin(k_{z1}d)/Y_{TM(E)1} \\ jY_{TM(E)1}\sin(k_{z1}d) & \cos(k_{z1}d) \end{bmatrix} \tag{4.25}$$

and the parameters of this Π network are

$$\begin{aligned} Y_{0e(h)} &= -jY_{TM(E)1}\csc(k_{z1}d) \\ Y_{1e(h)} &= jY_{TM(E)1}\left[\csc(k_{z1}d) - \cot(k_{z1}d)\right] \end{aligned} \tag{4.26}$$

and $Y_{2e(h)} = Y_{TM(E)2}$.

Then, according to the network theory, one can establish the following relations

$$\begin{bmatrix} V_1 \\ I_2 \end{bmatrix} = \begin{bmatrix} K_{11} & K_{12} \\ K_{21} & K_{22} \end{bmatrix} \begin{bmatrix} I_{g1} \\ V_{g2} \end{bmatrix} \tag{4.27}$$

where

$$\begin{aligned} K_{11} &= \left.\frac{V_1}{I_{g1}}\right|_{V_{g2}=0} = \frac{1}{Y_0+Y_1+Y_2} \\ K_{12} &= \left.\frac{V_1}{V_{g2}}\right|_{I_{g1}=0} = \frac{Y_0}{Y_0+Y_1+Y_2} \\ K_{21} &= \left.\frac{I_2}{I_{g1}}\right|_{V_{g2}=0} = -\frac{Y_0}{Y_0+Y_1+Y_2} \\ K_{22} &= \left.\frac{I_2}{V_{g2}}\right|_{I_{g1}=0} = Y_1 + \frac{Y_0(Y_1+Y_2)}{Y_0+Y_1+Y_2} \end{aligned} \tag{4.28}$$

According to the equivalence in (4.16) and (4.10), $I_{ge1} = -\tilde{J}_{u1}$, $I_{gh1} = \tilde{J}_{v1}$, $V_{ge2} = -\tilde{M}_{v2}$, $V_{gh2} = -\tilde{M}_{u2}$, $V_{e1} = \tilde{E}_{u1}$, $V_{h1} = -\tilde{E}_{v1}$, $I_{e2} = \tilde{H}_{v2}$, $I_{h2} = \tilde{H}_{u2}$, and eq.(4.27) becomes

$$\begin{bmatrix} \tilde{E}_{u1} \\ \tilde{E}_{v1} \\ \tilde{H}_{u2} \\ \tilde{H}_{v2} \end{bmatrix} = \begin{bmatrix} -K_{e11} & 0 & 0 & -K_{e12} \\ 0 & -K_{h11} & K_{h12} & 0 \\ 0 & K_{h21} & -K_{h22} & 0 \\ -K_{e21} & 0 & 0 & -K_{e22} \end{bmatrix} \begin{bmatrix} \tilde{J}_{u1} \\ \tilde{J}_{v1} \\ \tilde{M}_{u2} \\ \tilde{M}_{v2} \end{bmatrix} \tag{4.29}$$

By considering the transformation (4.3), (4.29) becomes

$$[\mathbf{F}] = [\mathbf{T}]^{-1} [\mathbf{K}] [\mathbf{T}] [\mathbf{S}] \tag{4.30}$$

where

$$[\mathbf{K}] = \begin{bmatrix} -K_{e11} & 0 & 0 & -K_{e12} \\ 0 & -K_{h11} & K_{h12} & 0 \\ 0 & K_{h21} & -K_{h22} & 0 \\ -K_{e21} & 0 & 0 & -K_{e22} \end{bmatrix}, \quad [\mathbf{F}] = \begin{bmatrix} \tilde{E}_x \\ \tilde{E}_y \\ \tilde{H}_x \\ \tilde{H}_y \end{bmatrix}, \tag{4.31}$$

$$[\mathbf{S}] = \begin{bmatrix} \tilde{J}_x \\ \tilde{J}_y \\ \tilde{M}_x \\ \tilde{M}_y \end{bmatrix}, \quad [\mathbf{T}] = \begin{bmatrix} \cos\phi & \sin\phi & 0 & 0 \\ -\sin\phi & \cos\phi & 0 & 0 \\ 0 & 0 & \cos\phi & \sin\phi \\ 0 & 0 & -\sin\phi & \cos\phi \end{bmatrix} \tag{4.32}$$

and $\cos\phi = -\frac{k_x}{\beta}$, $\sin\phi = -\frac{k_y}{\beta}$, $\beta = \sqrt{k_x^2 + k_y^2}$.

Therefore, the Green's function is

$$[\mathbf{G}] = [\mathbf{T}]^{-1}\,[\mathbf{K}]\,[\mathbf{T}] \tag{4.33}$$

and

$$[\mathbf{G}] = \begin{bmatrix} \tilde{G}_{ExJx} & \tilde{G}_{ExJy} & \tilde{G}_{ExMx} & \tilde{G}_{ExMy} \\ \tilde{G}_{EyJx} & \tilde{G}_{EyJy} & \tilde{G}_{EyMx} & \tilde{G}_{EyMy} \\ \tilde{G}_{HxJx} & \tilde{G}_{HxJy} & \tilde{G}_{HxMx} & \tilde{G}_{HxMy} \\ \tilde{G}_{HyJx} & \tilde{G}_{HyJy} & \tilde{G}_{HyMx} & \tilde{G}_{HyMy} \end{bmatrix} \tag{4.34}$$

For example,

$$\begin{aligned} \tilde{G}_{ExJx} &= -K_{e11}\cos^2\phi - K_{h11}\sin^2\phi \\ \tilde{G}_{ExJy} &= (K_{h11} - K_{e11})\sin\phi\cos\phi \\ \tilde{G}_{ExMx} &= (K_{e12} - K_{h12})\sin\phi\cos\phi \\ \tilde{G}_{ExMy} &= -K_{h12}\sin^2\phi - K_{e12}\cos^2\phi \end{aligned} \tag{4.35}$$

Substituting (4.28) into (4.35) results in

$$\begin{aligned} \tilde{G}_{ExJx} &= -j\frac{Z_o}{k_o}\frac{\left(\varepsilon_r k_o^2 - k_x^2\right)k_{z2}\cos k_{z1}d + j\left(k_o^2 - k_x^2\right)k_{z1}\sin k_{z1}d}{T_m\ T_e}\sin k_{z1}d \\ \tilde{G}_{ExJy} &= \ j\frac{Z_o}{k_o}\frac{k_{z2}\cos k_{z1}d + jk_{z1}\sin k_{z1}d}{T_m\ T_e}k_x k_y \sin k_{z1}d \\ \tilde{G}_{ExMx} &= -j\frac{\left(\varepsilon_r - 1\right)}{T_m\ T_e}k_x k_y \sin k_{z1}d \\ \tilde{G}_{ExMy} &= -\frac{k_{z1}k_{z2}\varepsilon_r\cos k_{z1}d + j\left(k_o^2\varepsilon_r - k_x^2\varepsilon_r - k_y^2\right)\sin k_{z1}d}{T_m\ T_e} \end{aligned} \tag{4.36}$$

where

$$T_m = k_{z2}\varepsilon_r \cos k_{z1}d + jk_{z1} \sin k_{z1}d$$
$$T_e = k_{z1} \cos k_{z1}d + jk_{z2} \sin k_{z1}d \tag{4.37}$$

Eq.(4.36) is exactly the same as those obtained by using the field matching process.

4.6 Conclusions

A unified network approach is developed in this chapter for the evaluation of spectral domain Green's functions of multilayer dielectrics. The electromagnetic wave modes in the multilayer dielectrics is decomposed into two modes and equivalent transmission line is obtained for each mode. Different electric and magnetic currents are replaced by appropriate electric current and voltage generators. The electric and magnetic fields are equivalent to electric currents and voltages in the network. Then the spectral domain Green's functions can be obtained by evaluating appropriate parameters of the network. Analytical results for a single layer grounded dielectric layer are provided to validate the technique. Consequently, the lengthy derivation process of deriving the spectral domain Green's function for multilayer dielectrics becomes a simple and systematic procedure of evaluating the parameters of a ladder network by using the network approach. It is ideal for the development of a general software to evaluate efficiently the spectral domain Green's functions.

Chapter 5 A UNIFIED SPECTRAL DOMAIN FULL WAVE TECHNIQUE FOR MULTILAYER PRINTED STRUCTURES

In this chapter, a unified spectral domain technique is developed for the full wave analysis of multi–layer printed structures. The multilayer dielectric extends to infinity in two dimensions and stacks up in the third dimension. By a Fourier Transformation, the electromagnetic boundary value problem of multilayer printed structures is transformed into spectral domain and solved by using the moment method in the spectral domain. Various types of radiating elements and feeding structures are considered in the analysis. A nodal based basis function is proposed along with other types of basis functions to model different shapes of structures.

5.1 A Generalized Printed Structure with Multilayer Dielectrics

A generalized open printed structure with multilayer dielectrics is defined in Fig.5.1. This structure represents most common types of open printed transmission lines, printed passive components, and printed antennas, and forms a building block for various printed structures used in the analysis. Its basic element is a dielectric layer with different printed circuits. The printed circuit on the surface of dielectric layer is represented in a complementary form of dielectric and conductor, i.e., if one part is covered with conductor, then the other part is covered with dielectric surface. In the following section, an outline of different parts of the structure shown in Fig.5.1 is presented.

5.1.1 Dielectric layers

The multilayer dielectric is assumed to extend to infinity in the $x-$ and $y-$ directions and stack up in the $z-$ direction. The lossy dielectric is treated automatically by using a complex dielectric constant.

5.1.2 Geometry of radiating elements

Both printed patches and slots can be used as printed antenna radiating elements, and the most frequently used radiating element shapes are rectangles and circles. However, in some cases, other shapes may also be used to fulfilled special requirements such as the circular polarization. Therefore, arbitrary shape radiating elements(patches or slots) is also included in the present model.

5.1.3 Feeding types

Among all five feeding techniques discussed before, the microstrip feeding structures(either direct or electromagnetically coupled feeds) have more attractive features than the coaxial probe feeding, especially when they are used in a large array. Therefore, the direct microstrip line or coupled feeds are used as the general feeding structure in the analysis model. For completeness, a model for probe feeding is also developed.

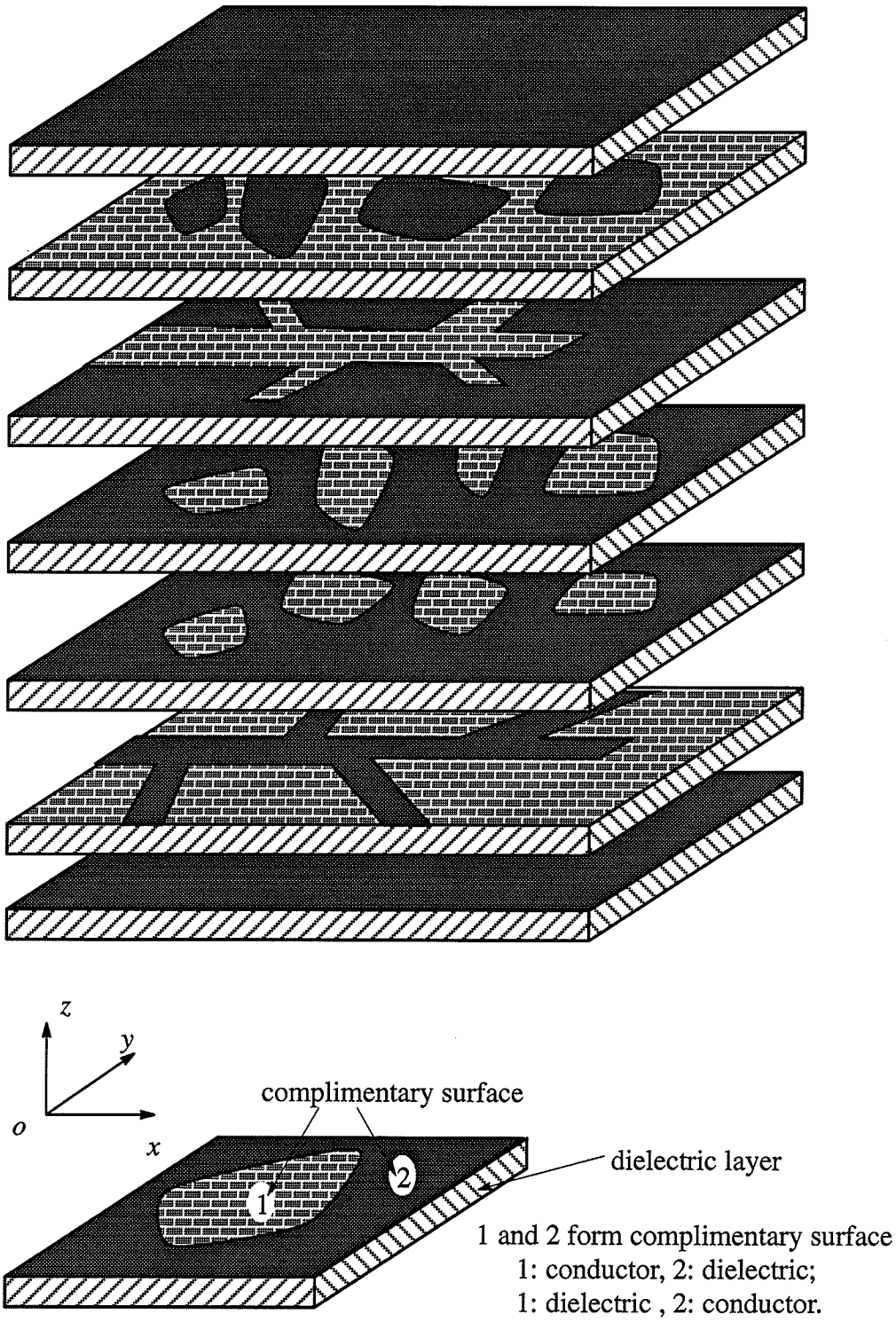

Fig.5.1. A generalized printed structure with multilayer dielectrics

5.2 A Unified Spectral Domain Technique

In this section, the moment method is applied in the spectral domain to develop a unified technique for the analysis of printed structures with multilayer dielectrics.

The spectral domain moment method analysis starts with the modeling of patches printed on the dielectrics and slots etched on the conducting planes. As it is known, the perfectly conductor patch can be modelled by using either surface patches or wire grid models. But, in [43][44], it has been proven that the wire grid modelling is equivalent to a surface patch modelling with subsectional basis functions. Therefore, in the present study, the surface patches are used to model perfectly conductor patches, i.e., the conducting patches are replaced by electric currents and vanishing of the tangential electric fields is enforced on their surface.

For a printed slot, the equivalent magnetic currents are assumed over the slot aperture and the conductor aperture is closed according to the equivalence principle(Fig.5.2). The equivalent magnetic currents on both sides of the closed conducting plane can be evaluated according to the electric fields as

$$\mathbf{M}_s = -\hat{\mathbf{n}} \times \mathbf{E}_s = \hat{\mathbf{x}} M_{sx} + \hat{\mathbf{y}} M_{sy} \tag{5.1}$$

The continuity conditions for the tangential magnetic fields should be enforced in the moment method solution, which can be satisfied by assuming $\mathbf{M}_s^i = -\mathbf{M}_s^j$.

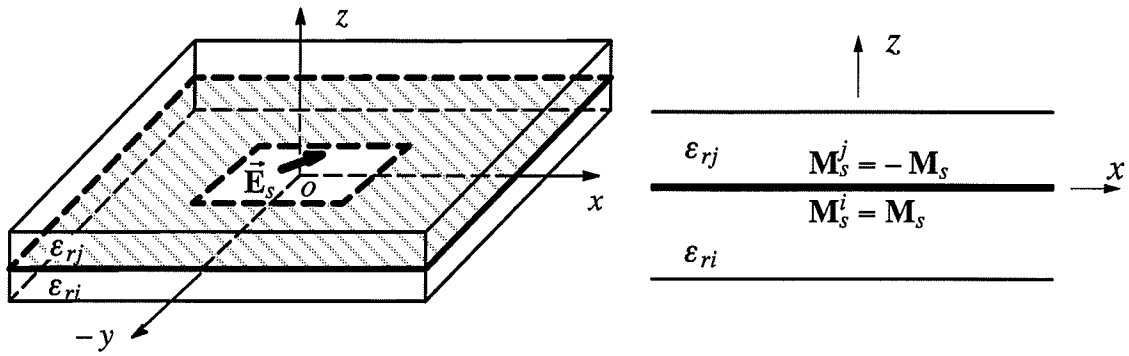

Fig.5.2. A printed slot and its equivalent model.

In summary, all the conducting patches are replaced by electric currents and the slots by equivalent magnetic currents. The total electromagnetic fields produced by all these planar currents can be evaluated by using the spectral domain Green's functions as follows

$$\begin{aligned}\mathbf{E}_{tot} = &\int_{S_J} \mathbf{J}(x_o, y_o) \cdot \left\{ \int_{-\infty}^{+\infty}\int \tilde{\tilde{\mathbf{G}}}_{EJ}(k_x, k_y) e^{jk_x(x-x_o)} e^{jk_y(y-y_o)} dk_x dk_y \right\} dx_o dy_o \\ &+ \int_{S_M} \mathbf{M}(x_o, y_o) \cdot \left\{ \int_{-\infty}^{+\infty}\int \tilde{\tilde{\mathbf{G}}}_{EM}(k_x, k_y) e^{jk_x(x-x_o)} e^{jk_y(y-y_o)} dk_x dk_y \right\} dx_o dy_o \end{aligned} \tag{5.2}$$

$$\begin{aligned}\mathbf{H}_{tot} = &\int_{S_J} \mathbf{J}(x_o, y_o) \cdot \left\{ \int_{-\infty}^{+\infty}\int \tilde{\tilde{\mathbf{G}}}_{HJ}(k_x, k_y) e^{jk_x(x-x_o)} e^{jk_y(y-y_o)} dk_x dk_y \right\} dx_o dy_o \\ &+ \int_{S_M} \mathbf{M}(x_o, y_o) \cdot \left\{ \int_{-\infty}^{+\infty}\int \tilde{\tilde{\mathbf{G}}}_{HM}(k_x, k_y) e^{jk_x(x-x_o)} e^{jk_y(y-y_o)} dk_x dk_y \right\} dx_o dy_o \end{aligned} \tag{5.3}$$

where $\mathbf{J}$ and $\mathbf{M}$ represent all planar electric and equivalent magnetic currents in the multilayer dielectric structure, and $\tilde{\tilde{\mathbf{G}}}$ is the dyadic Green's function in the spectral domain

which is composed of the corresponding scalar Green's functions discussed in the last chapter. For the planar currents considered here, the dyadic Green's function has the following form

$$\tilde{\bar{\mathbf{G}}} = \hat{\mathbf{x}}(\hat{\mathbf{x}}\tilde{G}_{xx} + \hat{\mathbf{y}}\tilde{G}_{yx} + \hat{\mathbf{z}}\tilde{G}_{zx}) + \hat{\mathbf{y}}(\hat{\mathbf{x}}\tilde{G}_{xy} + \hat{\mathbf{y}}\tilde{G}_{yy} + \hat{\mathbf{z}}\tilde{G}_{zy}) \tag{5.4}$$

which can be evaluated from (4.13) by using coordinate transformation (4.3).

the subscripts E and H in (5.2) and (5.3) represent the electric and magnetic fields and the subscripts J and M represent electric and magnetic currents, respectively.

As it is known, the tangential electric field on a perfect conductor should vanish and the tangential magnetic fields must be continuous across the printed slot. Since the electric currents can exist only on the conducting patch and the equivalent magnetic currents are present only in the printed slot area, the following equations can be used to enforce these boundary conditions from the principle of moment method

$$< \mathbf{H}^{u}_{tot} - \mathbf{H}^{d}_{tot} , \mathbf{M} >= 0 , \qquad \text{through slot aperture} \tag{5.5}$$

$$< \mathbf{E}_{tot} , \mathbf{J} >= 0 , \qquad \text{on conducting patch} \tag{5.6}$$

where the superscript u represents the total field in the region above the slot and the superscript d indicates that the field region is below the slot, and electric and magnetic fields are the total fields produced by all the currents as given in (5.2) and (5.3).

By expanding the electric and equivalent magnetic currents in (5.5) and (5.6) in terms of the basis functions with unknown expansion coefficients, one can finally obtain the following matrix equation

$$[Z]\,[a] = [F] \tag{5.7}$$

where $[a]$ is the coefficient matrix and the elements of $[Z]$ and $[F]$ matrices have similar expressions given by

$$\begin{matrix} Z_{mn} \\ F_m \end{matrix} = \int_{-\infty}^{+\infty}\int \tilde{T}_m^*(k_x, k_y)\ \tilde{G}(k_x, k_y)\ \tilde{S}_n(k_x, k_y)\ dk_x\ dk_y \tag{5.8}$$

where $\tilde{G}(k_x, k_y)$ is the corresponding Green's function, $\tilde{S}_m(k_x, k_y)$ is the Fourier transform of the electric or magnetic currents for the evaluation of $\tilde{Z}_{mn}$, or the exciting current when $\tilde{F}_m$ is evaluated, and $\tilde{T}_m^*(k_x, k_y)$ is the conjugate of the Fourier transform of the testing function, which is equal to that of the basis function when a Galerkin's testing procedure is used.

When there are vertical posts in the structure, they can initially be replaced by vertical electric currents and then, one additional term of Green's functions should be added as given in (4.13) to account for these vertical electric currents. In the method of moment, as well, the boundary condition on the surface of conducting post should also be enforced. The above procedure is repeated by adding appropriate terms with respect to the vertical currents and boundary conditions in the equations.

5.3 Basis Functions for Various Currents

5.3.1 Domain based basis functions

The electric and equivalent magnetic currents exist only within a finite region in the spatial domain. Therefore, the most straightforward way of approximating these currents is to de-

fine a type of function in these regions, i.e., the entire domain basis functions, or in their subregions, i.e., the subdomain or subsectional basis functions. The basis functions defined in this way are classified as the domain based basis functions. Conventionally, the entire domain basis functions and the subsectional basis functions are used separately. The entire domain basis functions converge quickly but can only be used in the structure with regular shapes. The subsectional basis functions have more flexibility but converge slowly. In this section, a mixed set of basis functions composed of both entire domain and subsectional basis functions is proposed to save computation time.

Consider the slotted patch as shown in Fig.5.3. It is difficult to use entire domain basis functions on this patch, since the current over the slot is zero. To overcome the problem, in the present technique, two different types of sub–divisions for x– and y– directed currents are used, as shown in Fig.5.3a and b respectively. Then in each sub–patch, either the entire domain or subsectional basis functions can be used. Further, each subregion can be sub–divided again if finer divisions are required for subsectional basis functions. By using this technique, fewer terms of basis functions are needed as compared with conventional subsectional basis functions that are used for such irregular shaped patches.

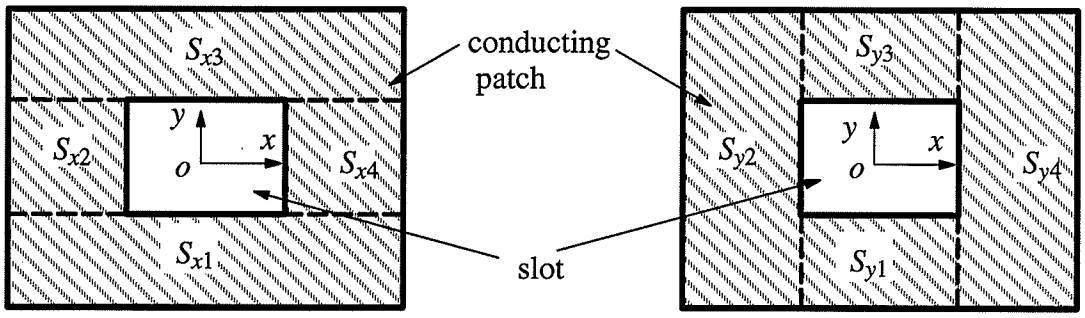

(a) division for x–directed current (b) division for y–directed current

Fig.5.3. Mixed basis functions for an irregular current patch

For instance, on the subregion S_{x1} , the longitudinal distribution of the $x-$ directed current can be expanded by using the entire domain basis functions as shown in Fig.5.4a

$$f_{xn}(x) = \sin\frac{n\pi}{l}(x - l/2) \qquad \text{for } |x| < l/2 \tag{5.9}$$

or using the subsectional basis functions as shown in Fig.5.4b

$$f_{xn}(x) = \frac{\sin k_o(l_n - |x - x_{cn}|)}{\sin k_o l_n} \qquad \text{for } |x - x_{cn}| < l_n \tag{5.10}$$

For the transverse distribution, the basis functions, can be either constant as shown in Fig.5.5a, as

$$f_x(y) = 1/w \ , \quad |y| < w/2 \tag{5.11}$$

or take a more appropriate form of Fig.5.5b to satisfy the edge conditions as

$$f_x(y) = 1/\sqrt{(w/2)^2 - x^2} \ , \quad |y| < w/2 \tag{5.12}$$

Fourier transforms of these basis functions are given in Appendix B.

When multiple patches are considered, the computation effort can be reduced by using a pretreatment technique, discussed in [45][46], and adopted in combination with the domain based basis functions for each individual patch.

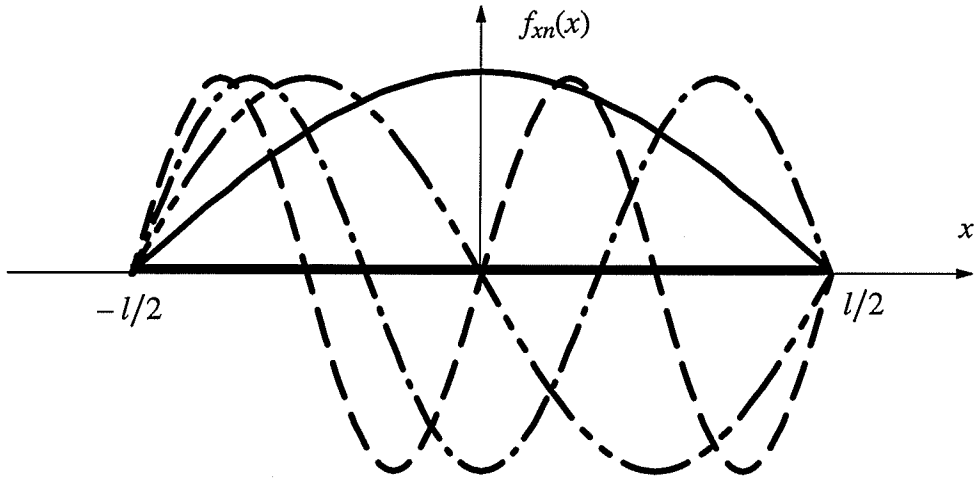

(a) Entire domain basis function

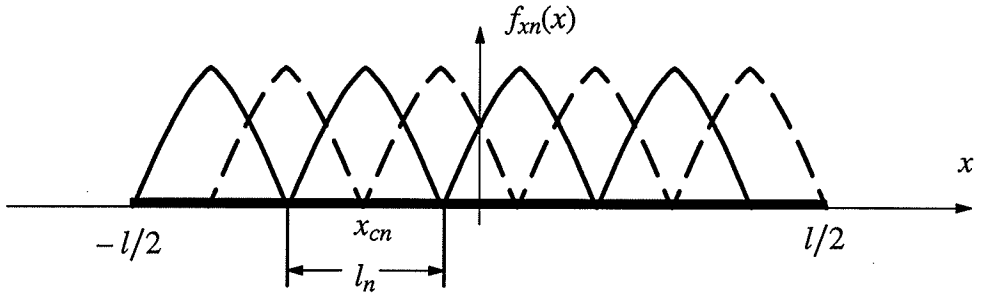

(b) Subsectional basis function

Fig.5.4. Basis functions for the longitudinal distribution

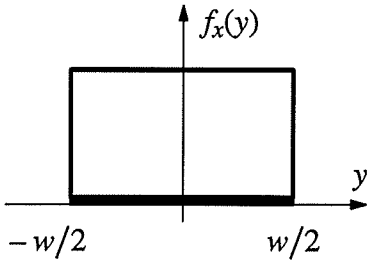

(a) no edge effect

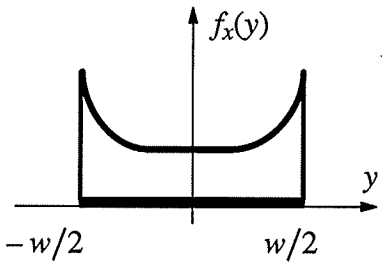

(b) edge effect

Fig.5.5. Basis functions for the transverse distribution

5.3.2 Nodal based basis functions

The domain based basis function discussed in the last section is defined in a rectangular region and cannot be used for arbitrary shaped patches. Instead, the triangular domain basis functions[47] are used, which are more efficient for analyses in the space domain. For this reason, they are also used in the spatial domain analysis of the microstrip antennas. The triangular basis functions can also be applied in the spectral domain moment method. However, since the vectorial basis functions defined in each triangle is arbitrarily directed, it is not easy to derive their Fourier transform expressions and the arbitrarily directed current will need more computation time to implement the moment method in the spectral domain. Therefore, in this section, a nodal based basis function is proposed for the spectral domain moment methods. The current on the entire area is first approximated by those on the nodes rather than in the subdomains. Then, the current at each node is decomposed into two orthogonal components in order to obtain a simpler Fourier transform expression and reduce computation time. Such nodal based basis functions can be used to approximate electric currents on a conducting surface or equivalent magnetic currents on a slot. The current is continuous all over the arbitrary area and satisfies the edge current boundary conditions.

A patch with an arbitrary geometry is divided into a number of subregions by a set of nodes as shown in Fig.5.6. These subregions may have any shapes but here only triangular subregions are considered. Then the electric current within each subregion is expressed as a linear combination of those at its vertices, i.e., three nodes in a triangular subregion. These nodal electric currents are arbitrarily directed. However, they can be decomposed into two orthogonal components to be treated separately. For example, the electric current at node n, in Fig.5.6, can be assumed as a combination of two components along $\hat{\mathbf{x}}-$ and $\hat{\mathbf{y}}-$ directions, giving $\mathbf{I}_n = \hat{\mathbf{x}}\, I_{nx} + \hat{\mathbf{y}}\, I_{ny}$. These current components are in general independent of each other, except when the node falls at the patch edge where the normal compo-

nent of electric current vanishes. For the edge node m shown in Fig.5.6, the edge boundary condition can be fulfilled by enforcing the following equation on the node current components

$$I_{mx} \sin\theta_{mt} - I_{my} \cos\theta_{mt} = 0 \tag{5.13}$$

In addition to enforcing the edge current condition, eq.(5.13) can be used to reduce numerical computation effort. In practice, numerical experience shows that this edge boundary condition will automatically be fulfilled even if it is not considered explicitly in the expression of the basis functions, as long as the surface sub–division is fine enough.

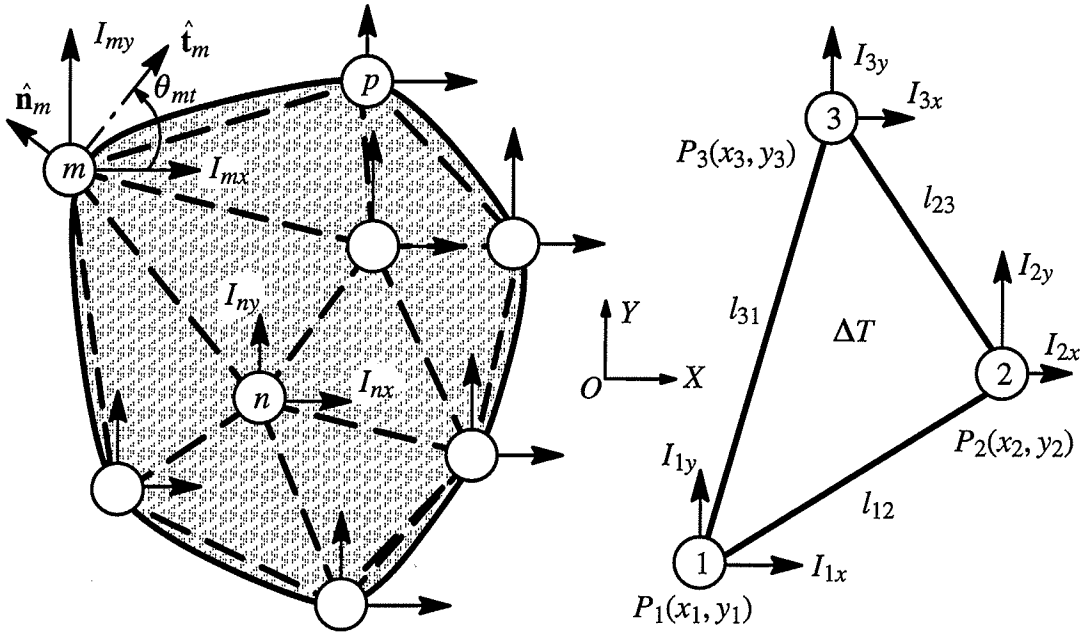

division of the entire patch a single subregion with three nodes

Fig.5.6. A nodal based division for an arbitrary shaped patch

Now, to present the method in detail, consider a triangular subregion ΔT with three nodes shown in Fig.5.6. The nodal electric current components at these three nodes are

$\{I_{iv} | i = 1,2,3\}$, where subscripts v represents $\hat{\mathbf{x}}-$ or $\hat{\mathbf{y}}-$ component. The electric current $I_{v\Delta T}$ in this subregion can be expressed in terms of the nodal currents as

$$I_{v\Delta T}(x,y) = \sum_{i=1}^{3} \left(C_{i0} + C_{i1}x + C_{i2}y\right) I_{iv} \tag{5.14}$$

where $C_{i0} = \frac{1}{2A}(x_{i+1}y_{i+2} - x_{i+2}y_{i+1})$, $C_{i1} = \frac{1}{2A}(y_{i+1} - y_{i+2})$, $C_{i2} = \frac{1}{2A}(x_{i+2} - x_{i+1})$ and A is the area of subregion ΔT.

The above constants are determined by enforcing the subregion current to be equal to nodal current at each node. Therefore, currents expressed by (5.14) in each subregion are continuous over the entire region.

In the spectral domain, (5.14) becomes

$$\tilde{I}_{v\Delta T}(k_x, k_y) = \sum_{i=1}^{3} \left(C_{i0}\tilde{F}_0 + C_{i1}\tilde{F}_1 + C_{i3}\tilde{F}_3\right) I_{iv} \tag{5.15}$$

where $\tilde{F}_0$, $\tilde{F}_1$ and $\tilde{F}_2$ are the Fourier transforms of $F_0 = 1$, $F_1 = x$ and $F_2 = y$ in the subregion ΔT, respectively, which are defined by

$$\tilde{F}(k_x, k_y) = \int\int_{\Delta T} F(x,y)\ \exp\left(-jk_x x\right)\ \exp\left(-jk_y y\right)\ dx\,dy \tag{5.16}$$

and given in Appendix B.

If there are N nodes over the entire patch and the $n-$ th node is shared by M_n subregions, then the electric current in the spectral domain is

$$\tilde{I}_{v\,\mathrm{tot}}(k_x, k_y) = \sum_{n=1}^{N} \tilde{D}_n(k_x, k_y)\; I_{nv} \tag{5.17}$$

where

$$\tilde{D}_n(k_x, k_y) = \sum_{i=1}^{M_n} \left(C_{ni0}\tilde{F}_{n0} + C_{ni1}\tilde{F}_{n1} + C_{ni2}\tilde{F}_{n2} \right) \tag{5.18}$$

Expression (5.18) in combination with the edge current condition (5.13) forms the spectral domain expression for the two components of electric current on the patch. They can be applied in the spectral domain moment method to determine unknown electric current components at each node and then the electric current distribution on the entire patch.

The nodal based basis functions proposed above are ideal for representation of currents over arbitrary shape patch, and the surface electric currents are continuous over the entire area. Also, only two orthogonal current components need to be considered which simplifies the analysis procedure and saves computation time. Furthermore, they can be used in conjunction with other type fo basis functions in the spectral domain moment method without any additional effort.

5.3.3 Semi–infinite transmission lines

The basis functions discussed above are for finite size structures. For planar transmission lines, the distribution of the current in the transmission direction can be expressed by sinusoidal functions which yield dirac–delta (δ) functions after Fourier transformation. Therefore, one needs only to approximate the transverse distribution and the moment method is reduced into a one dimensional problem in the spectral domain.

When the infinite planar transmission line is terminated as shown in Fig.5.7a, the currents in the line can be divided into three parts[48], the infinite line current, the reflected current,

and the higher order mode current in the vicinity of the termination. Thus, the longitudinal distribution of the current can be modeled by using the entire domain traveling wave modes along with the semi–infinite line and the subsectional sinusoidal modes in the vicinity of the open end, as shown in Fig.5.7b.

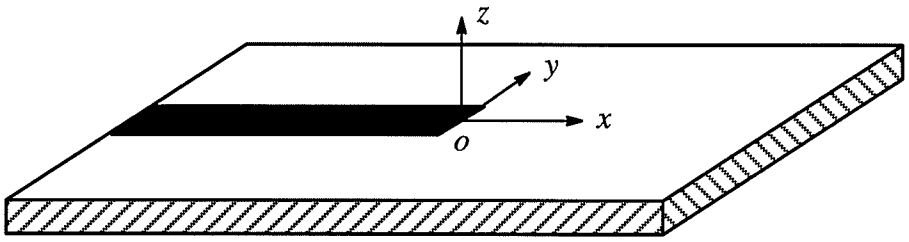

(a) a terminated planar transmission line

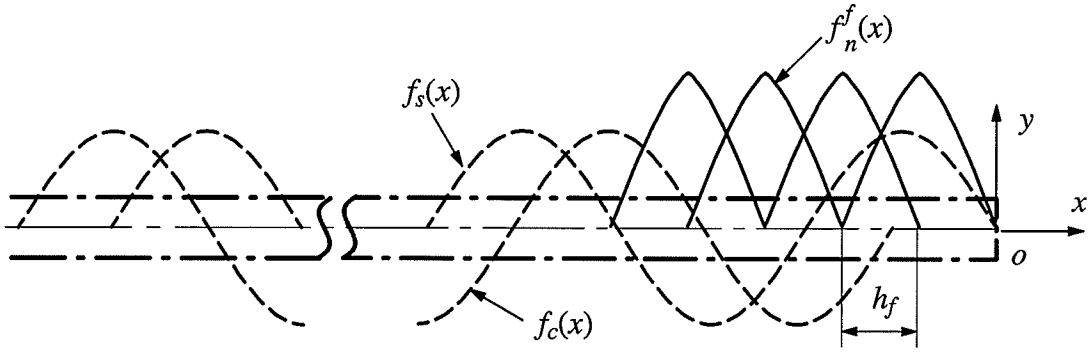

(b) basis functions for the longitudinal distribution of current

Fig.5.7. Basis functions for a semi–infinite planar transmission line

For small widths of the feedline, the transverse component of the electric surface current on the line is very small, as compared with the longitudinal one. Therefore for simplicity, only the longitudinal component is considered in the analysis, which can be expressed as

$$J_{fx}(x,y) = g_f(y)\left[(1-R)f_c(x) - j(1+R)f_s(x) + \sum_{n=1}^{N_f} I_n^f f_n^f(x)\right] \tag{5.19}$$

where $g_f(y)$ is the transverse distribution of the current which may include the edge effect or be assumed simply as constant for a narrow feedline, R is the reflection coefficient along the line to be determined, and I_n^f are coefficients of subsectional basis functions.

Expressions for $f_c(x)$, $f_s(x)$, and $f_n^f(x)$ in (5.19) are

$$f_c(x) = \cos k_e x \qquad \text{for } -\infty < x < -\pi/2k_e \tag{5.20}$$

$$f_s(x) = \sin k_e x \qquad \text{for } -\infty < x < 0 \tag{5.21}$$

$$f_n^f(x) = \frac{\sin k_e(h_f - |x + nh_f|)}{\sin k_e h_f} \qquad \text{for } |x + nh_f| < h_f \tag{5.22}$$

where k_e is the wavenumber of the infinite microstrip line with the same width as the feedline, and h_f is the length of the sinusoidal roof top basis function. Usually these subsectional rooftop terms can be terminated after one or two waveguide wavelengths away from the open end of the feedline.

Fourier transforms of these basis functions are also given in Appendix B.

5.3.4 Vertical current

The subsectional basis function can be used to model the vertical electric current on the post or feeding probe as shown Fig.5.8. It should be noted that the appropriate current distribu-

tion should be assumed on the patch directly connected to the vertical current to enforce the continuity of the current at the connection point, especially when the current on the patch is modelled by the subsectional basis functions.

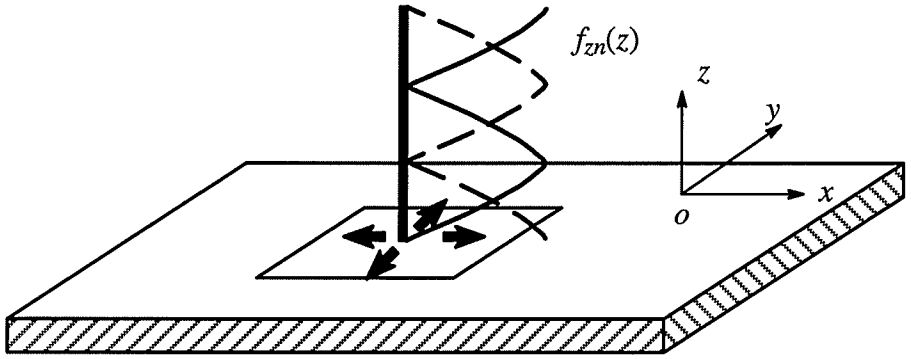

Fig.5.8. Model of a vertical current and current continuity

5.4 Far Field Radiation Pattern

The coordinate system used to evaluate far field radiation pattern is shown in Fig.5.9. For simplicity, the original point is at the upper interface of the top dielectric layer.

Assume that the electric fields at the upper interface of the top dielectric layer as shown in Fig.5.9 is $\tilde{E}_x(k_x, k_y, 0^+)$, $\tilde{E}_y(k_x, k_y, 0^+)$, $\tilde{E}_z(k_x, k_y, 0^+)$. Since the space above this interface is free space extending to infinity, the electric field beyond this interface is

$$\tilde{E}_s(k_x, k_y, z) = \tilde{E}_{s0} \exp(-jk_z z) \tag{5.23}$$

where subscript s represents x , y , or z , respectively, $\tilde{E}_{s0} = \tilde{E}_s(k_x, k_y, 0^+)$ and $k_z = \sqrt{k_o^2 - k_x^2 - k_y^2}$.

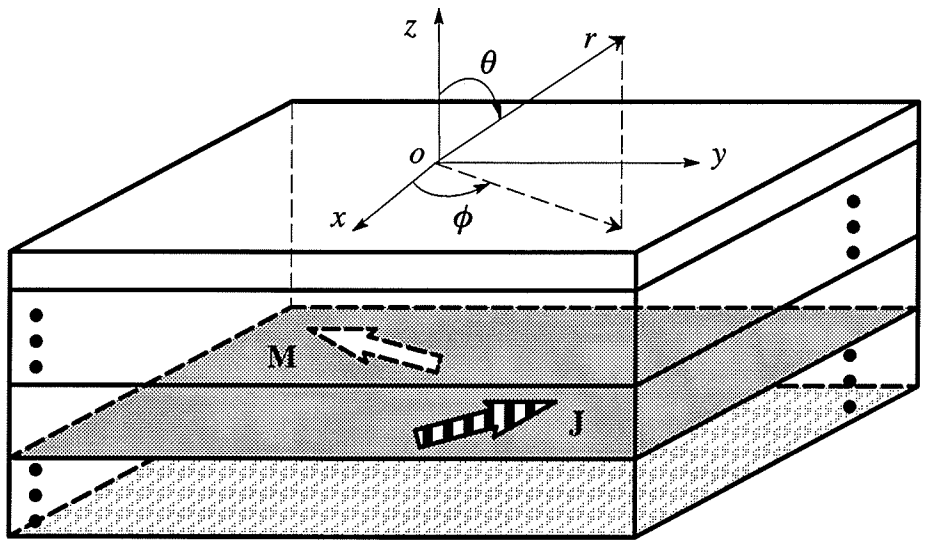

Fig.5.9. The coordinate system for far field evaluation

Therefore, by using the inverse Fourier transformation, the space domain expressions for electric fields in this area can be written as

$$E_s(x,y,z) = \frac{1}{4\pi^2}\int_{-\infty}^{\infty}\int \tilde{E}_{s0}\ \exp(-jk_z z)\ \exp(jk_x + jk_y)\ \mathrm{d}k_x\ \mathrm{d}k_y \tag{5.24}$$

or

$$E_s(x,y,z) = \frac{1}{4\pi^2}\int_{-\infty}^{\infty}\int \tilde{E}_{s0}\ \exp\left[-j\left(k_x x + k_y y + k_z z\right)\right]\ \mathrm{d}k_x\ \mathrm{d}k_y \tag{5.25}$$

By using the stationary phase method, the integration in (5.25) can be approximated to yield

$$E_s(x,y,z) \approx j\frac{k_o}{2\pi}\frac{\exp(-jk_o r)}{r}\cos\theta\ \tilde{E}_{s0} \tag{5.26}$$

where $k_x = -k_o \sin\theta \cos\phi$, $k_y = -k_o \sin\theta \sin\phi$.

And, $\beta^2 = k_x^2 + k_y^2 = k_o^2 \sin^2\theta$, $k_z = \sqrt{k_o^2 - \beta^2} = k_o \cos\theta$, and $k_x = -\beta \cos\phi$, $k_y = -\beta \sin\phi$.

The electromagnetic field components in a spherical coordinate system can be obtained from

$$\begin{aligned} E_r &= \left(E_x \cos\phi + E_y \sin\phi\right) \sin\theta + E_z \cos\theta \\ E_\theta &= \left(E_x \cos\phi + E_y \sin\phi\right) \cos\theta - E_z \sin\theta \\ E_\phi &= -E_x \sin\phi + E_y \cos\phi \end{aligned} \tag{5.27}$$

and substituting (5.26) into (5.27) yields

$$\begin{aligned} E_r &\approx j\frac{k_o}{2\pi}\frac{\exp(-jk_o r)}{r}\cos\theta \left[\left(\tilde{E}_{x0}\cos\phi + \tilde{E}_{y0}\sin\phi\right)\sin\theta + \tilde{E}_{z0}\cos\theta\right] \\ E_\theta &\approx j\frac{k_o}{2\pi}\frac{\exp(-jk_o r)}{r}\cos\theta \left[\left(\tilde{E}_{x0}\cos\phi + \tilde{E}_{y0}\sin\phi\right)\cos\theta - \tilde{E}_{z0}\sin\theta\right] \\ E_\phi &\approx j\frac{k_o}{2\pi}\frac{\exp(-jk_o r)}{r}\cos\theta \left[-\tilde{E}_{x0}\sin\phi + \tilde{E}_{y0}\cos\phi\right] \end{aligned} \tag{5.28}$$

Now, from (4.3) in the last chapter, we get

$$\begin{aligned} E_r &\approx j\frac{k_o}{2\pi}\frac{\exp(-jk_o r)}{r}\cos\theta \left(\tilde{E}_{u0}\sin\theta + \tilde{E}_{z0}\cos\theta\right) \\ E_\theta &\approx j\frac{k_o}{2\pi}\frac{\exp(-jk_o r)}{r}\cos\theta \left(\tilde{E}_{u0}\cos\theta - \tilde{E}_{z0}\sin\theta\right) \\ E_\phi &\approx j\frac{k_o}{2\pi}\frac{\exp(-jk_o r)}{r}\cos\theta \ \tilde{E}_{v0} \end{aligned} \tag{5.29}$$

and (4.6) gives

$$\tilde{E}_{z0} = -\frac{\beta}{k_z}\tilde{E}_{u0} \tag{5.30}$$

which provide the final expressions for the far field components as

$$E_r \approx 0$$

$$E_\theta \approx j\frac{k_o}{2\pi}\frac{\exp(-jk_o r)}{r}\tilde{E}_{u0} \tag{5.31}$$

$$E_\phi \approx j\frac{k_o}{2\pi}\frac{\exp(-jk_o r)}{r}\cos\theta\ \tilde{E}_{v0}$$

Therefore, the far field radiation patterns can be obtained using (5.31), in which $\tilde{E}_{u0}$ and $\tilde{E}_{v0}$ is the spectral domain electric fields components at the interface of $z = 0^+$ produced by electric/magnetic currents, which can be evaluated by multiplying the Fourier Transforms of currents and their corresponding spectral domain Green's functions as given in the last chapter.

5.5 Conclusions

This chapter provided a unified spectral domain technique for the full wave analysis of multilayer printed structures. The analysis was based on the spectral domain Green's functions derived in the last chapter. The technique was described along with various basis functions for different shapes of the structures. Simple expressions for the evaluation of far field radiation pattern were also derived.

Chapter 6 CHARACTERISTICS OF APERTURE COUPLED MICROSTRIP ANTENNAS

Aperture coupled microstrip antennas were first proposed in 1985[13]. Subsequently, the rectangular patch fed by a rectangular coupling aperture was analyzed by using various techniques[49]–[55] and considering only the longitudinal component of the electric surface current and equivalent magnetic current. However, the inclusion of both radiating patch current components and accurate treatment of the exciting slot provide more accurate solutions for the antenna input impedance and radiation characteristics. In particular, the cross–polarization can be determined accurately. This is significant since the cross–polarization is an important parameter of the antenna, but its low relative level requires accurate far field computation to yield a meaningful result.

In this chapter, various radiating elements fed by microstrip lines through several kinds of feeding geometries at arbitrary positions on the ground plane are analyzed[56][57]. The input impedances at the feedline are evaluated for the purpose of the feed network design. The electric current distribution on the feedline and radiating elements along with the equivalent magnetic current distribution on the coupling aperture are evaluated for better understanding of the operating mechanism of the antenna. The radiation pattern by the entire antenna and the coupling aperture are also calculated to evaluate the performance of the aperture coupled microstrip antennas. Finally, design considerations for the aperture coupled microstrip antennas are discussed.

6.1 Basic Performances

In this section, the basic performances of an aperture coupled microstrip antenna is studied. The structure is a rectangular patch fed with a centered rectangular coupling aperture as shown in Fig.6.1.

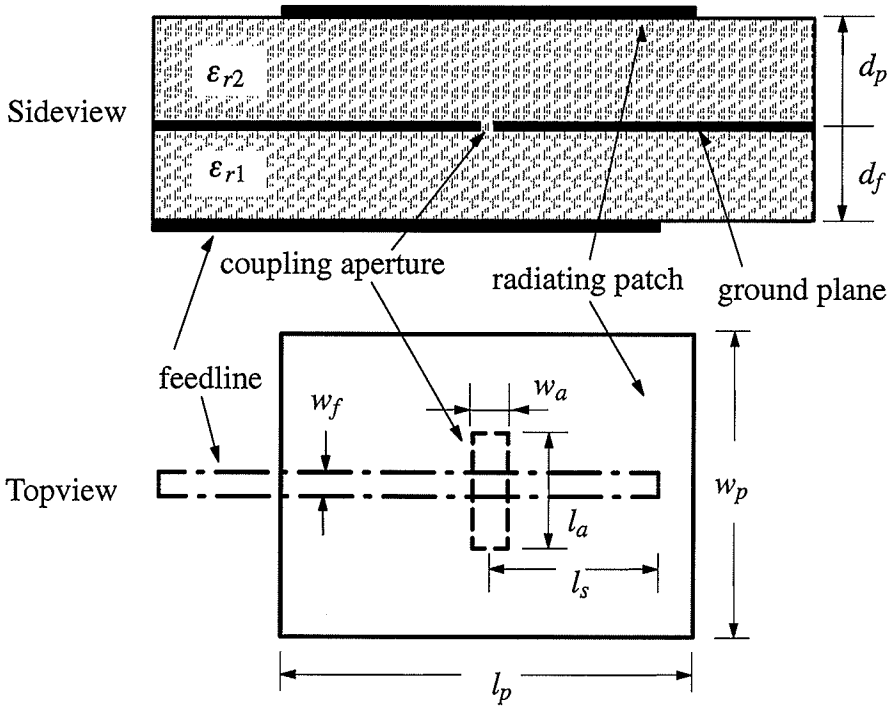

$\varepsilon_{r1} = \varepsilon_{r2} = 2.54$, $d_f = d_p = 1.6$ mm , $w_f = 4.4$ mm , $l_s = 1.2$ cm ,

$l_a = 1.1$ cm , $w_a = 1.6$ mm , $l_p = 4$ cm , $w_p = 3$ cm .

Fig.6.1. Rectangular patch with centered coupling aperture

6.1.1 Input impedance

The input impedance of this antenna over a very wide bandwidth is shown in Fig.6.2. It shows two resonances for the antenna. The first resonance is due to the resonance of the

patch, while the second one is mainly due to the resonance of the coupling slot. It is clear that the resonance frequency of the slot is much higher than that of the aperture coupled microstrip antenna, i.e., at the operating frequency of the antenna, the slot is not effectively excited.

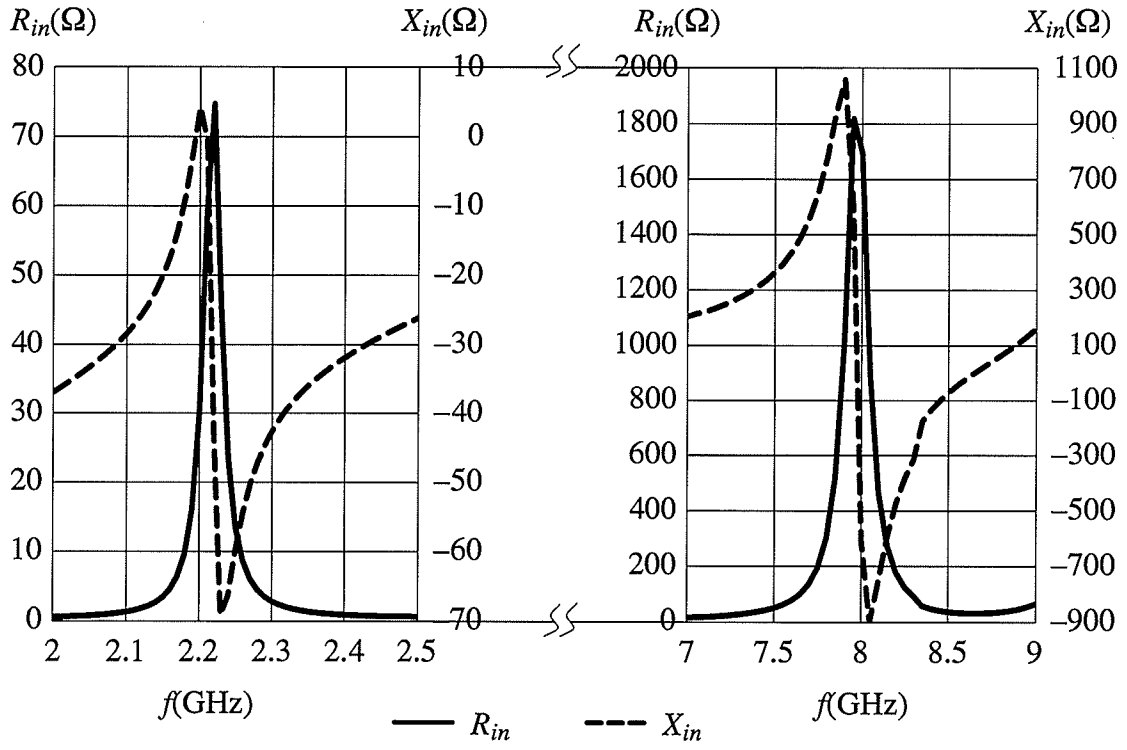

Fig.6.2. Resonances of the antenna and coupling aperture

6.1.2 Current distributions

In the previous analysis, the equivalent magnetic current on the coupling aperture was approximated by a single term sinusoidal function. However, It is found that the accuracy of the results for this current depends on the form of its representation by the selected functions. Here, different number of subsectional sinusoidal basis functions are used and the computed results are shown in Fig.3c. It clearly shows that a single term approximation is not sufficient and additional terms are needed to provide a convergent solution.

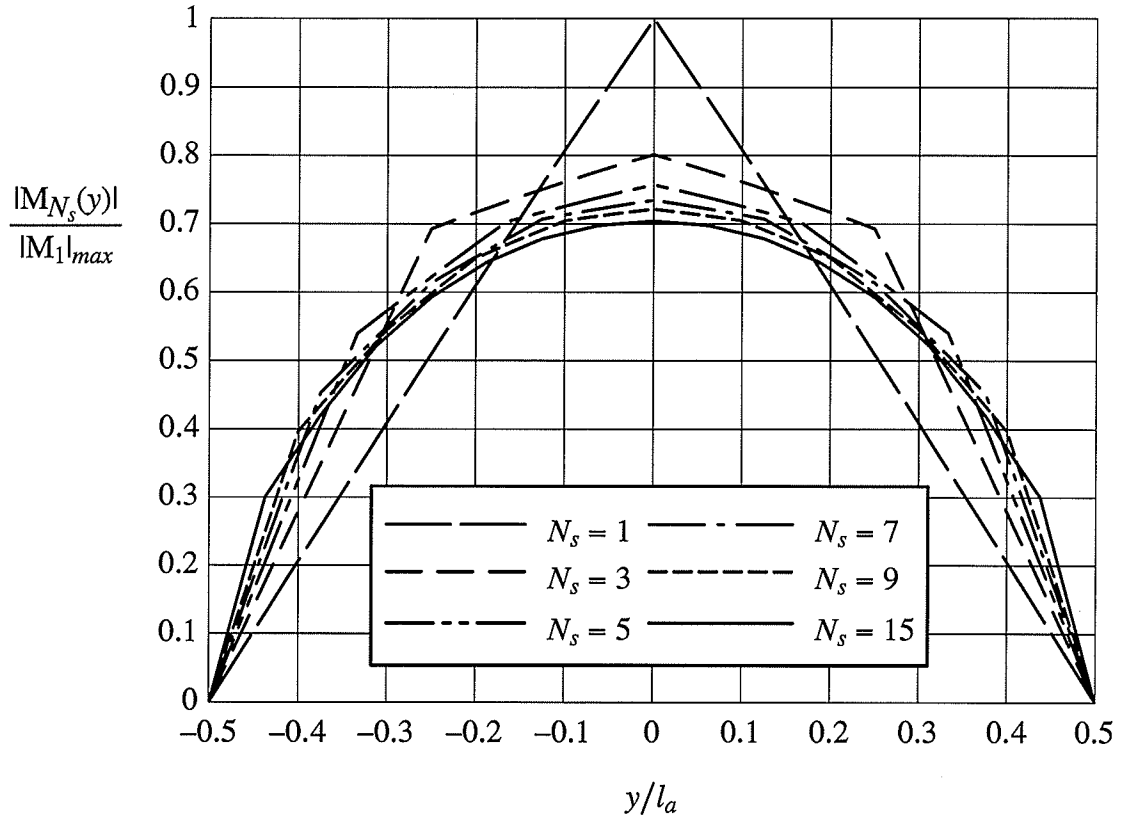

N_s -- the number of subsection terms used in the aperture

Fig.6.3. Normalized equivalent magnetic current on the slot aperture.

For the rectangular patch with a centered rectangular coupling aperture, Fig.6.4 shows the electrical surface current distribution on the patch and the equivalent magnetic current distribution on the coupling aperture. The magnitude of the longitudinal, i.e., the copolar, current component is symmetric with respect to the center point and in phase on almost the entire surface except in the vicinity of the patch center(Fig.6.4a). The magnitude of transverse, i.e., the crosspolar, current component is also symmetric with respect to the patch center, but out of phase on two sides(Fig.6.4b). These results indicate a proper excitation of the dominant mode and a strong influence of the coupling aperture on the patch currents. The latter is evident from perturbation of both amplitudes and phases of the patch currents as observed in the figure.

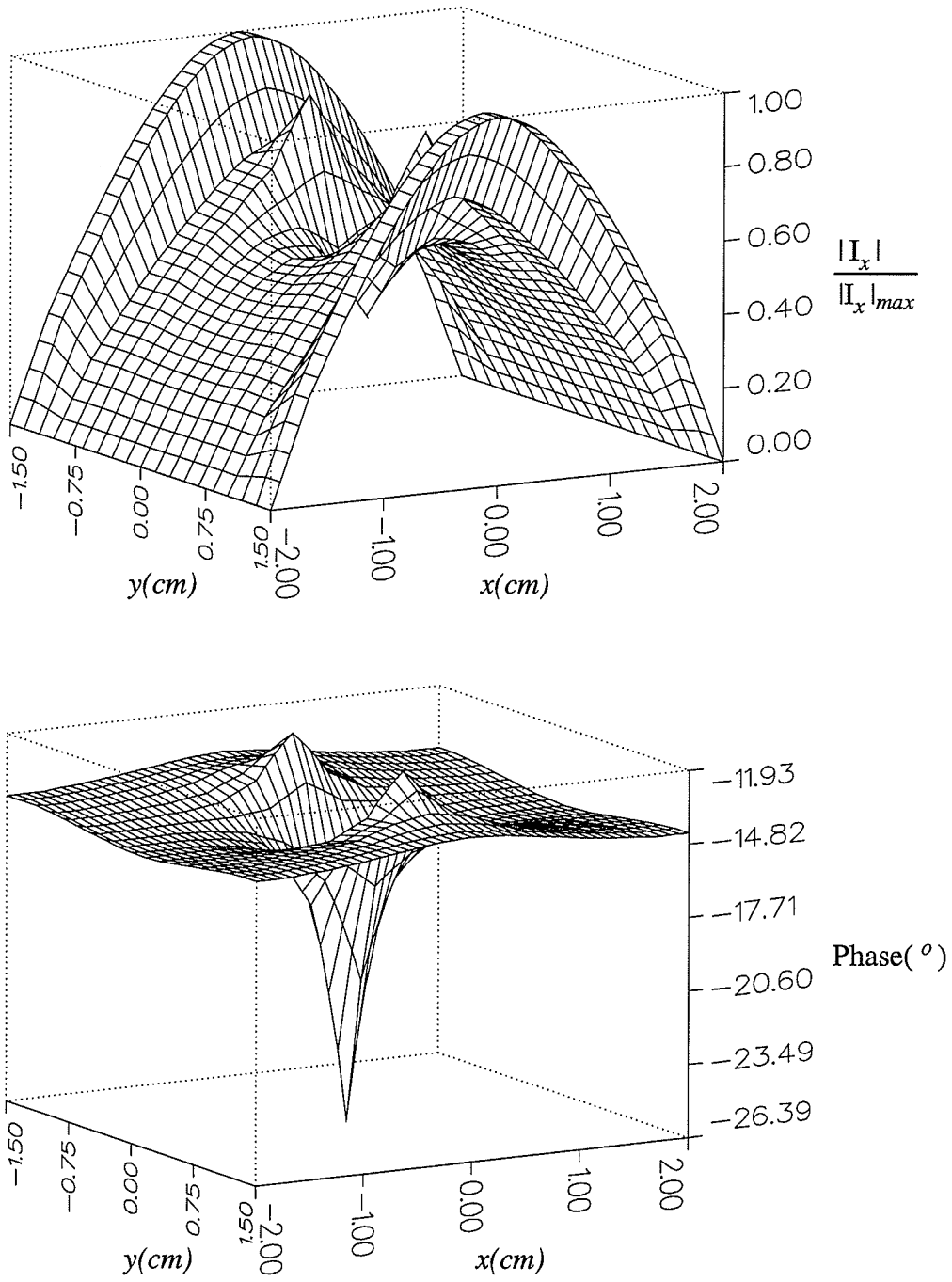

(a) magnitude and phase distribution of the longitudinal electric currents

Fig.6.4. Electric current distribution on the patch

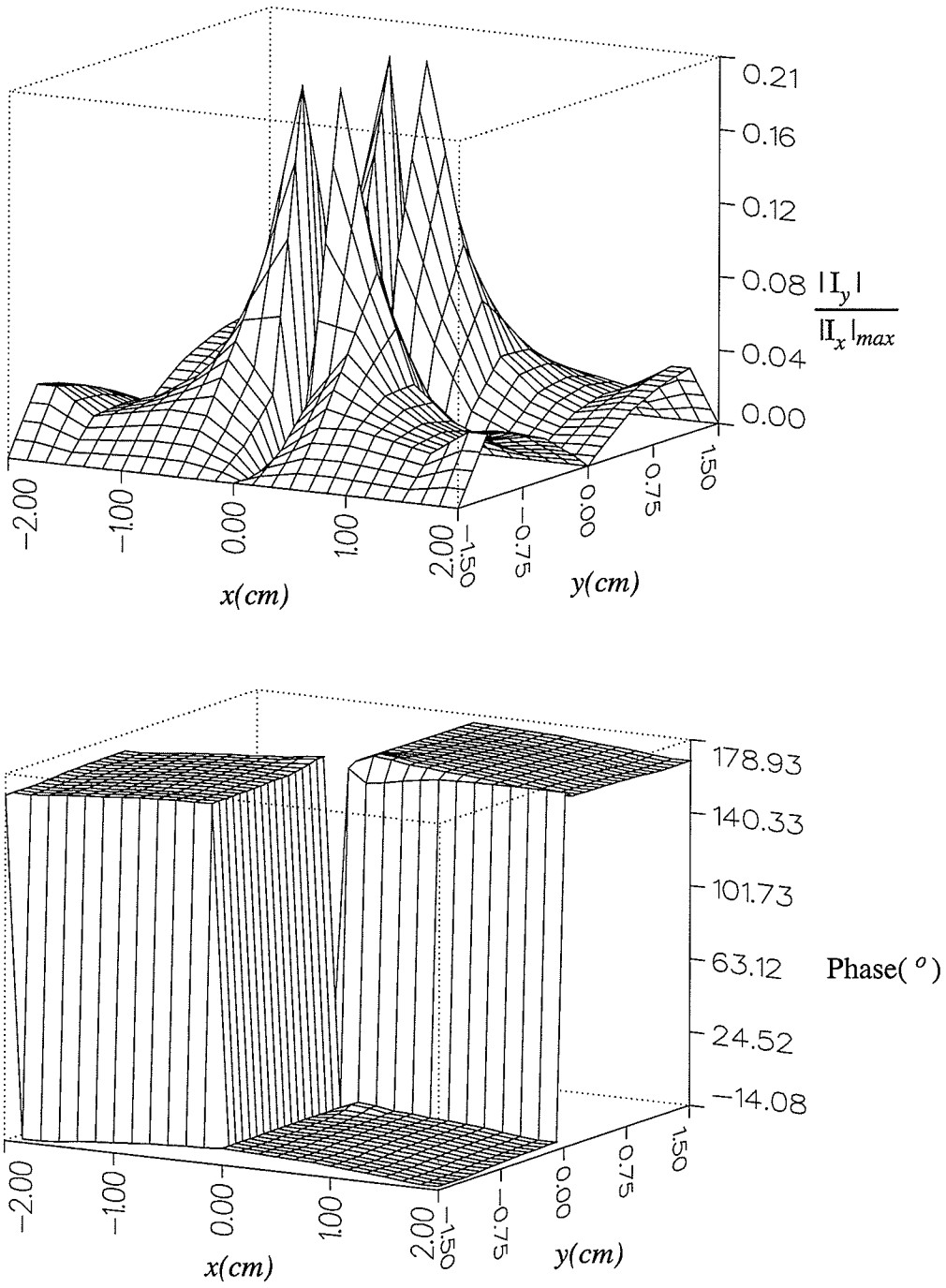

(b) magnitude and phase distribution of the transverse electric currents.

Fig.6.4 (continued)

6.1.3 Radiation Patterns

The co–polar and cross–polar radiation patterns are also evaluated and shown in Fig.6.5a. It shows that the cross polarization is small in the vicinity of broadside and becomes zero on the broadside. This indicates the superiority of the aperture coupling type feeding method for microstrip antennas, over other methods, by yielding a considerably lower cross–polarization level.

The coupling aperture radiates also in the backward direction, below the ground plane. This back radiation is a loss and a main disadvantage of the aperture coupled microstrip antennas. Its co– and cross–polar radiations, normalized by the maximum co–polar radiation, are also computed and shown in Fig.6.5b. It shows that the backward radiation from the coupling aperture is very small as compared with the forward radiation of the antenna, which is an anticipated result because the coupling aperture is not effectively excited at this frequency.

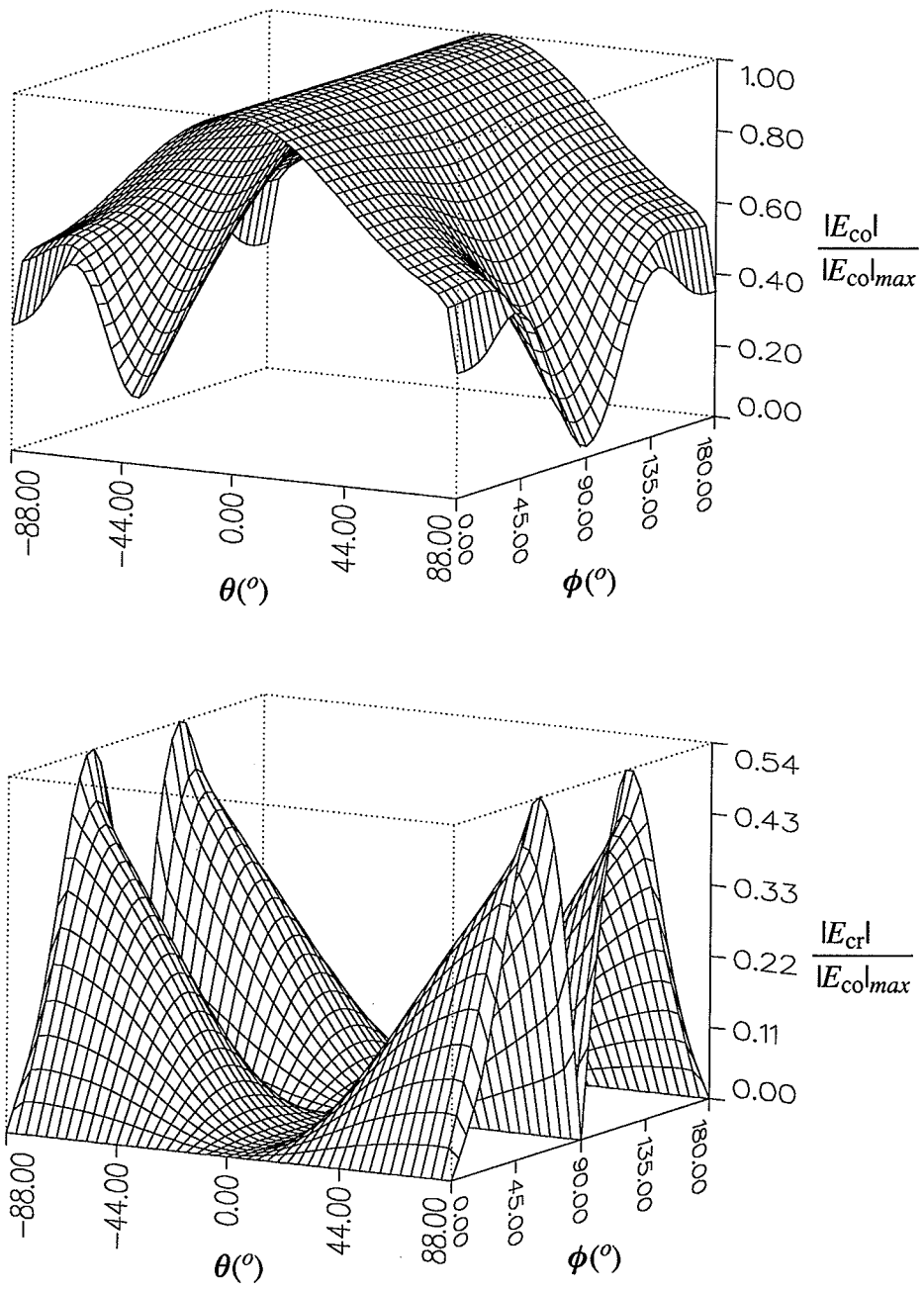

(a) Radiation patterns in the forward direction

Fig.6.5. Radiation field patterns of the rectangular patch.

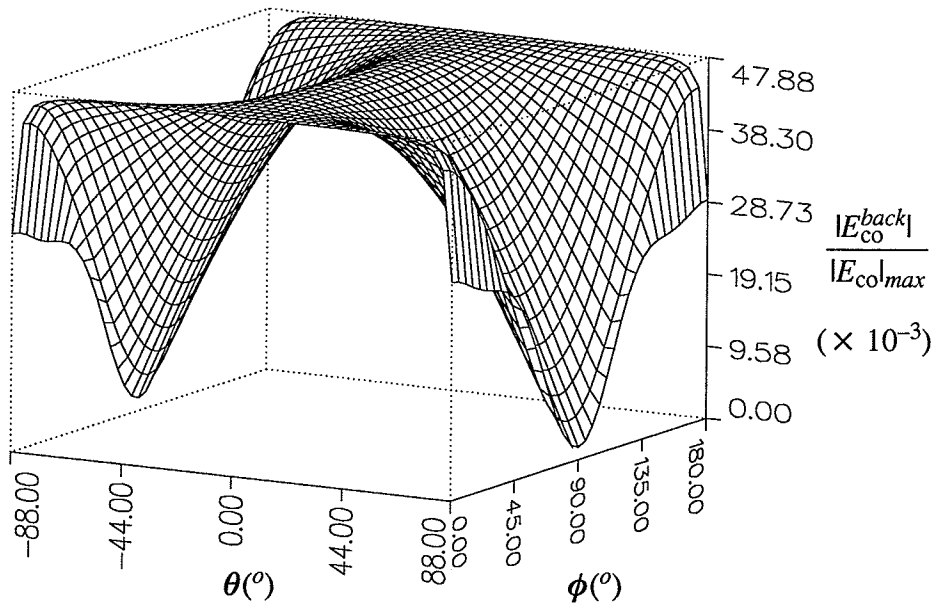

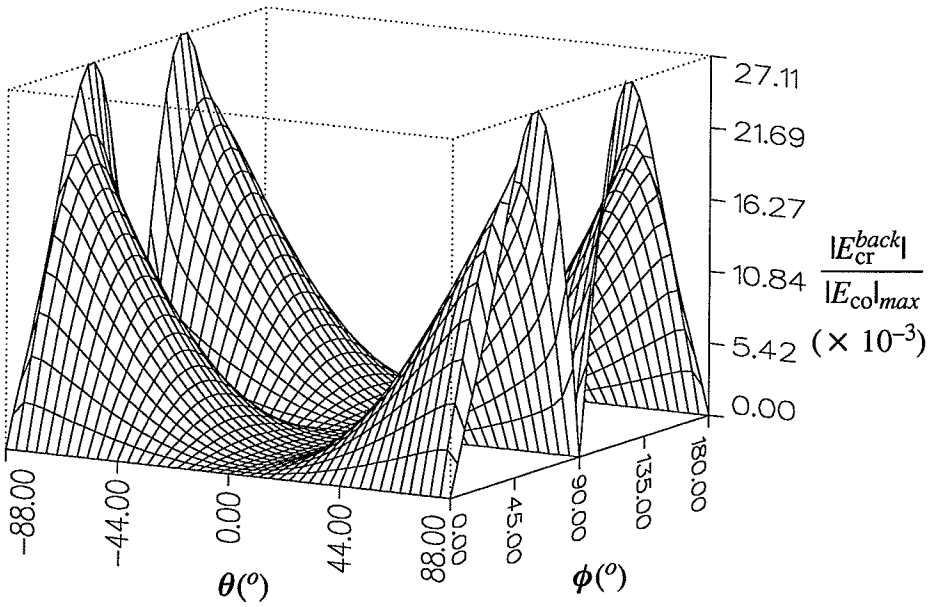

(b) Backward slot radiation patterns

Fig.6.5 (continued)

6.2 Parameter Studies of Rectangular Patch and Aperture

In this section, effects of various parameters on aperture coupled microstrip antenna performances are studied for a rectangular patch fed by a rectangular coupling aperture.

6.2.1 Open end stub length of the feedline

The effect of the open end stub length on the input impedance of antenna is studied in Fig.6.6. It shows that it affects only the input reactance, but not the bandwidth, of the antenna. When the stub length is changed, there is almost no change in the input resistance. The reactance curve, on the other hand, moves up or down with the stub length, but its derivative with respect to the frequency remains unchanged.

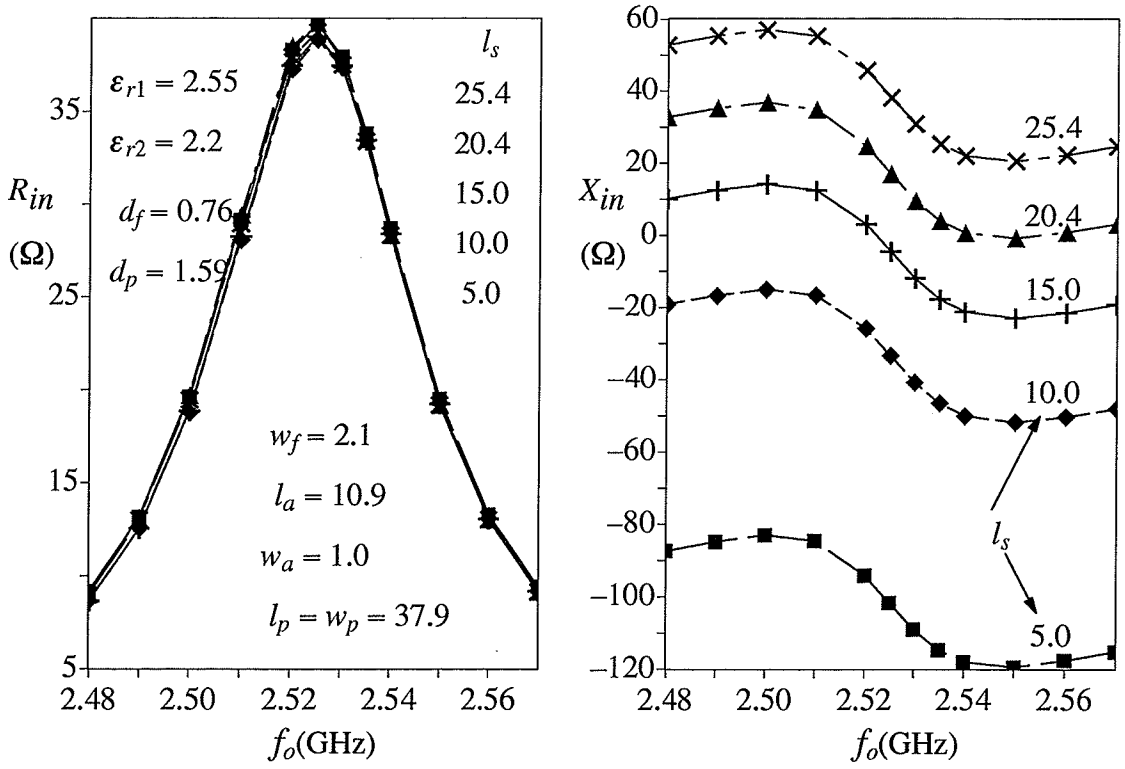

Fig.6.6. Effects of the open end stub length

6.2.2 Displacement of the coupling aperture

The coupling aperture is often shifted from the center of the patch as shown in Fig.6.7 to adjust input impedance of the antenna[49]. However, this results in an asymmetric excitation and as shown in Fig.6.8, it increases the relative magnitude of the transverse current distribution, i.e., the cross–polar current, on the patch. As a result, the cross polarization of the far field also increases. For a symmetric excitation, i.e., a centrally located aperture, the cross–polarization shown in Fig.6.9a is identically zero in the principal planes and the broadside. As shown in Fig.6.9b, shifting the coupling aperture along the symmetric x–axis, does not affect the cross–polarization. However, for a shift along the asymmetric y–axis, the cross–polarization in the principal planes become non–zero. They are shown in Fig.6.9c for a y–axis shift and in Fig.6.9d for a combined x– and y– shift of the aperture. The latter results show non–vanishing cross–polarization in both principal planes and along the broadside. Therefore, the centered coupling aperture will give the best cross polarization performance as long as the linear polarization is concerned.

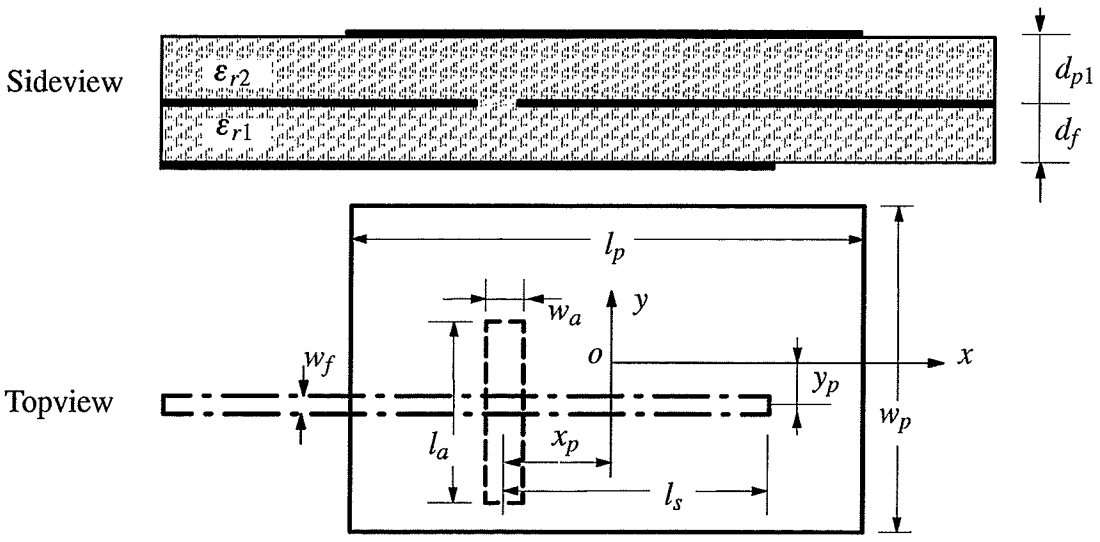

Fig.6.7. A rectangular patch with displaced coupling aperture

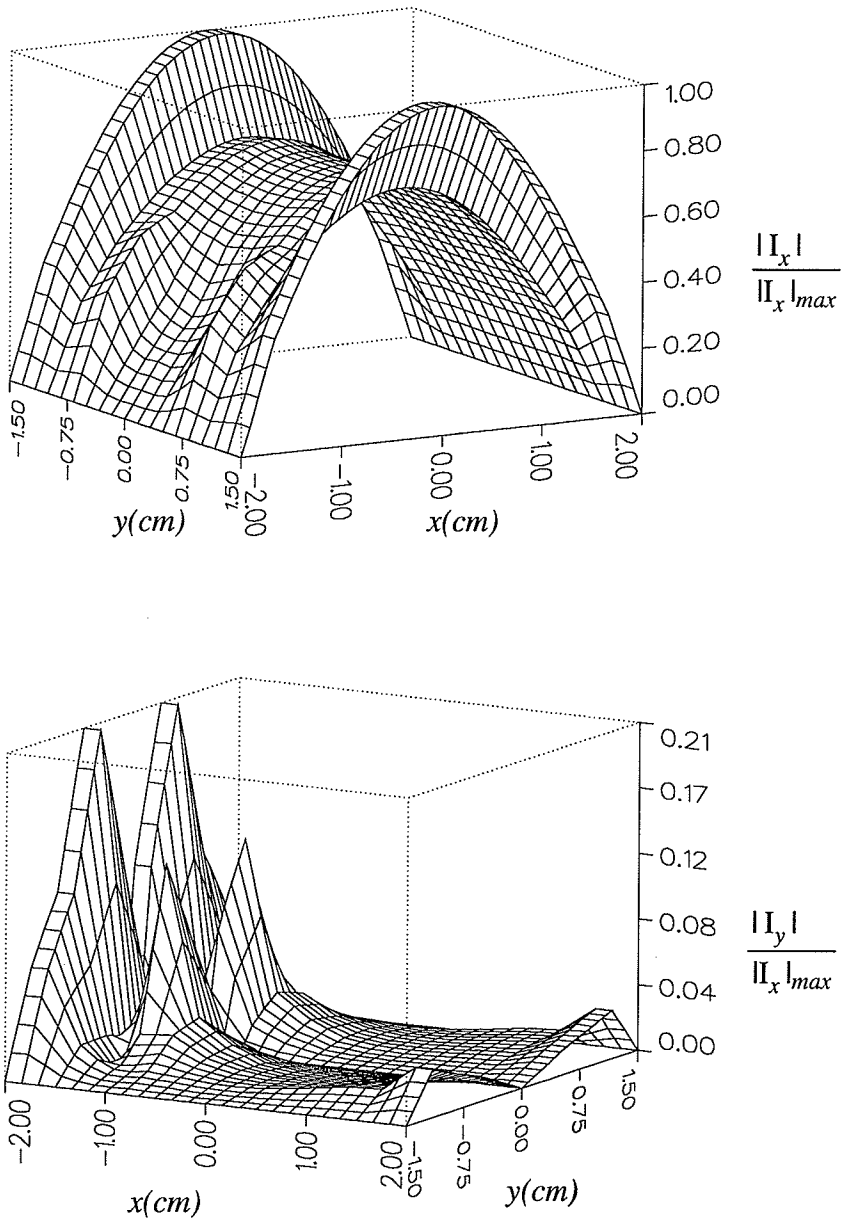

(a) aperture shifted along x–direction: $x_p = 1.5$ cm, $y_p = 0$

Fig.6.8. Effects of coupling aperture position on patch current distribution.

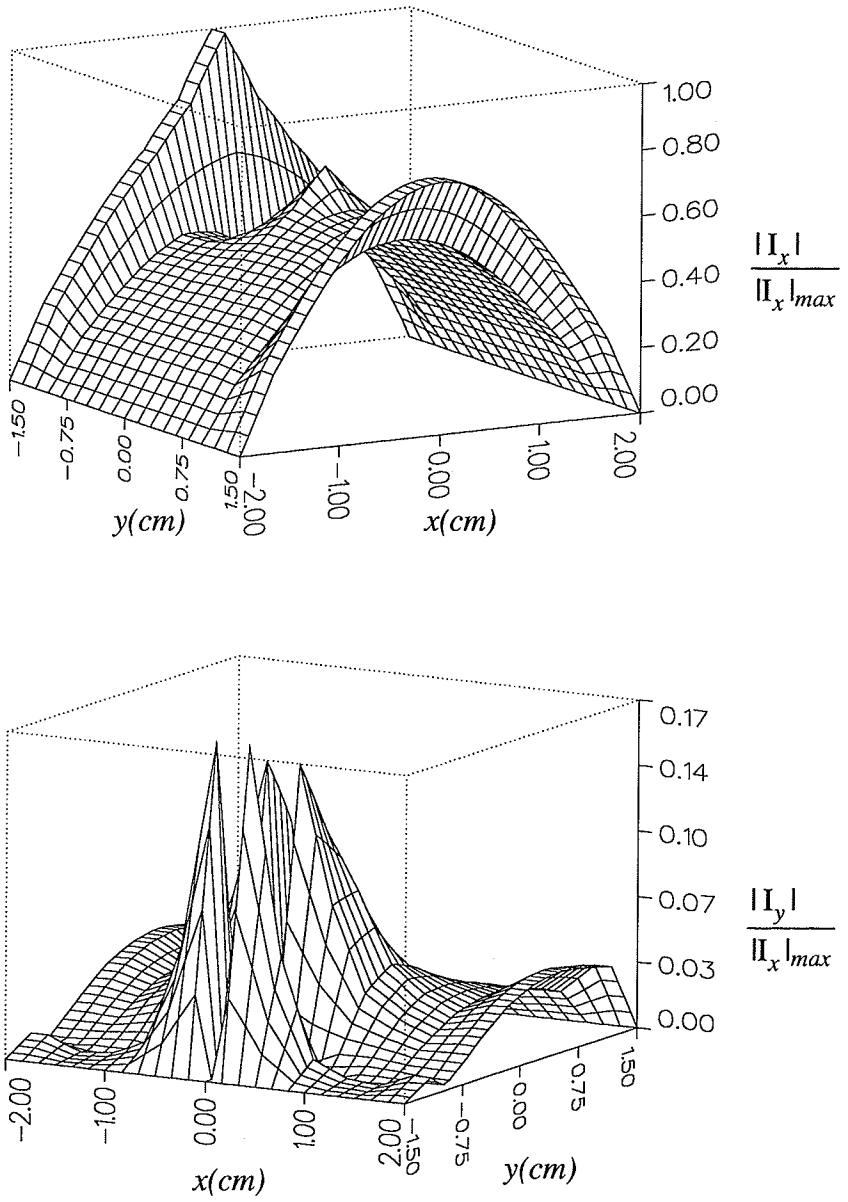

(b) aperture shifted along y–direction: $x_p = 0, \quad y_p = 0.8\ cm$

Fig.6.8 (continued)

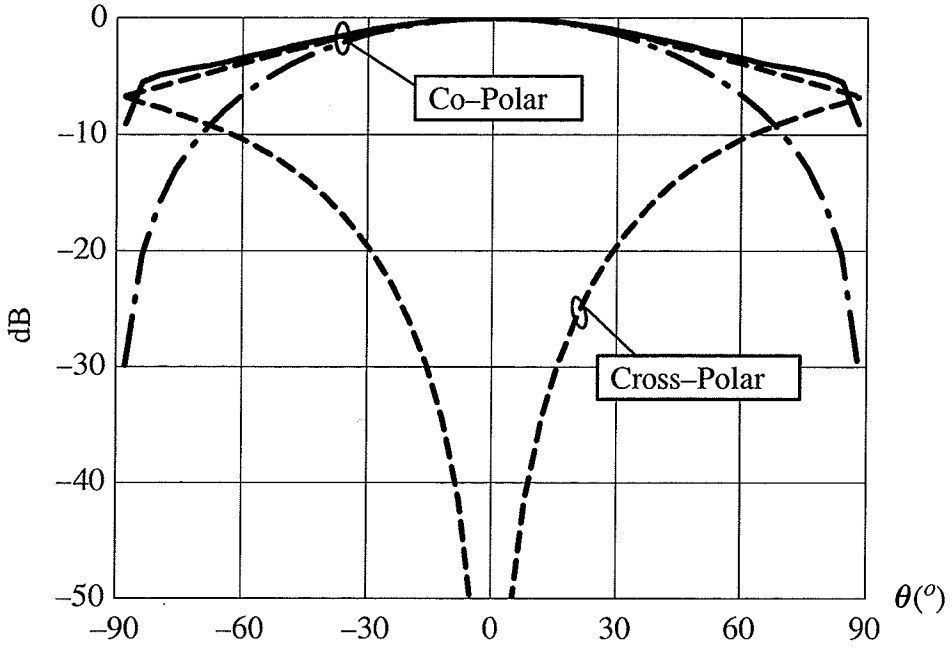

(a) centered aperture: $x_p = 0,\ \ y_p = 0$

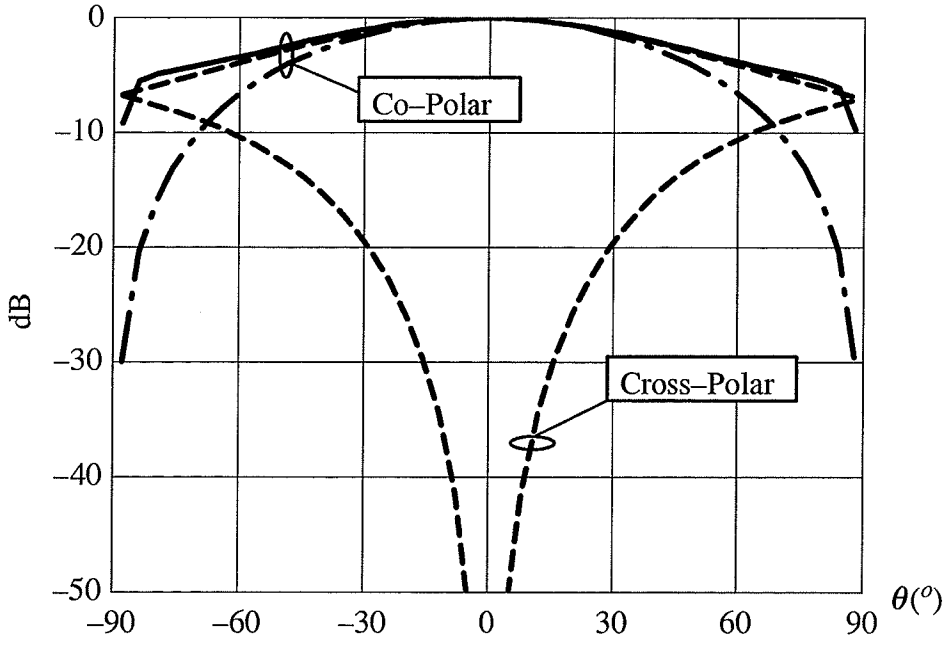

(b) aperture shifted along x–direction; $x_p = 1.5$ cm , $y_p = 0$

Fig.6.9. Effects of coupling aperture position on radiation performance.

——— $\phi = 0^o$, – – – – $\phi = 45^o$, —·— $\phi = 90^o$

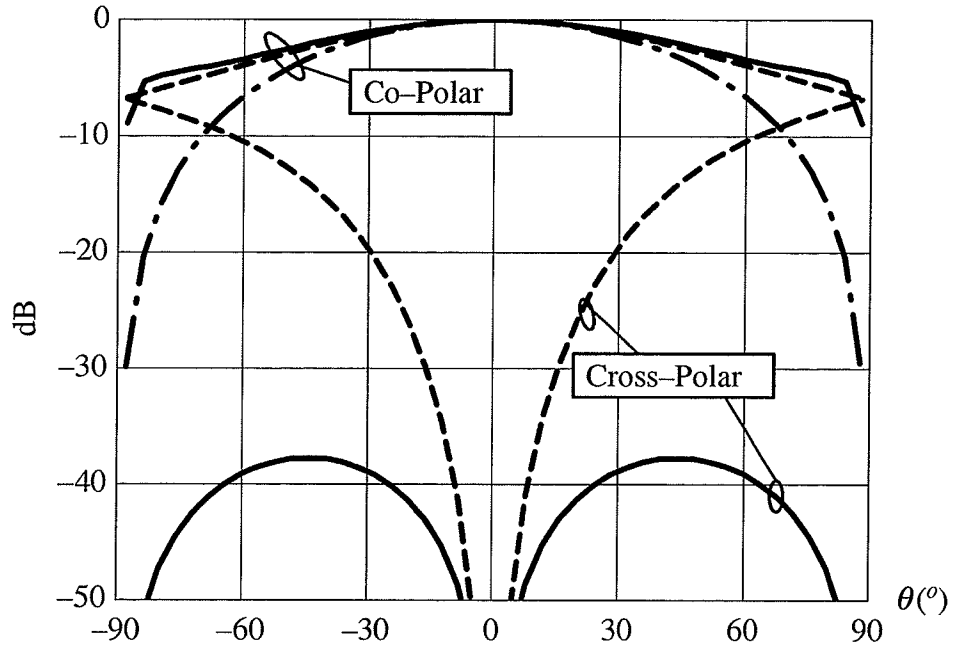

(c) aperture shifted along y–direction: $x_p = 0$, $y_p = 0.8$ cm

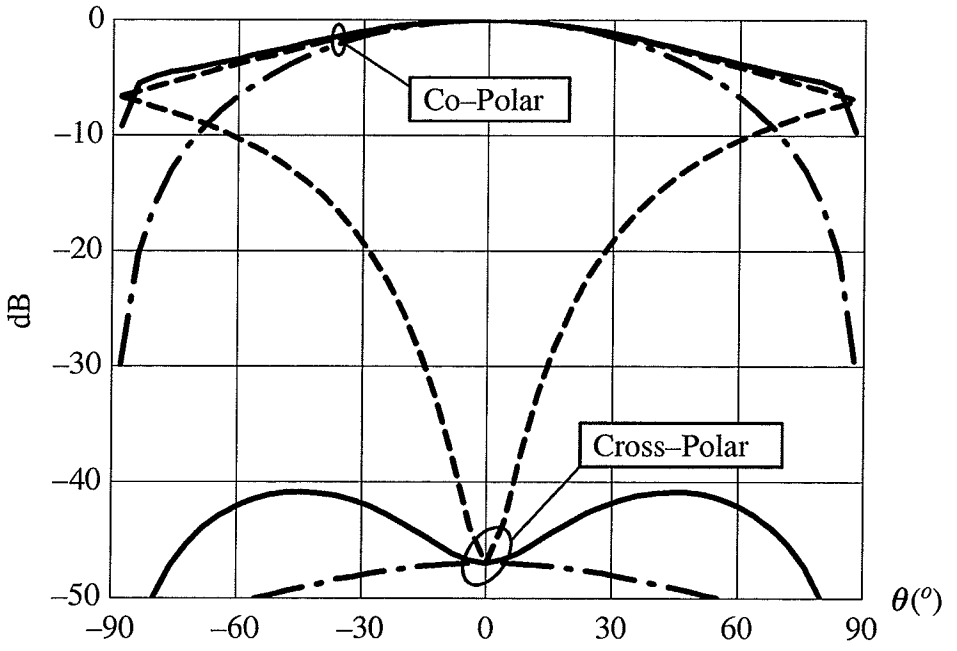

(d) aperture shifted along both x– and y–direction: $x_p = 1.5$ cm , $y_p = 0.8$ cm

Fig.6.9 (continued)

6.2.3 Size of the coupling aperture

The coupling between the patch and feedline can be adjusted by changing the size of the coupling aperture. The computed input impedance values for different coupling aperture widths are compared in Fig.6.10. Both input resistance and reactance increase with the aperture width, but the operating frequency decreases. As expected the back radiation also increases with the slot width. This is shown in Fig.6.11, which shows the back radiation being nearly proportional to the slot width.

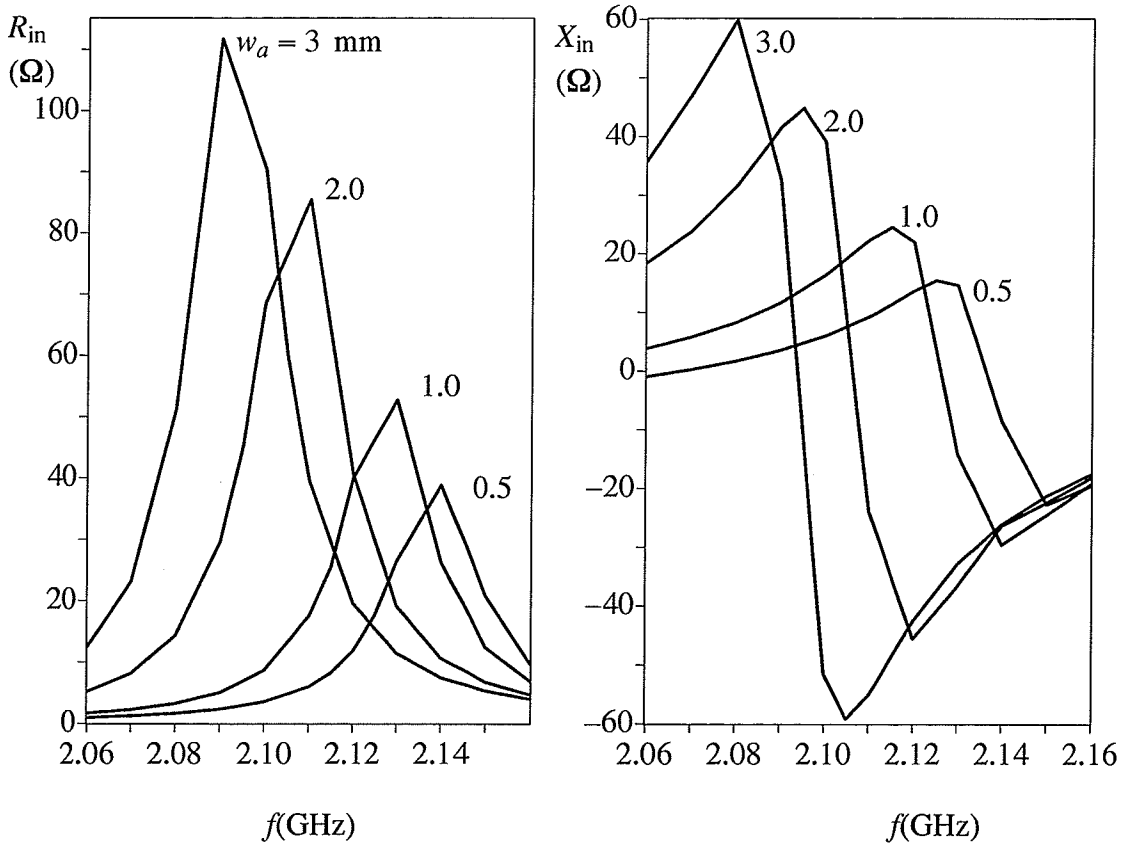

Fig.6.10. Effects of coupling aperture width on input impedance.
($\varepsilon_{r1} = \varepsilon_{r2} = 2.54$, $d_f = d_p = 1.6$ mm , $w_f = 4.4$ mm ,
$l_s = 2.0$ cm , $l_a = 1.2$ cm , $l_p = 4.2$ cm , $w_p = 3$ cm)

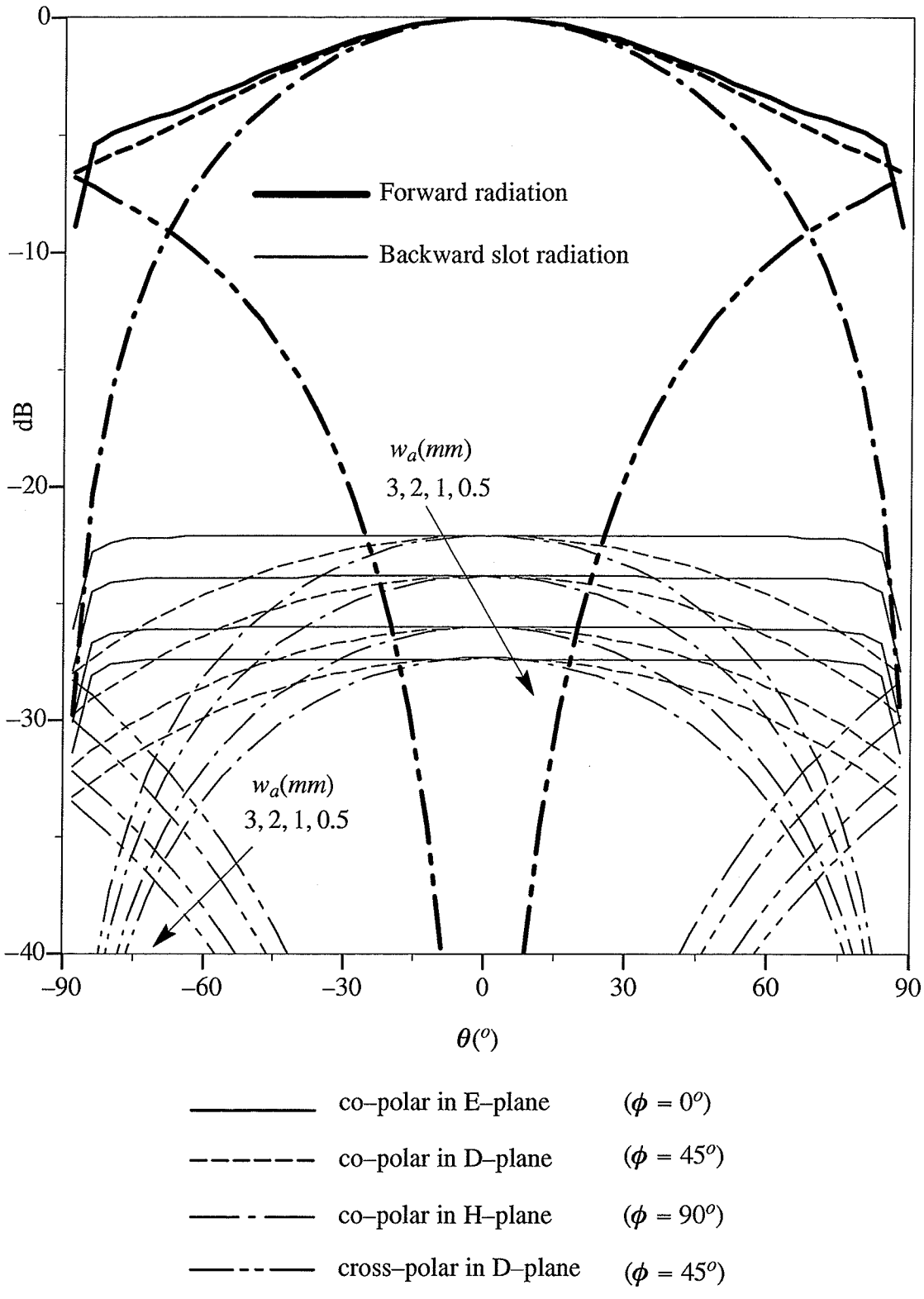

Fig.6.11. Effects of coupling aperture width on radiation performance.

6.3 Other Shapes of Coupling Apertures and Radiating Elements

6.3.1 End and center loaded coupling apertures

To study the effects of the coupling aperture shape on the antenna parameters, two configurations of Fig.6.12 are selected. The computed input impedances are shown and compared with results of $w_a = w_{ac}$ in Fig.6.13. It shows that for these irregular coupling apertures, the coupling efficiency is high, and results in an increase in the transverse electric surface current. This means that the slot transverse dimension should not be too large, otherwise the cross polarization of the far field in the direction away from the broadside will increase. The backward radiation may also change when the shape of the coupling aperture is changed.

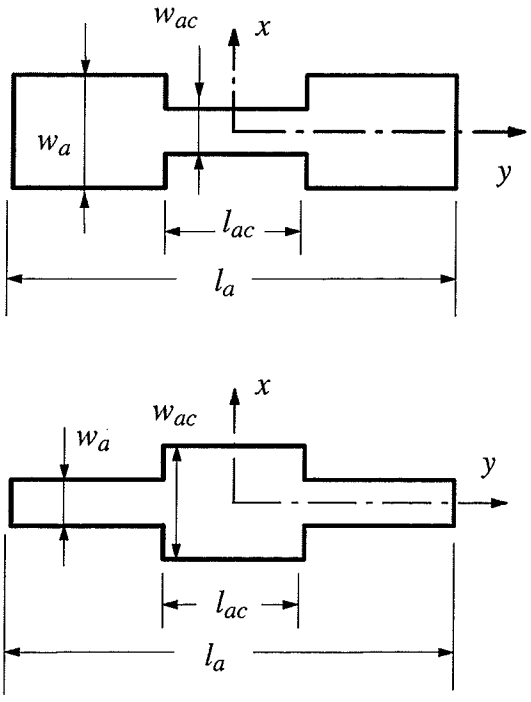

Fig.6.12. End and center loaded coupling apertures

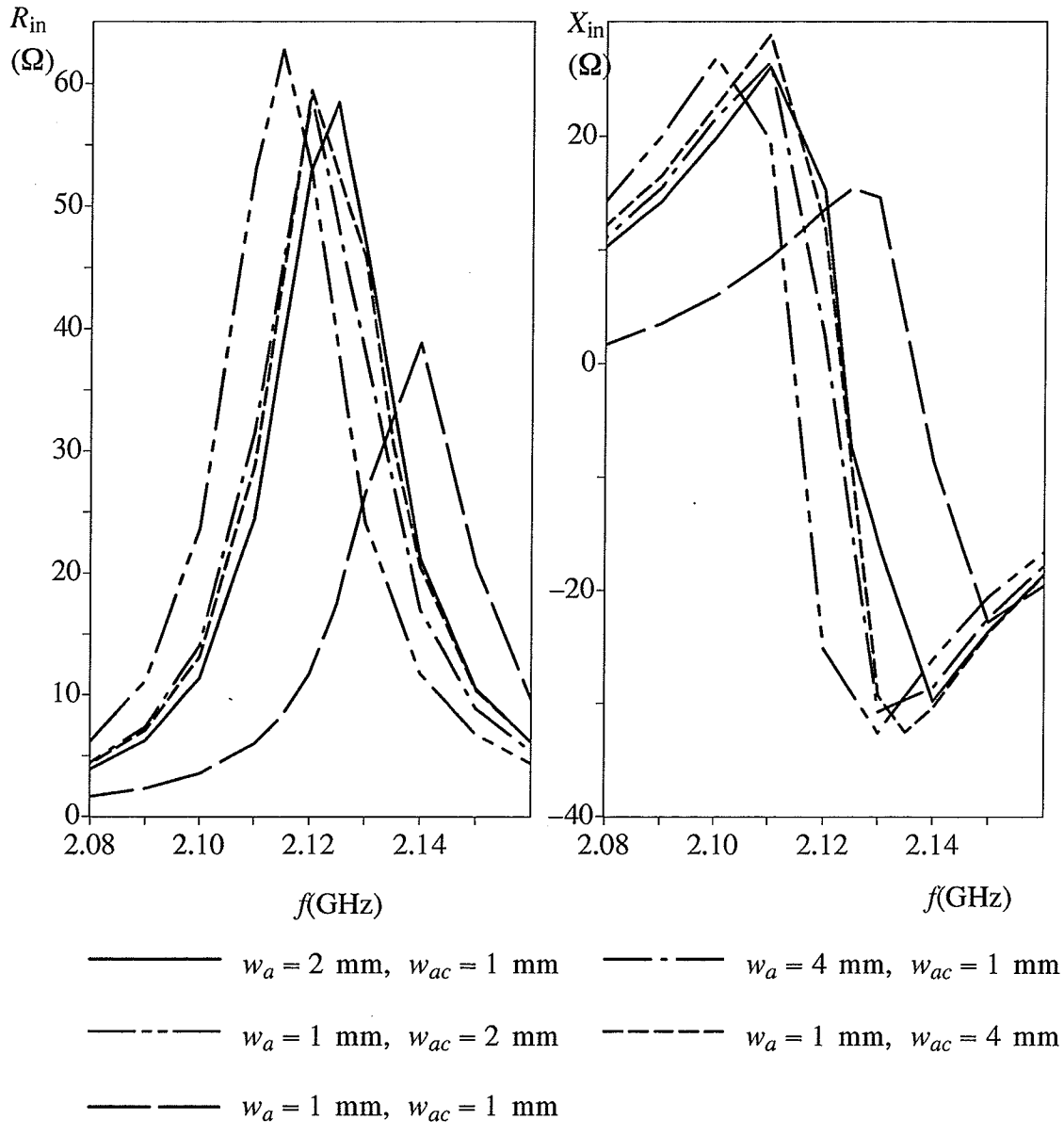

Fig.6.13. Input impedance for different aperture shapes ($l_{ac} = l_c/3$).
(other parameters are the same as in Fig.6.10)

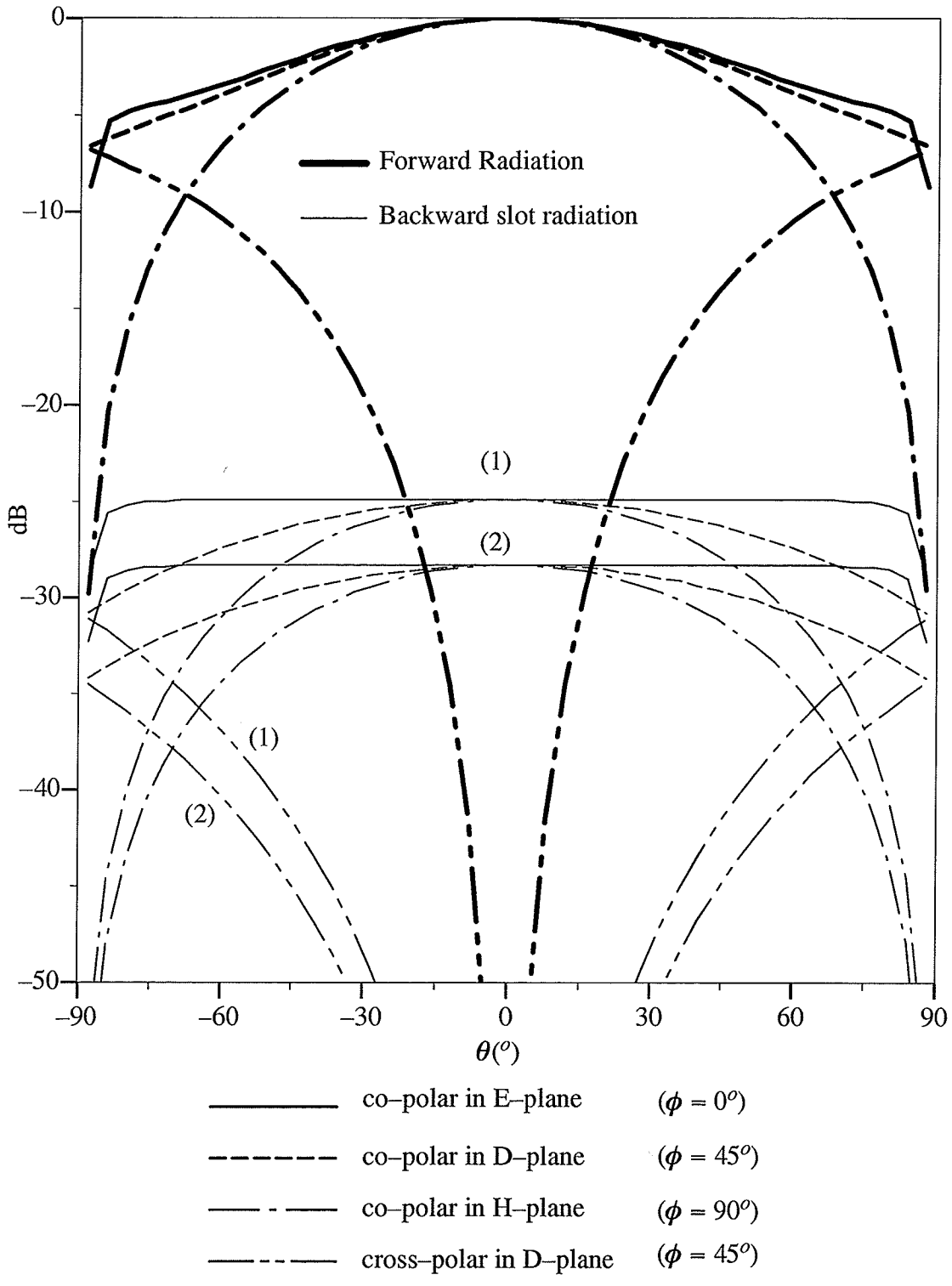

Fig.6.14. Effects of coupling aperture shape on radiation performance.

6.3.2 Loop antennas

The loop antenna can be used in arrays to improve aperture distribution or add symmetry to polarization. When the circumference of the circle is $2\pi r = \lambda_g$, the loop is equivalent to two dipoles excited in phase. The electric current distributions of a single loop (at f=5.4 GHz) and twin loops (at f=5.6 GHz) are shown in Fig.4.

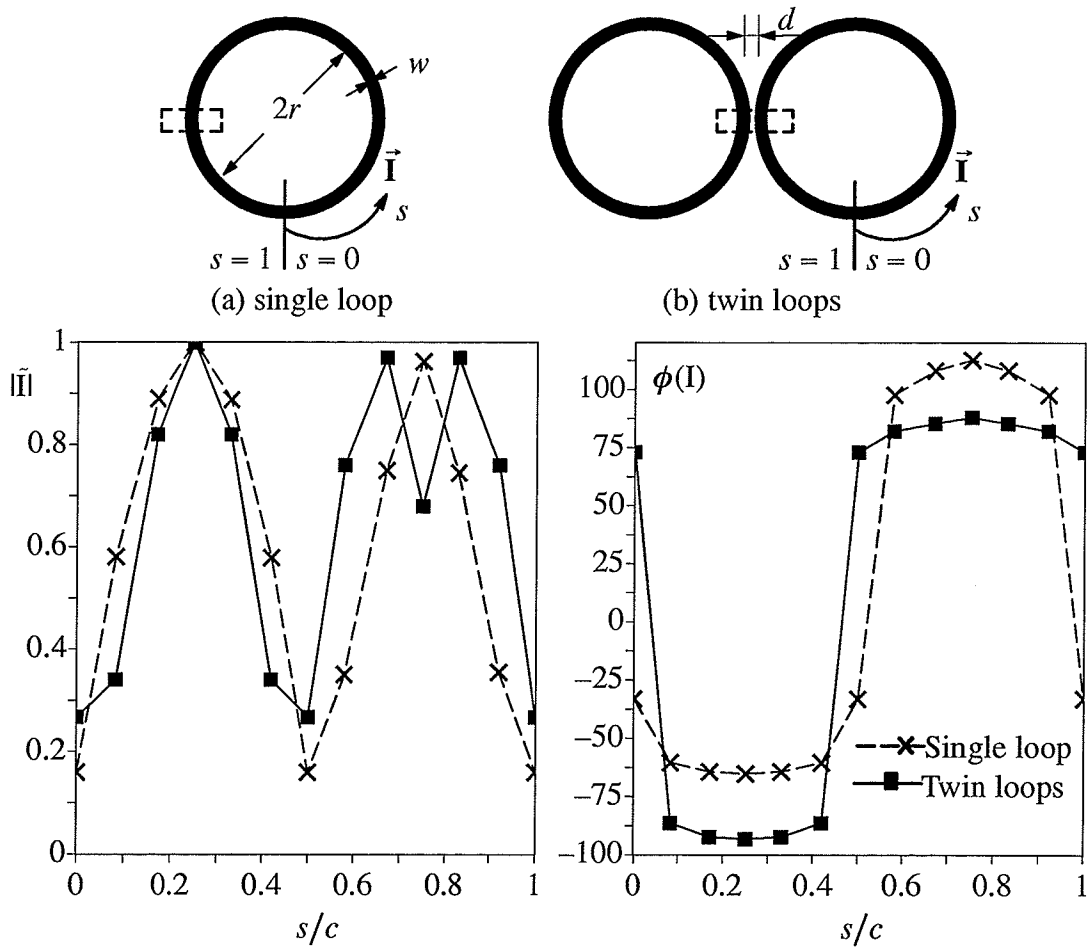

(a) single loop (b) twin loops

(c) Normalized magnitude distributions (d) Phase distributions

$c = 2\pi r = 80$ mm $w = 0.5$ mm $d = 0.1$ mm

Fig.6.15. Electric current distributions of loops.

6.3.3 Triangular elements

Other shapes of radiating elements may also be used in the aperture coupled microstrip antennas. For example, the input impedance for an equilateral triangle patch fed with a rectangular coupling aperture as shown in Fig.6.16a is presented in Fig.6.16b. It shows similar performance as a rectangular patch as shown on the same figure for comparison, although cross polarization may be higher for the triangle patch.

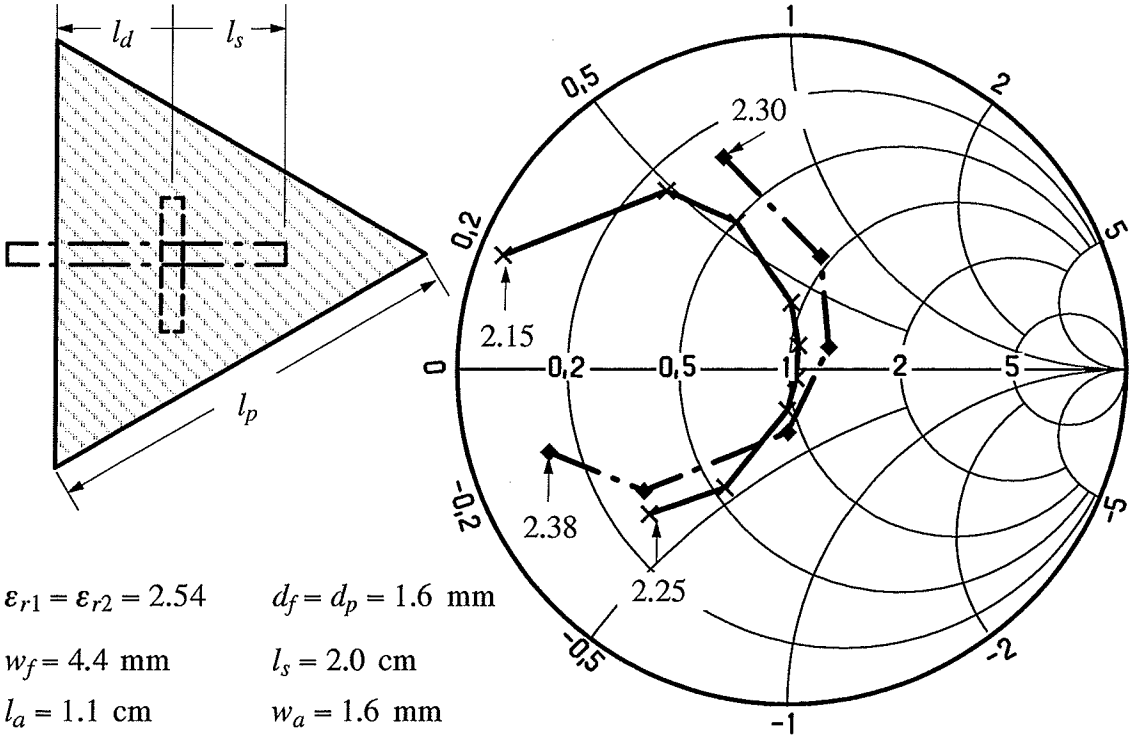

(a) an equilateral triangular patch (b) input impedance

Fig.6.16. Performance of aperture coupled triangular patch

6.4 Design Considerations

The design of aperture coupled microstrip antenna is similar to that of other types of microstrip antennas. As it was discussed before, the shape, size and position of the coupling aperture can be used to adjust the antenna performance, that is, more parameters are needed to be determined in the design. In this section, design considerations for a regular aperture coupled microstrip antenna are presented.

The first step is to select the shapes of both radiating element and coupling aperture. For a linearly polarized antenna, a rectangular patch and rectangular coupling aperture should be adopted to achieve the lowest cross polarization. For the patches, other shapes such as triangular, may also be chosen to reduce its area, assuming that higher cross polarization level can be tolerated. For the circular polarization, both square and circular patches are the natural choices. The coupling aperture can be a single or two rectangular slots.

Usually, the types and thickness of the dielectric substrates are determined by other considerations. For the antenna, thicker substrates with lower dielectric constants are preferred, while for the feedline, thinner substrates with higher dielectric constant are selected.

The second step is to determine the dimensions and positions of the feedline, coupling aperture, and patch. The width of the feedline is determined by the required characteristic impedance. The length of the open end stub can be used to adjust the reactance of the antenna. Its initial lengths plus the end effect should be around $\lambda_g/4$, where λ_g is the wavelength of the feedline. The patch can be designed as in a regular microstrip antenna. However, the width of the patch can always be used to adjust the resistance of the antenna at resonance. The coupling aperture is usually placed just above the feedline to maximize its coupling

and minimize the cross polarization. The length of the coupling aperture should be selected such that its resonance frequency is much higher than the operating frequency of the antenna. The width of the coupling aperture can be set around one to two tenth of its length. For the linear polarization, the coupling aperture should be perpendicular to the patch and the feedline. The aperture should be placed beneath the center of the patch in order to reduce the cross polarization of the antenna. Even when a displacement from this center point of the coupling aperture is needed, such as for the impedance matching in an array, it should be done along the symmetry plane of the patch in the longitudinal direction.

Chapter 7 BANDWIDTH ENHANCEMENT TECHNIQUES FOR PRINTED ANTENNAS

The narrow bandwidth is one of the major disadvantages of microstrip antennas. Consequently, several techniques have been developed to increase their bandwidth. One technique uses low dielectric constant or thick substrates. This thick dielectric can be a single layer or multilayers as shown in Fig.7.1a, or a cover layer as shown in Fig.7.1b. This technique is simple but has limited applications. The dielectric type is often determined by other factors. A thick dielectric may excite higher order mode surface waves which cause a gain loss and increased spurious radiation and mutual coupling in the arrays. Other techniques use parasitic elements which can be stacked (Fig.7.1c) or made coplanar(Fig.7.1d) or be their combinations. In the stacked structure, an additional dielectric layer is needed, but this double layer structure increases the mutual coupling between the array elements. However, it does not increase the element size. In the coplanar structure, the thickness is not increased, but the out of phase mode[58] between the feeding patch and parasitic elements may be excited which decreases sharply the antenna directivity, and must be avoided.

In stead of large bandwidths, multi–frequency capability may also be expected in some applications, where the antenna is required to operate at several discrete frequency bands that are far from each other and narrow individually.

In this chapter, the wide bandwidth properties of subarrays composed of coplanar and stacked parasitic elements are investigated. Then, a dual frequency technique is proposed

for a single patch over a single layer substrate by simply slotting the radiating patch. Finally, techniques are proposed to achieve multi–frequency operation for aperture coupled microstrip antennas.

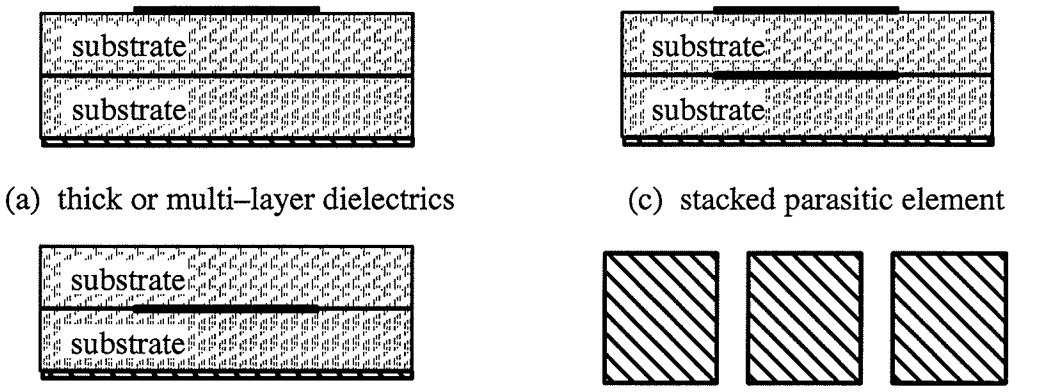

(a) thick or multi–layer dielectrics

(c) stacked parasitic element

(b) dielectric cover layer

(d) coplanar parasitic elements

Fig.7.1. Wideband techniques for microstrip antennas.

7.1 Coplanar Subarray of Parasitic Elements

The subarrays composed of coplanar parasitic elements have been used to widen bandwidth of probe fed microstrip antennas[58]. In this section, such subarrays fed by an aperture coupling[59] as shown in Fig.7.2a are studied to widen the antenna bandwidth. They offer an additional feature in a simplified feed network, where several elements can be fed by only one coupling aperture and the parasitic radiation from the aperture can be reduced.

It has been reported that a multi–frequency operation can be achieved if several elements of different sizes are fed directly by a single aperture[60], as in Fig.7.2b. However, this will increase the length of the coupling aperture and increase its parasitic and backward radi-

ations. Therefore, a subarray as shown in Fig.7.2c is considered here[59], where only one patch is fed directly by the coupling aperture and other elements are excited through electromagnetic coupling between them.

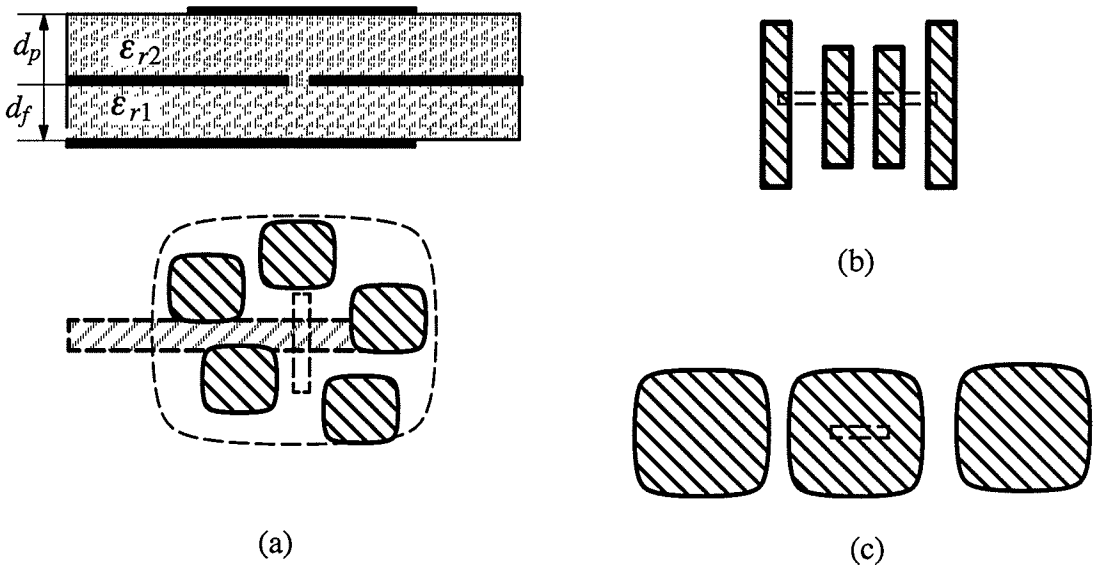

Fig.7.2. Coplanar aperture coupled microstrip subarray

The parasitic elements can be placed to form a linear subarray, as shown in Fig.7.3, or a cross subarray as in Fig.7.4. The input impedances for the linear and cross subarrays are shown in Fig.7.5. It shows that a wider bandwidth can be achieved by using parasitic elements in either linear or cross subarray. A cross subarray may have better bandwidth performance than a linear array. However, it should be noted that all subarrays have negative reactances, which can be eliminated by using a longer open end stub for the feedline as discussed earlier.

The radiation pattern of these subarrays are shown in Fig.7.6 and Fig.7.7. The directivity of the subarray is larger than that of a single patch as shown in the figure.

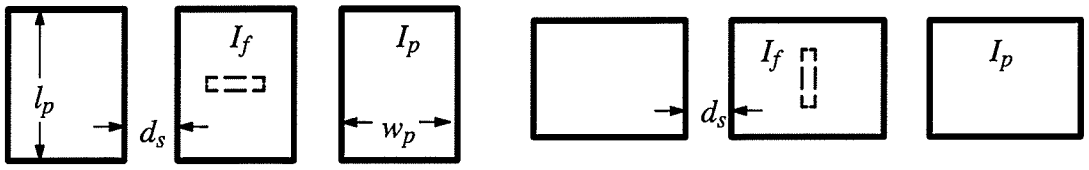

(a) 3–element H–plane subarray (b) 3–element E–plane subarray

Fig.7.3. Aperture coupled linear microstrip subarrays

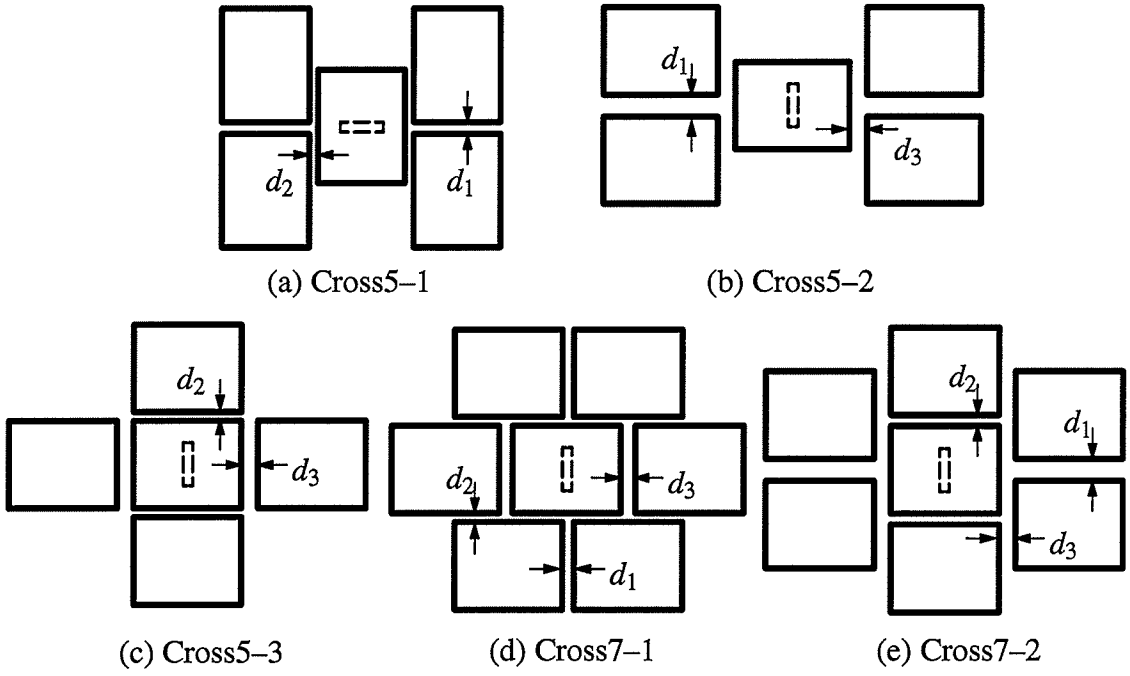

(a) Cross5–1 (b) Cross5–2

(c) Cross5–3 (d) Cross7–1 (e) Cross7–2

Fig.7.4. Aperture coupled cross microstrip subarrays

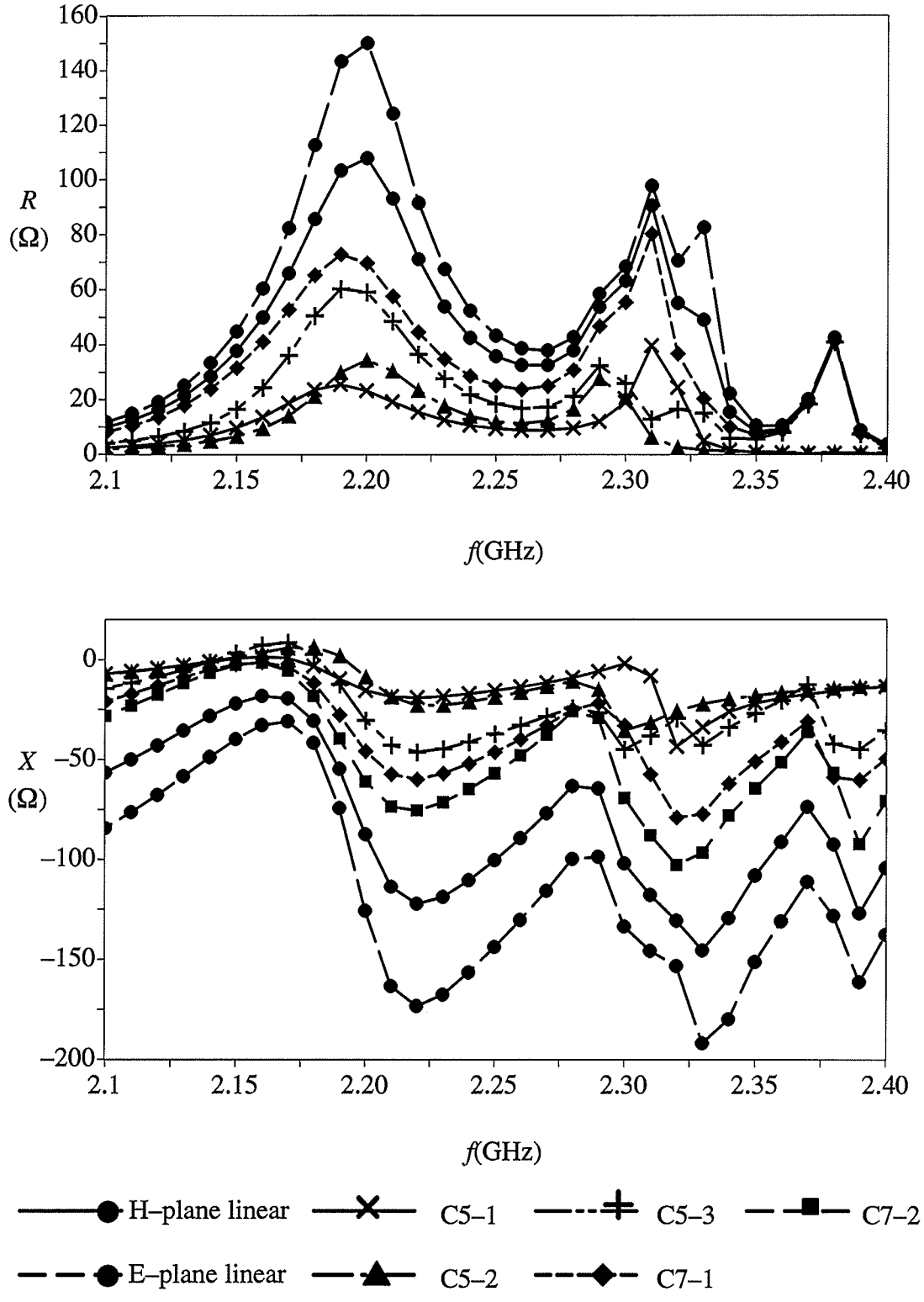

Fig.7.5. Input impedances of H– and E–plane linear and cross subarrays.

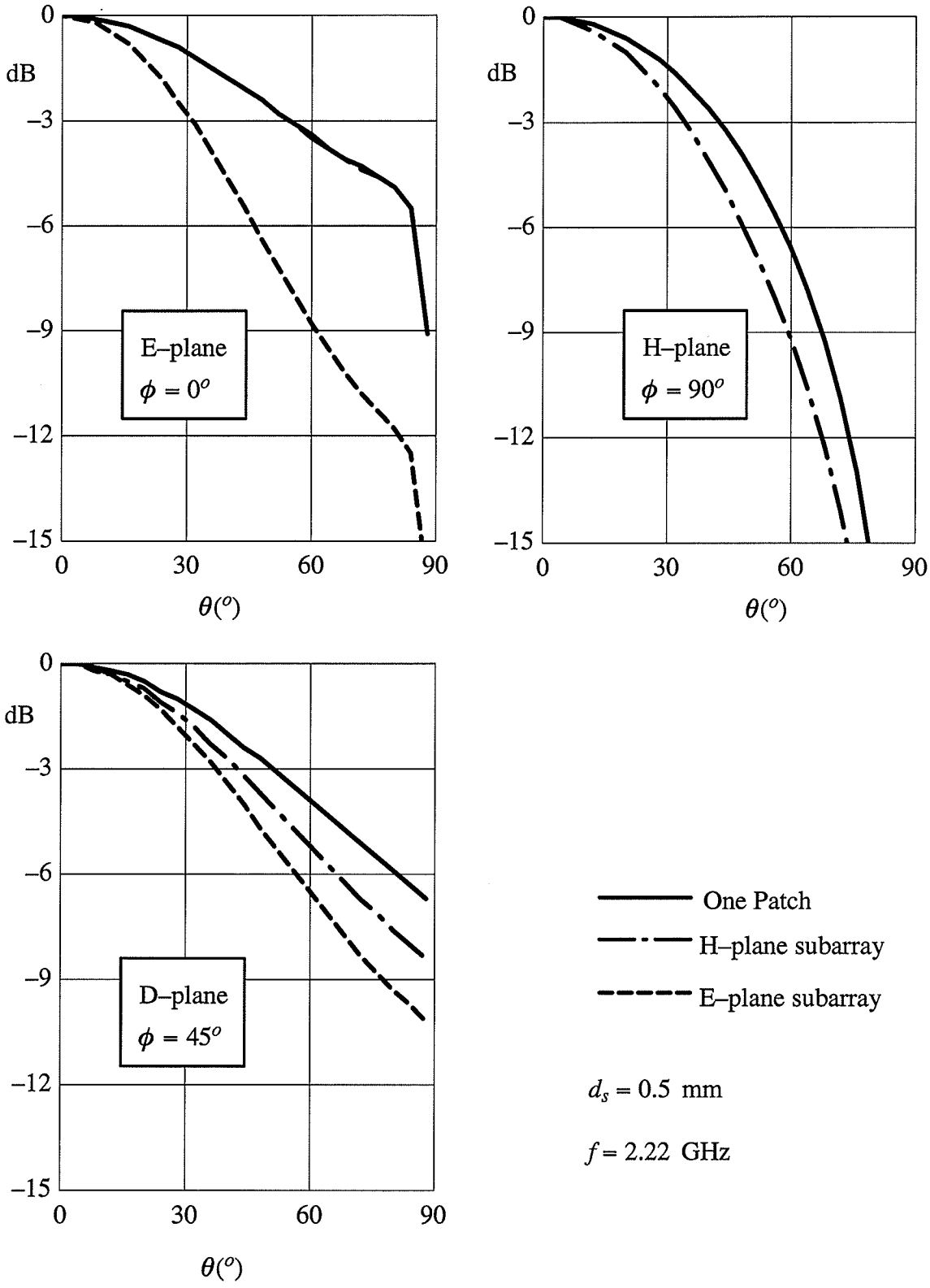

Fig.7.6. Radiation Patterns of H– and E–plane linear subarrays

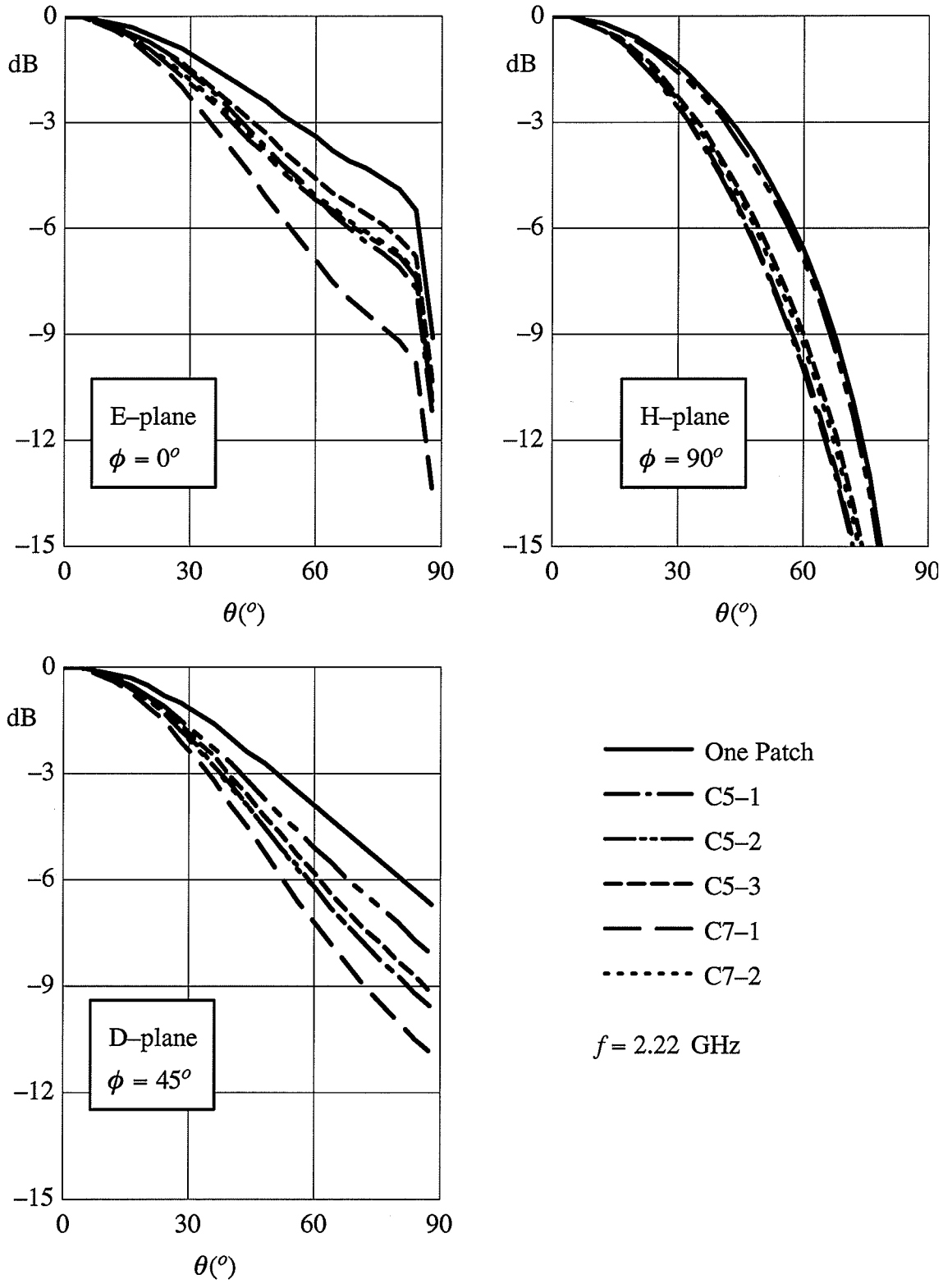

Fig.7.7. Radiation Patterns of cross subarrays

7.2 Stacked Parasitic Subarrays

The bandwidth of microstrip antennas can be increased by using stacked parasitic elements[61][62] as shown in Fig.7.8a. The two stacked patches are resonant at two different frequencies, and their coupling affects the bandwidth of the antenna. Results for one stacked structure is compared with the non–stacked case shown in Fig.7.8b.

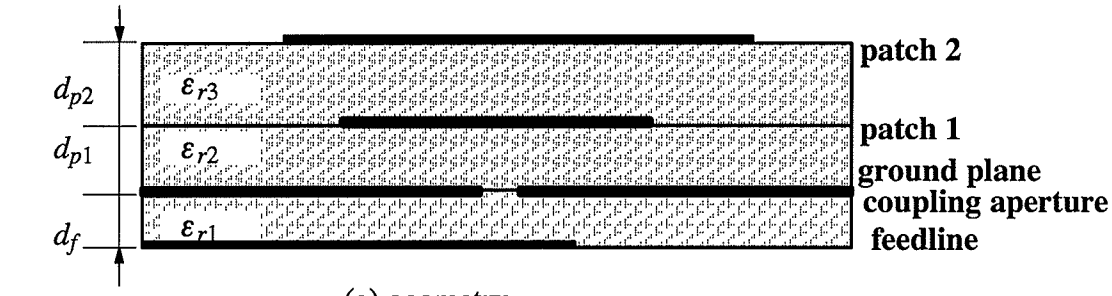

(a) geometry

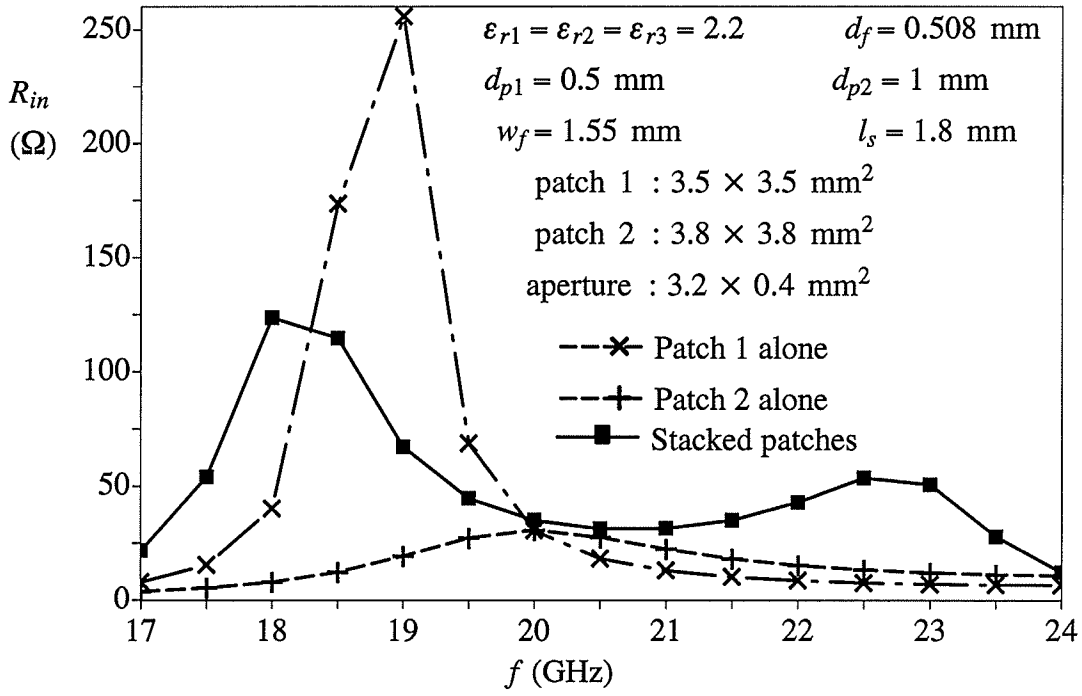

(b) characteristics

Fig.7.8. Characteristics of a stacked aperture coupled microstrip antennas

The stacked parasitic subarray in Fig.7.9 is formed by substituting patch 2 in the stacked antenna with a subarray. The characteristics of such subarray of probe feeding has been studied[63]. Here, characteristics of aperture coupling is studied. In Fig.7.10, input impedance of a subarray with four upper patches and one lower patch is presented.

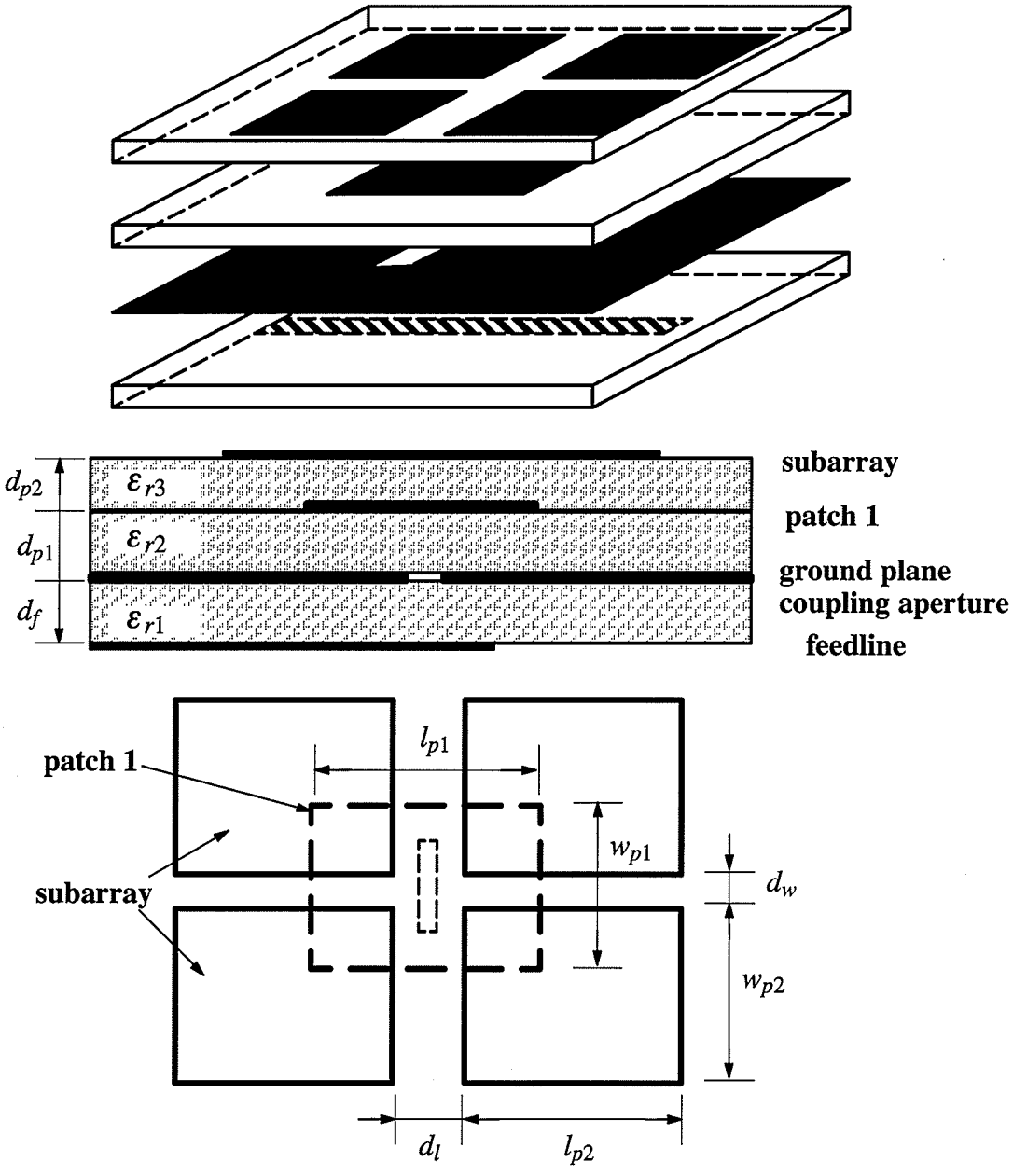

Fig.7.9. Stacked parasitic subarray fed by aperture coupling

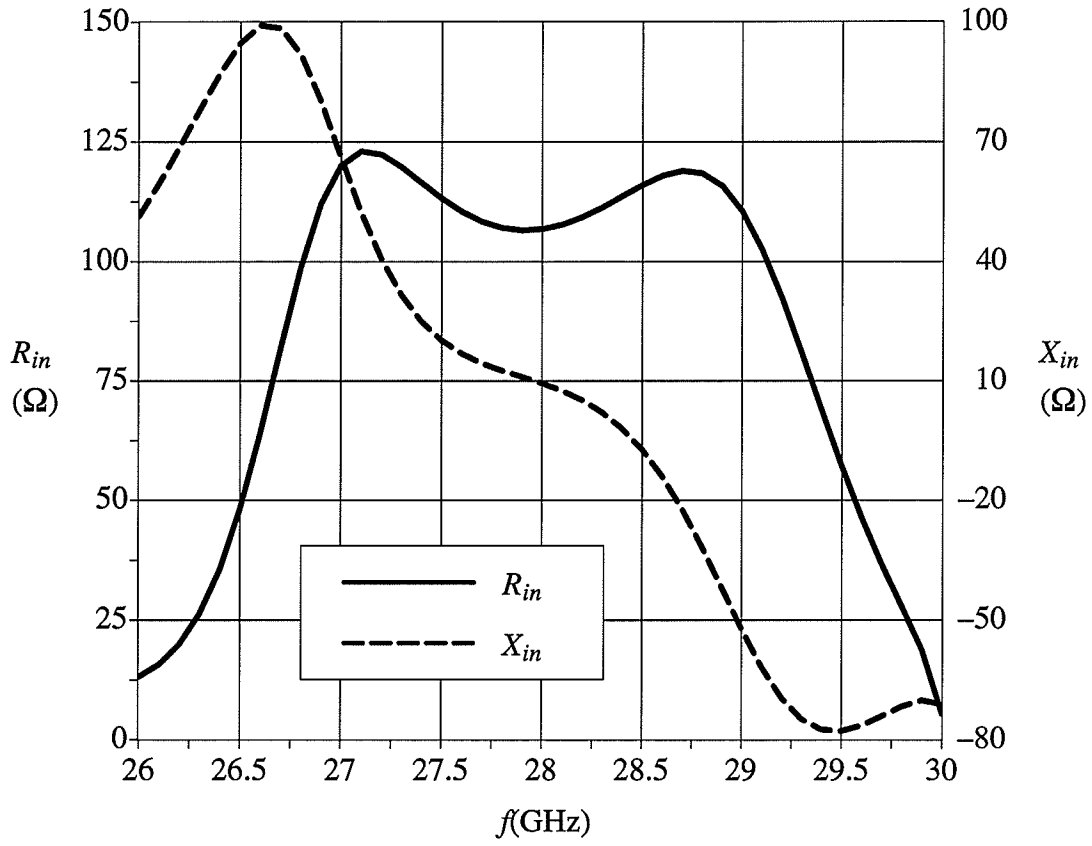

$\varepsilon_{r1} = 9.8$, $d_f = 0.254$ mm , $w_f = 0.27$ mm , $l_s = 0.9$ mm ,

$\varepsilon_{r2} = \varepsilon_{r3} = 2.5$, $d_{p1} = 0.254$ mm, $d_{p2} = 0.381$ mm,

$l_a = 1.8$ mm , $w_a = 0.35$ mm , $l_{p1} = 2.7$ mm , $w_{p1} = 5.3$ mm,

$l_{p2} = 2.4$ mm , $w_{p2} = 3.2$ mm, $d_l = 2.8$ mm , $d_w = 1.4$ mm .

Fig.7.10. Characteristics of stacked parasitic subarray

The radiation patterns of the antenna shown in Fig.7.9 and dimensions given in Fig.7.10 are evaluated and shown in Fig.7.11 for two different frequencies. Radiation patterns of individual parts of the antenna are also evaluated and ploted in the same figure to show their contributions to the radiation of the whole antenna.

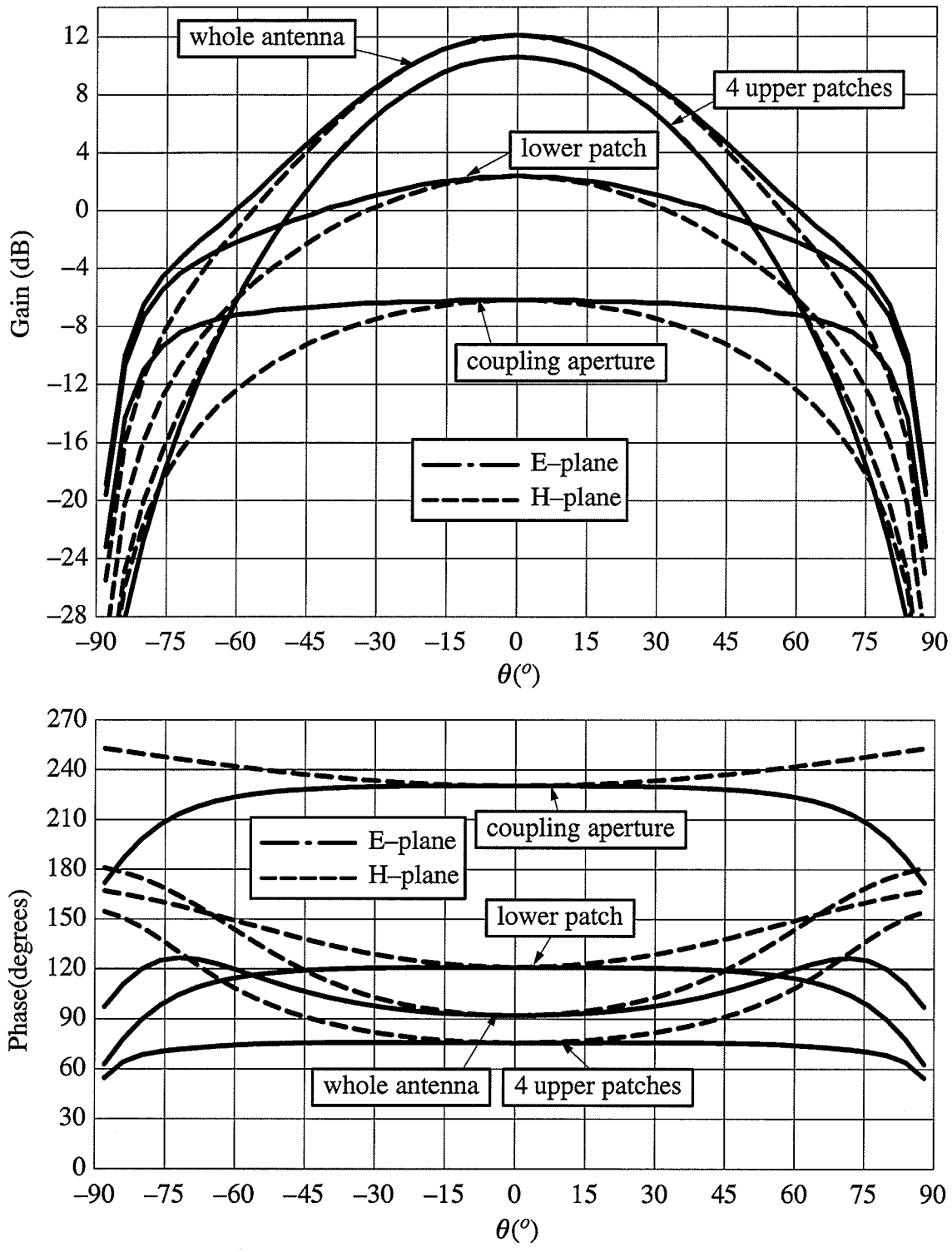

(a) f=28.4 GHz

Fig.7.11. Radiation patterns of antenna shown in Fig.7.9 and Fig.7.10.

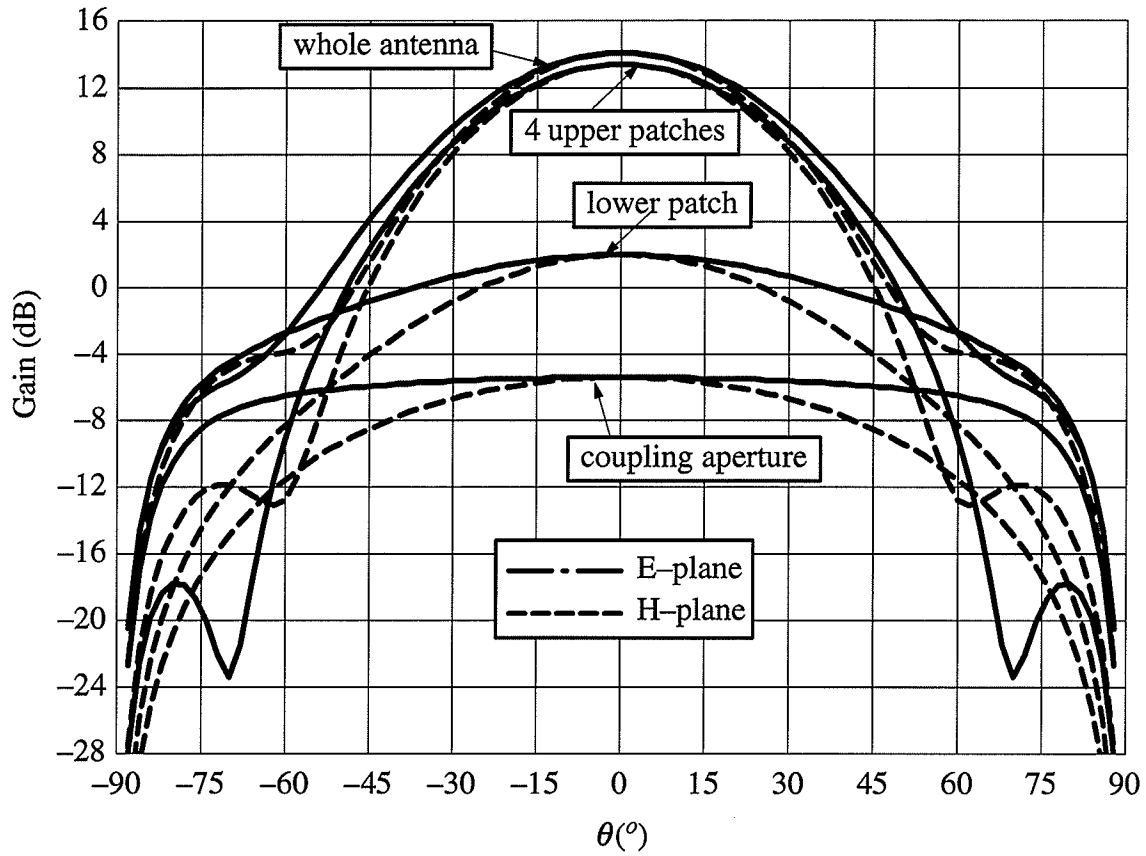

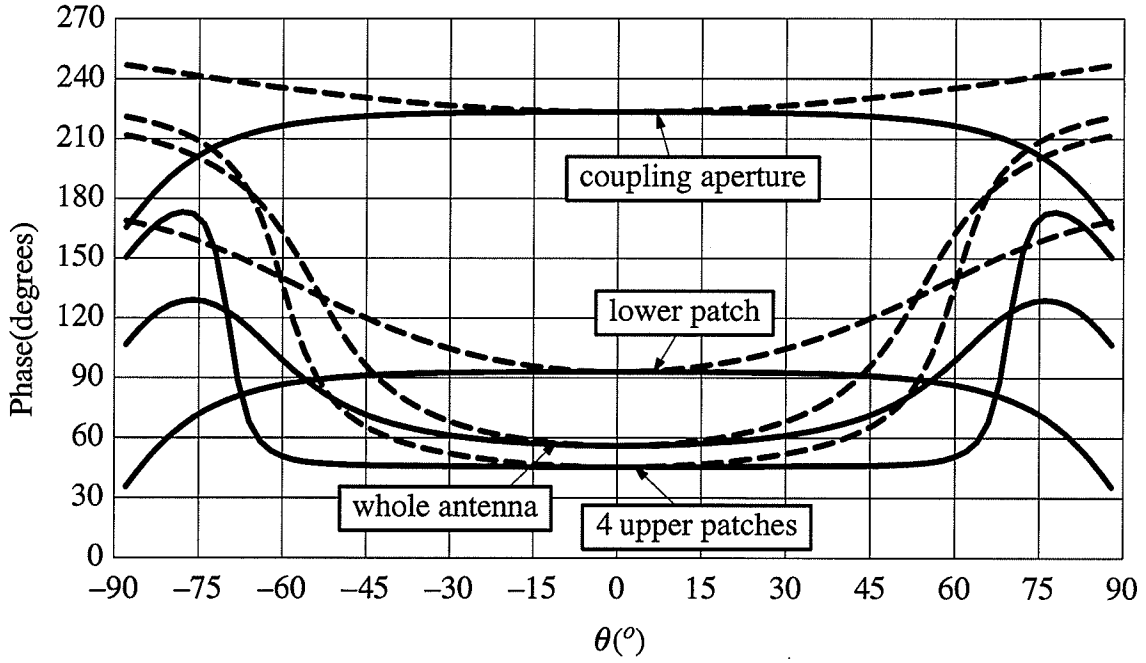

(b) f=29.5 GHz

Fig.7.11 (continued)

7.3 Dual Frequency Operation of Slotted Patches

The slotted patches, as shown in Fig.7.12, can be designed to achieve dual or multi– frequency operation[64][65]. The single centrally slotted patch will not be effectively excited and the shift of the slot from the center will increase the cross polarization. The double–slotted patch with two symmetric parts removed from the patch will be excited effectively. The bandwidth may be increased by selecting the dimensions so that the two lowest modes (the lowest mode of a regular patch and the lowest mode of a rectangular ring) couple to each other appropriately. The other feature of the slotted patch is that it may be used to tune the frequency of the antenna by changing the slot position or the area of the patch. The multi–frequency operation is possible by introducing additional slots on the patch.

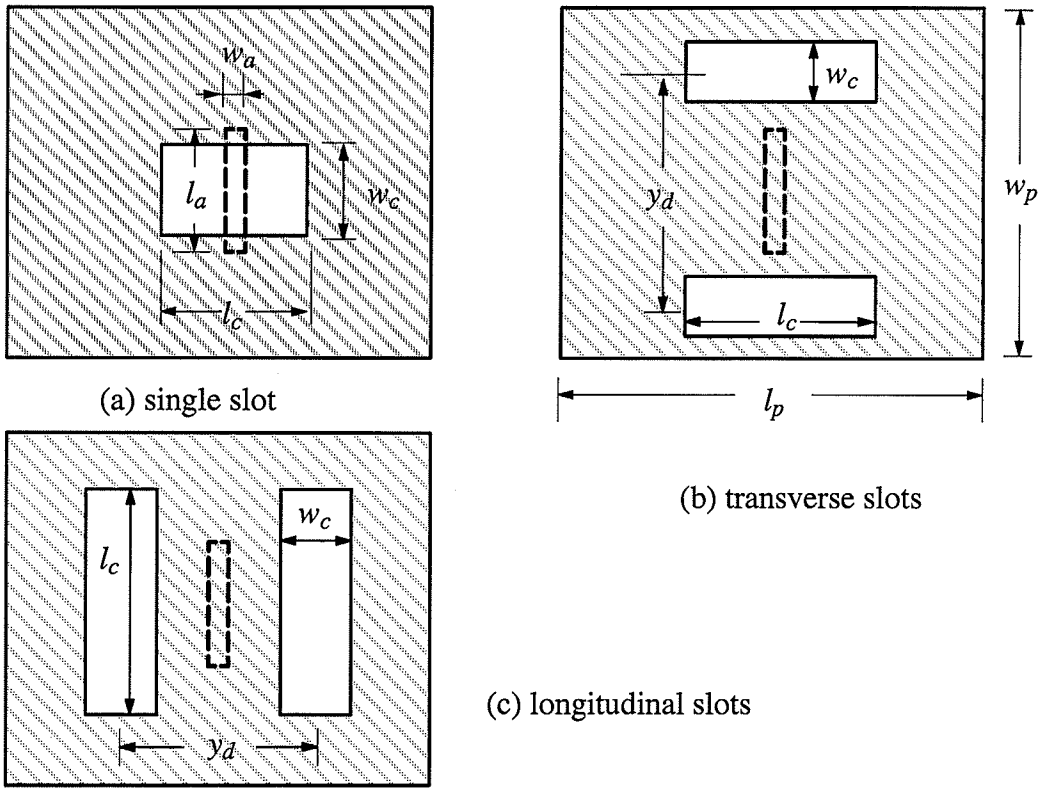

(a) single slot

(b) transverse slots

(c) longitudinal slots

Fig.7.12. Aperture coupled microstrip antennas with slotted patches.

The computed input impedance of the antenna of Fig.7.12c, is shown in Fig.7.13, which clearly shows two distinct resonant frequencies, and the upper resonance is in the vicinity of the patch resonance. Since the resonance frequencies are due to the coupling between the slots and the patch, they can be modified by the size, location and orientation of the slot, a property that was also confirmed by calculation.

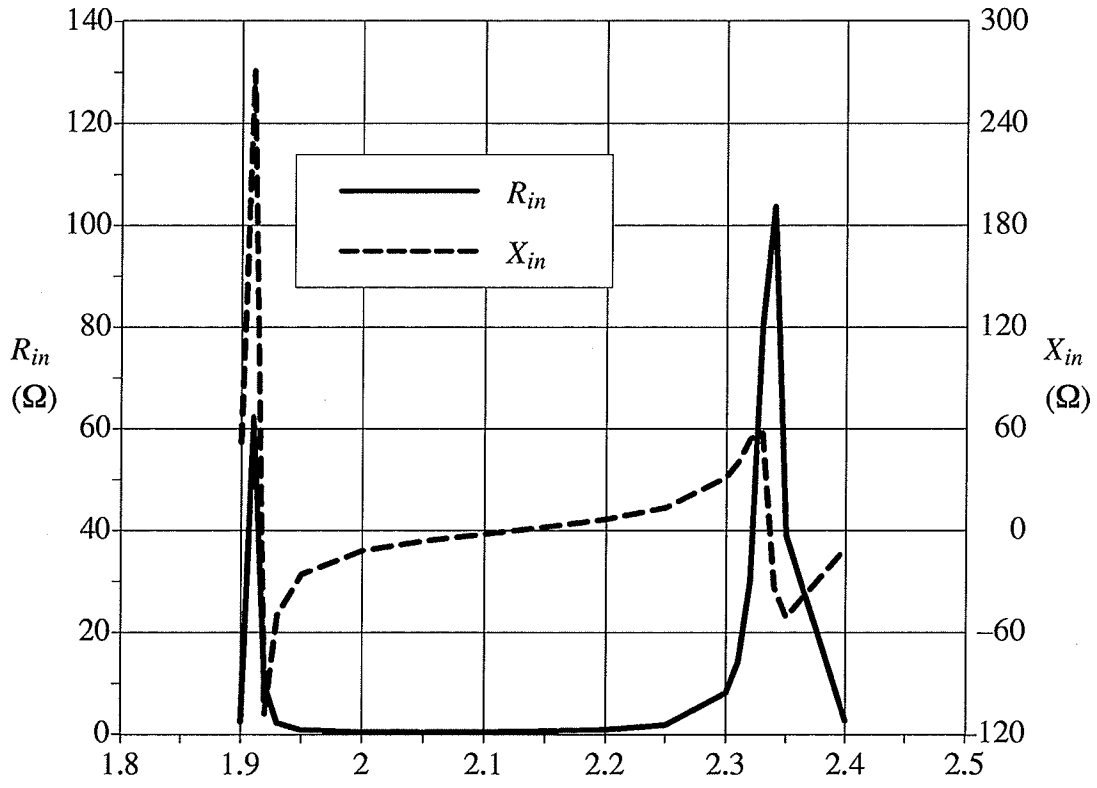

$\varepsilon_{r1} = 2.54$, $\varepsilon_{r2} = 2.33$, $d_f = d_p = 1.6$ mm , $w_f = 4.4$ mm ,

$l_s = 2.0$ cm, $l_a = 1.1$ cm, $w_a = 1.0$ mm , $l_p = 4$ cm, $w_p = 3$ cm ,

$w_c = 8$ mm, $l_c = 14$ mm, $y_d = 14$ mm .

Fig.7.13. Dual frequency operation of longitudinal double slotted patch

7.4 A Class of Multi–frequency Operation Techniques

The antenna bandwidth can be increased from about 3% to over 10% by using coplanar parasitic elements or stacked structures discussed in this chapter. A dual frequency operation can also be achieved by using slotted patches. The two operating frequencies of the slotted patch with aperture coupling can be tuned by adjusting the position and sizes of the slots on the patch. However, the tuning range can not be very large without deteriorating the gain and cross polarization performance of the antenna. On the other hand, in some applications, the antenna is required to operate at several discrete frequencies that are far from each other and over narrow bandwidths around individual operating frequencies, i.e., a multi–frequency operation is required over a very large frequency range.

Therefore, a new technique is proposed here to achieve multi–frequency operation at widely separately operating frequencies. The basic structure of multi–frequency operation antennas are shown in Fig.7.14.

In Fig.7.14a, the antenna is composed of three dielectric layers with a slotted ground plane to separate layer 1 from layer 2 and 3. The microstrip feedline is placed on layer 1 below the ground plane while patch 1 is placed on layer 2 and patch 2 is placed on layer 3 above the ground plane. As it is known, patch 1 and patch 2 may couple to each other to form a relatively wideband antenna. However, when the difference between dimensions of these two patches is very large, their resonances may not couple well to each other. For instance, when patch 2 is much smaller than patch 1, it can not be excited effectively through patch 1, due to its blockage. On the other hand, when patch 1 is much smaller than patch 2, then while both patches are strongly excited, patch 1 cannot radiate through patch 2. In the present structure, this problem is overcome. In order to excite this smaller patch 2 effectively

at the higher operating frequency, a small slot is used at the center of patch 1. This slot will allow patch 2 to be effectively excited at the higher operating frequency.

Since an appropriately slotted patch itself can achieve dual frequency operation, it can be used to achieve even more operating frequencies. For example one additional operating frequency may be achieved if patch 1 is slotted at two sides as shown in Fig.7.14b, where two top patches are excited separately by these two slots on patch 1 rather than a new centered slot. Therefore, there are many possibilities and combinations to form multi–frequency operation and adjust resonance performances of the antenna.

An example of a dual frequency operation is shown in Fig.7.15. The two operating frequencies of the antenna are at 2.27 GHz and 4.04 GHz. It is found that their separation can be adjusted by changing the size of the slot on patch 1 in Fig.7.14a.

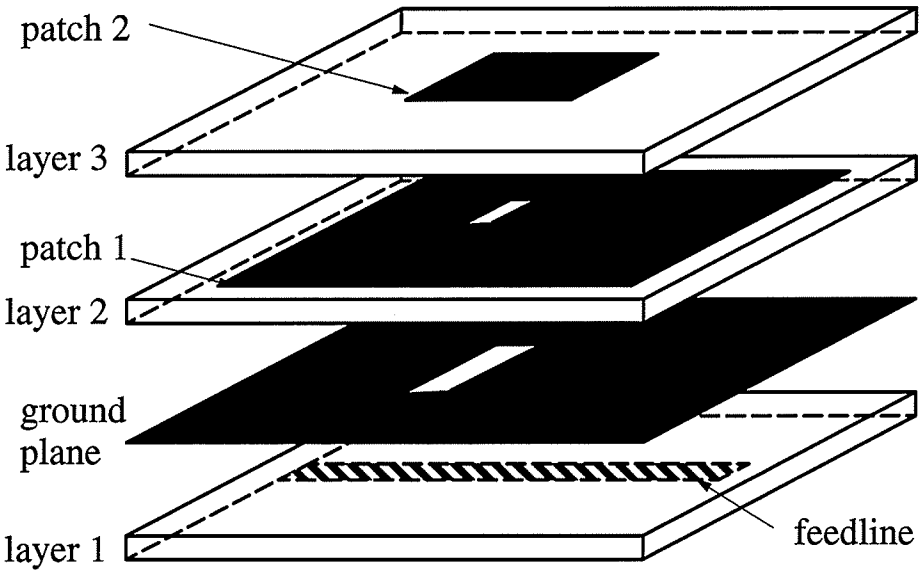

(a) dual frequency operation

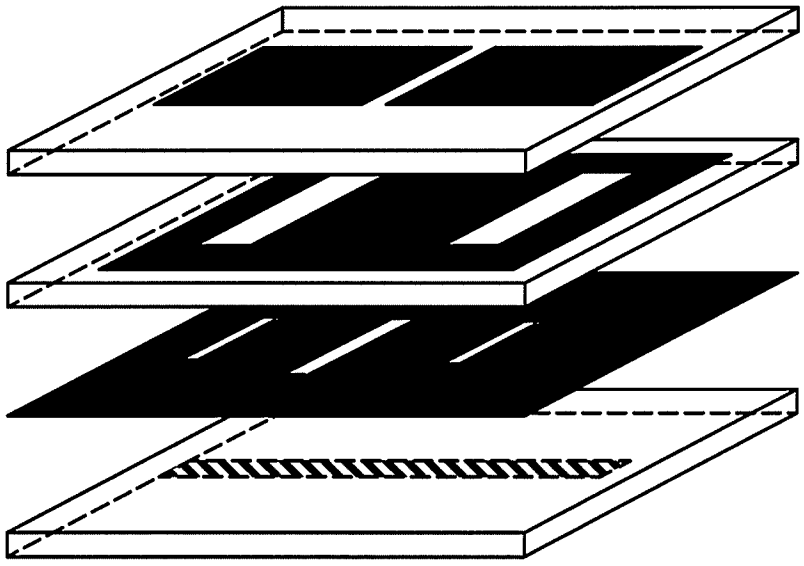

(b) multi–frequency operation

Fig.7.14. Geometry of a class of multi–frequency operation antennas

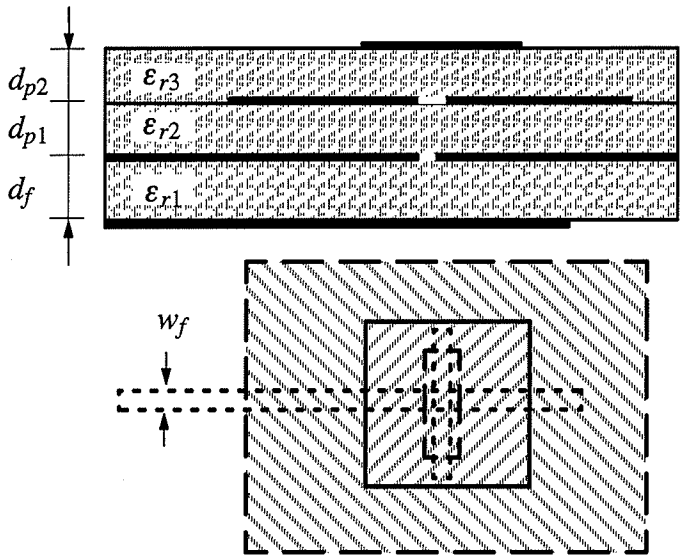

(a) geometry

$\varepsilon_{r1} = \varepsilon_{r2} = \varepsilon_{r3} = 2.54$

$d_f = 1.6$ mm

$d_{p1} = d_{p2} = 0.8$ mm

$w_f = 4.4$ mm

$l_a = 1$ cm

$w_a = 1$ mm

$l_s = 4$ mm

$w_s = 2$ mm

$l_{p1} = 4$ cm

$w_{p1} = 2.4$ cm

$l_{p2} = 2$ cm

$w_{p2} = 2.4$ cm

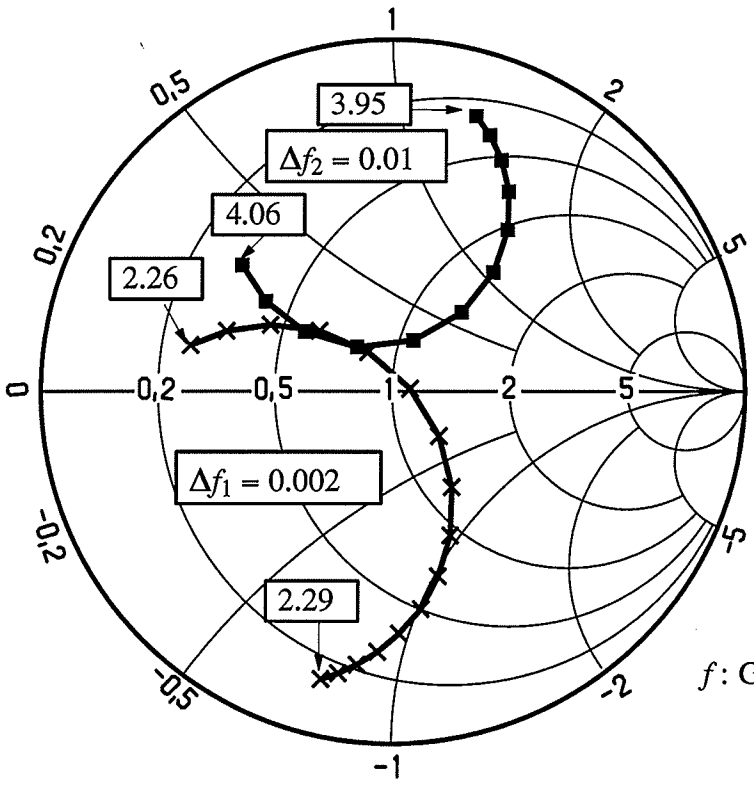

(b) input impedance loci

Fig.7.15. Characteristics of a dual frequency operating antenna

Chapter 8 CONCLUSIONS

8.1 Summary

This thesis presents the work on a space domain full wave analysis for open printed transmission lines, a unified spectral domain full wave analysis for multilayer printed antennas, and a set of bandwidth enhancement techniques for printed antennas. As applications of the theoretical analysis techniques, the open single and coupled microstrip lines of finite width dielectrics, and the aperture coupled microstrip antennas are studied.

As a theoretical basis for the entire thesis, the electromagnetic boundary value problem of multilayer dielectrics is discussed in the form of vectorial auxiliary potential functions. It shows that two potential function types are essentially the same and a general solution to such problem can be obtained either in the space domain or in the spectral domain.

As an example of space domain solution, a full wave technique is developed for open printed transmission lines. This technique is based on the method of lines. Its most attractive feature is that it can give full wave results for open printed transmission lines of finite width dielectrics. It is then applied to study single and coupled microstrip lines of finite width dielectrics.

When the problem is solved in the spectral domain, the first step is to evaluate the spectral domain Green's functions. Traditionally, this needs a very lengthy and complicated deriva-

tion. Therefore, a network approach is developed to evaluate spectral domain Green's functions of multilayer structure. It is a simple and systematic procedure and very suitable for the development of a general computer program for arbitrary layers of dielectrics. As an example, analytical results for a single layer grounded dielectric with both electric and magnetic currents are presented, which are exactly the same as those obtained by the field matching process.

Then, a unified spectral domain full wave technique is developed for printed antennas with multilayer dielectrics. Different types of feeding structures and radiating elements with arbitrary shapes of geometries are considered in the technique. The expression for the far field radiation patterns are also presented by a set of simple formulations, that do not require calculation of integrals.

This technique is then applied to study the aperture coupled microstrip antennas. Basic characteristics of the antenna are evaluated that considers all the components of electric and magnetic currents and fields. Parameter studies are presented with respect to different coupling apertures and radiating elements of various geometries.

The narrow bandwidth has been one major drawback of printed antennas. Consequently, several techniques are proposed to enhance their bandwidth performance. Subarrays of coplanar or stacked parasitic elements can widen the bandwidth and increase directivity. Slotted patches can achieve dual–frequency operation with only one patch and a single feed. Finally, a class of techniques is presented to achieve the multi–frequency operation.

8.2 Future Research

With ongoing development of the fabrication techniques, more and more printed transmission lines and antennas will be used in microwave and monolithic integrated circuits. Their

design will also rely more and more on the theoretical analysis. Therefore, there is a need for accurate modelling of these structures. A full wave analysis is undoubtedly needed. However, how to generate the full wave results quickly and at low cost, to fulfil the requirement of a computer aided design, is still an area in need for large effort. On the other hand, attention should also be paid to the treatment of other kinds of dielectric materials and active components which are used more and more frequently in the microwave and monolithic integrated circuits to achieve high performance. The effect of finite dielectrics on the antenna performance should also be considered in an accurate full wave model.

So far, several techniques have been developed to enhance performances of printed antennas. Good results are obtained for single elements or subarrays. The next step is the application of these techniques to antenna arrays by using these wideband or multi–frequency operating antennas as array elements. It is expected that enhanced bandwidth performance will also be obtained for the arrays. However, mutual coupling between elements should be considered in the array applications.

Appendix A NETWORK THEORY

This appendix presents the necessary network theory for the evaluation of spectral domain Green's functions in Chapter 4.

A.1 Basic Network Matrices

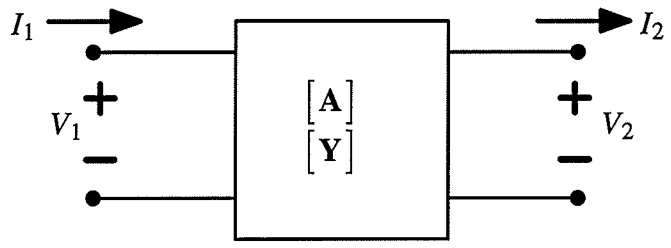

Fig.A.1. A two port network

The $[\mathbf{A}]$ and $[\mathbf{Y}]$ matrices of the two port network in Fig.A.1 are defined as

$$\begin{bmatrix} V_1 \\ I_1 \end{bmatrix} = \begin{bmatrix} A & B \\ C & D \end{bmatrix} \begin{bmatrix} V_2 \\ I_2 \end{bmatrix} \tag{A.1}$$

$$\begin{bmatrix} I_1 \\ -I_2 \end{bmatrix} = \begin{bmatrix} Y_{11} & Y_{12} \\ Y_{21} & Y_{22} \end{bmatrix} \begin{bmatrix} V_1 \\ V_2 \end{bmatrix} \tag{A.2}$$

Relation between the $[\mathbf{A}]$ matrix and $[\mathbf{Y}]$ matrix is

$$\begin{bmatrix} Y_{11} & Y_{12} \\ Y_{21} & Y_{22} \end{bmatrix} = \frac{1}{B} \begin{bmatrix} D & -|\mathbf{A}| \\ -1 & A \end{bmatrix} \tag{A.3}$$

where $|\mathbf{A}|$ is the determinant of the matrix $[\mathbf{A}]$.

The matrix $[\mathbf{A}]$ of the ladder connected network in Fig.A.2 is

$$[\mathbf{A}]_{\text{tot}} = [\mathbf{A}]_1 [\mathbf{A}]_2 \cdots [\mathbf{A}]_n \tag{A.4}$$

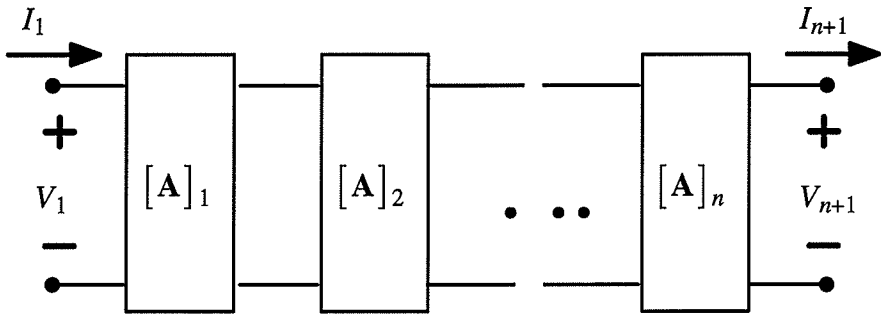

Fig.A.2. Ladder connection of two port networks

A.2 Network matrices for a transmission line section

The network parameter for the transmission line section shown in Fig.A.3 is

$$\begin{bmatrix} A & B \\ C & D \end{bmatrix} = \begin{bmatrix} \cos(k_e d) & j \sin(k_e d) / Y_e \\ j Y_e \sin(k_e d) & \cos(k_e d) \end{bmatrix} \tag{A.5}$$

where Y_e is the characteristic admittance and k_e is the wave number of the line.

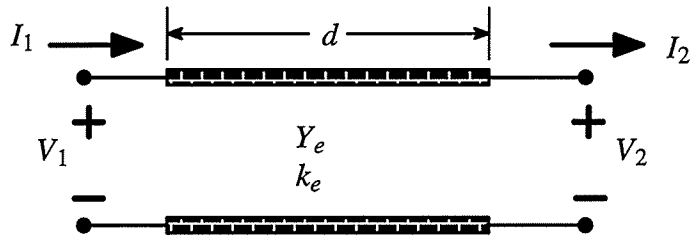

Fig.A.3. A transmission line section

A.3 An equivalent Π network

The reciprocal network in Fig.A.1 can be equivalent to a Π network as in Fig.A.4 with

$$Y_o = -Y_{12} = -Y_{21} = \frac{1}{B}$$

$$Y_1 = Y_{11} + Y_{12} = \frac{D-1}{B} \qquad \text{(A.6)}$$

$$Y_2 = Y_{22} + Y_{12} = \frac{A-1}{B}$$

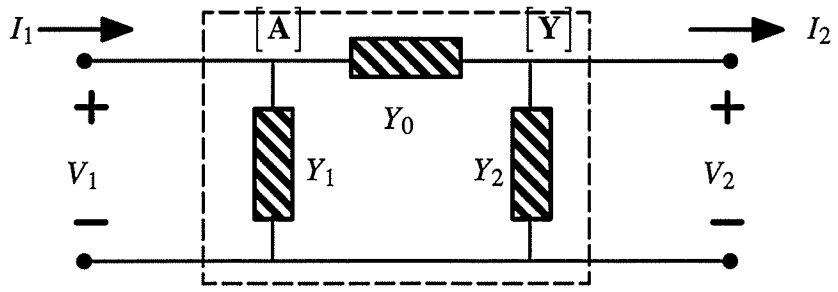

Fig.A.4. Equivalent Π network

Appendix B FOURIER TRANSFORM EXPRESSIONS OF BASIS FUNCTIONS

This appendix lists the Fourier Transform expressions of various basis functions used in Chapter 5. The definition of Fourier transform is

$$\tilde{Q}(k_x, k_y, z) = \int\int_{-\infty}^{\infty} Q(x, y, z)\, e^{-jk_x x}\, e^{-jk_y y}\, dx\, dy \tag{B.1}$$

B.1 One Dimensional Basis Functions

Expressions of Fourier transform of one dimensional basis functions are as follows

$$\begin{cases} f_{x\,n}(x) = \sin\dfrac{n\pi}{l}(x + l/2) & \text{for } |x| < l/2 \\ \tilde{f}(k_x) = \dfrac{n\pi/l}{k_x^2 - (n\pi/l)^2}\left[\cos n\pi\, \exp(-jk_x l) - \exp(jk_x l)\right] \end{cases} \tag{B.2}$$

$$\begin{cases} f(x) = \dfrac{\sin k_o(l - |x|)}{\sin k_o l} & \text{for } |x| < l \\ \tilde{f}(k_x) = \dfrac{2k_o}{k_o^2 - k_x^2}\dfrac{\cos k_x l - \cos k_o l}{\sin k_o l} \end{cases} \tag{B.3}$$

$$\begin{cases} f(x) = 1/w\ , \quad |x| < w/2 \\ \tilde{f}(k_x) = \dfrac{\sin(k_x w/2)}{k_x w/2} \end{cases} \tag{B.4}$$

$$\begin{cases} f(x) = 1/\sqrt{(w/2)^2 - x^2} \quad , \quad |x| < w/2 \\ \tilde{f}(k_x) = \dfrac{\pi w}{4} \mathrm{J}_0\left(\dfrac{w}{2}|k_x|\right) \end{cases} \tag{B.5}$$

$$\begin{cases} f(x) = \cos k_e x \qquad \text{for} \quad -x_o < x < 0 \\ \tilde{f}(k_x) = \dfrac{(k_e \sin k_e x_o + jk_x \cos k_e x_o)\exp(jk_x x_o) - jk_x}{k_e^2 - k_x^2} \end{cases} \tag{B.6}$$

$$\begin{cases} f(x) = \sin k_e x \qquad \text{for} \quad -x_o < x < 0 \\ \tilde{f}(k_x) = \dfrac{(k_e \cos k_e x_o - jk_x \sin k_e x_o)\exp(jk_x x_o) - k_e}{k_e^2 - k_x^2} \end{cases} \tag{B.7}$$

B.2 Two Dimensional Basis Functions

In the application of nodal based functions, Fourier transforms of several basis functions in the triangular area as shown in Fig.B.1 is needed, which can be evaluated by

$$\tilde{F}(k_x, k_y) = \int\int_{\Delta A} F(x,y)\ \exp(-jk_x x)\ \exp(-jk_y y)\ dx\,dy \tag{B.8}$$

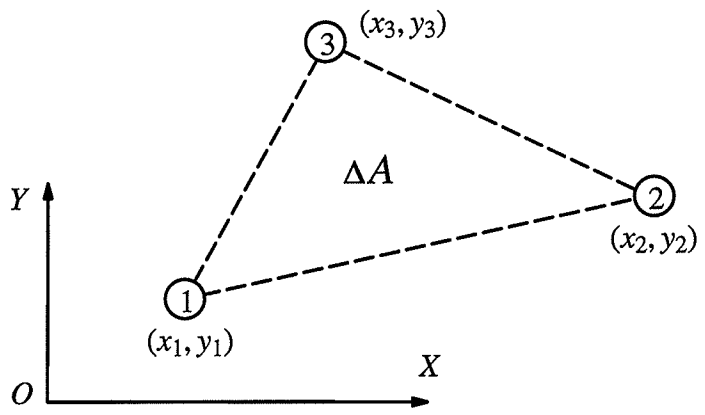

Fig.B.1. A triangle for two dimensional Fourier transform

The Fourier transform expressions are as follows

$$\begin{cases} F_0 = 1 \\ \tilde{F}_0(k_x, k_y) = \sum_{i=1}^{3} \dfrac{\exp\left[-j(k_x x_i + k_y y_i)\right] - \exp\left[-j(k_x x_{i+2} + k_y y_{i+2})\right]}{k_y\left[k_x + k_y t_{i(i+2)}\right]} \end{cases} \tag{B.9}$$

$$\begin{cases} F_1 = x \\ \tilde{F}_1(k_x, k_y) = j\dfrac{d}{dk_x}\tilde{F}_0(k_x, k_y) \\ \qquad = j\sum_{i=1}^{3} \dfrac{\left\{\begin{array}{l} -\left[1 + j(k_x + k_y t_{i(i+2)})x_i\right]\exp\left[-j(k_x x_i + k_y y_i)\right] \\ +\left[1 + j(k_x + k_y t_{i(i+2)})x_{i+2}\right]\exp\left[-j(k_x x_{i+2} + k_y y_{i+2})\right] \end{array}\right\}}{k_y\left[k_x + k_y t_{i(i+2)}\right]^2} \end{cases} \tag{B.10}$$

$$\begin{cases} F_2 = y \\ \tilde{F}_2(k_x, k_y) = j\dfrac{d}{dk_y}\tilde{F}_0(k_x, k_y) = -j\dfrac{\tilde{F}_0(k_x, k_y)}{k_y} \\ \qquad + j\sum_{i=1}^{3} \dfrac{\left\{\begin{array}{l} -\left[t_{i(i+2)} + j(k_x + k_y t_{i(i+2)})y_i\right]\exp\left[-j(k_x x_i + k_y y_i)\right] \\ +\left[t_{i(i+2)} + j(k_x + k_y t_{i(i+2)})y_{i+2}\right]\exp\left[-j(k_x x_{i+2} + k_y y_{i+2})\right] \end{array}\right\}}{k_y\left[k_x + k_y t_{i(i+2)}\right]^2} \end{cases} \tag{B.11}$$

References

[1] G. A. Deschamps, "Microstrip Microwave Antennas," presented at *the 3rd USAF Symposium on Antennas*, 1953.

[2] J. Q. Howell, "Microstrip Antennas," *IEEE Antennas and Propagation Symposium Digest*, 1972, pp.177–180.

[3] R. E. Munson, "Conformal Microstrip Antennas and Microstrip Phased Arrays," *IEEE Trans. Antennas and Propagation*, Vol. AP–22, pp.74–78, 1974.

[4] I .J. Bahl and P. Bhartia, *Microstrip Antennas*, Artech House, Dedham, Mass., 1980.

[5] J. R. James, P. S. Hall, and C. Wood, *Microstrip Antenna Theory and Design*, IEE Peter Peregrinus, London, UK, 1981.

[6] *IEEE Trans. Antennas and Propagation*, Vol. AP–29, No.1, 1981.

[7] J. R. James and P. S. Hall, eds., *Handbook of Microstrip Antennas*, Vol. I & II, IEE Peter Peregrinus Press, Stevenage, UK, 1989.

[8] J. M. Griffin and J. R. Forrest, "Broadband circular disc microstrip antenna," *Electronics Letters*, Vol.18, No.6, pp.266–269, 1982.

[9] P. S. Hall, "Probe compensation in thick microstrip patches," *Electronics Letters*, Vol.21, No.3, pp.606–607, 1987.

[10] R. C. Johnson and H. Jasik, eds., *Antenna Engineering Handbook*, Chapter 7, McGraw–Hill, 2nd ed., 1984.

[11] H. Legay and L. Shafai, "A high performance spider subarray of five microstrip patches," *IEEE Antennas and Propagation Symposium Digest*, 1993, pp.1394–1397.

[12] H. G. Oltman and D. A. Huebner, "Electromagnetically coupled microstrip dipoles," *IEEE Trans. Antennas and Propagation*, Vol. AP–29, pp.151–157, No.1, 1981.

[13] D. M. Pozar, "Microstrip antenna aperture–coupled to a microstripline," *Electronics Letters*, Vol.21, No.2, pp.49–50, 1985.

[14] R. F. Harrington, *Time Harmonic Electromagnetic Fields*, McGraw–Hill, NY, 1961.

[15] R. E. Collin, *Field Theory of Guided Waves*. IEEE Press, NY, 1991.

[16] A. Derneryd, "Linearly polarized microstrip antennas," *IEEE Trans. Antennas and Propagation*, Vol. AP–24, pp.846–851, 1976.

[17] A. Van de Capelle, "Transmission–line model for rectangular microstrip antennas," Chapter 10 in [7].

[18] Y. T. Lo, D. Solomon, and W. F. Richards, "Theory and experiment on microstrip antennas," *IEEE Trans. Antennas and Propagation*, Vol. AP–27, pp.137–145, 1979.

[19] K.C. Gupta, "Multiport network approach for modelling and analysis of microstrip patch antennas and arrays," Chapter 9 in [7].

[20] L.Shafai and A. Kishk, "Analysis of circular microstrip antennas," Chapter 2 in [7].

[21] J. R. Mosig, R. C. Hall and F. E. Gardiol, "Numerical analysis of microstrip patch antennas," Chapter 8 in [7] .

[22] N. K. Uznoglu, N. G. Alexopoulos, and J. G. Fikioris, "Radiation propertires of printed dipoles," *IEEE Trans. Antennas and Propagation*, Vol. AP–27, pp.853–858, 1979.

[23] D. M. Pozar, "Input impedance and mutual coupling of rectangular microstrip antennas," *IEEE Trans. Antennas and Propagation*, Vol. AP–30, pp.1191–1196, No.11, 1982.

[24] Y. L. Chow, J. J. Yang, D. G. Fang, and G. E. Howard, "A closed form for spatial Green's function for thick microstrip substarte," *IEEE Trans. Microwave Theory and Techniques*, Vol. MTT–39, pp.588–592, No.3, 1991.

[25] R. K. Hoffmann, *Handbook of Microwave Integrated Circuits*. Norwood, MA: Artech House, Inc., 1987.

[26] C. E. Smith and R. S. Chang, "Microstrip transmission line with finite–width dielectric," *IEEE Trans. Microwave Theory and Techniques*, Vol. MTT–28, pp.90–94, No.1, 1980

[27] C.E. Smith and R.S. Chang, "Microstrip with finite–width dielectric and ground plane," *IEEE Trans. Microwave Theory and Techniques*, Vol. MTT–33, pp.835–839, No.9, 1985.

[28] U. Schulz and R. Pregla, "A new technique for the analysis of the dispersion characteristics of planar waveguides," *AEÜ*, Vol.34, pp.84–88, 1980.

[29] R. Pregla and W. Pascher, "The Method of Lines," in *Numerical Techniques for Microwave and Millimeter Wave Passive Structures*, (T. Itoh, Ed.) Wiley, New York, pp.380–446, 1989.

[30] M. Thorburn, A. Agoston and V. K. Tripathi, "Computation of frequency–dependent propagation characteristics of microstriplike propagation structures with discontinuous layers," *IEEE Trans. Microwave Theory and Techniques*, Vol. MTT–38, pp.148–153, No.2, 1990.

[31] F. J. Schmuckle and R. Pregla, "The method of lines for the analysis of lossy planar waveguides," *IEEE Trans. Microwave Theory and Techniques*, Vol. MTT–38, pp.1437–1479, No.10, 1990.

[32] S. B. Worm, "Full–wave analysis of discontinuities in planar waveguides by the method of lines using a source approach," *IEEE Trans. Microwave Theory and Techniques*, Vol. MTT–38, pp.1510–1514, No.10, 1990.

[33] X. H. Yang and L. Shafai, "Extension of the method of lines to unbounded regions by using coordinate transformation," *Electronics Letters*, Vol.27, No.23, pp.2108–2110, 1991.

[34] X. H. Yang and L. Shafai, "Full wave approach for the analysis of open planar waveguides with finite width dielectric layers and ground planes," *IEEE Trans. Microwave Theory and Techniques*, Vol. MTT–44, pp.142–149, No.1, 1994.

[35] R. S. Martin and J. H. Wilkinson, "The impact QL–algorithm", *Numer. Math.*, Vol.12, pp.377–383, 1968.

[36] M. Kobayashi and F. Ando, "Dispersion Characteristics of Open Microstrip Lines," *IEEE Trans. Microwave Theory and Techniques*, Vol. MTT–35, pp.101–105, No.1, 1987.

[37] G. Kowalski and R. Pregla, "Dispersion characteristics of single and coupled microstrips," *AEÜ*, Vol.26, pp.276–280, 1972.

[38] J. A. Kong, *Theory of Electromagnetic Waves*, John Wiley & Sons, New York, 1975.

[39] J. R. Wait, *Electromagnetic Waves in Stratified Media*, MacMillan, New York, 1962

[40] T. Itoh, "Spectral domain immitantce approach for dispersion characteristics of generalized printed transmission lines," *IEEE Trans. Microwave Theory and Techniques*, Vol. MTT–28, pp.733–736, No.7, 1980.

[41] N. K. Das, and D. M. Pozar, "A generalized spectral–domain Green's function for multilayer dielectric substrates with application to multilayer transmission lines," *IEEE Trans. Microwave Theory and Techniques*, Vol. MTT–35, pp.326–335, No.3, 1987.

[42] L. Vegni, R. Cicchetti, and P. Capece, "Spectral dyadic Green's function formulation for planar integrated structures," *IEEE Trans. Antennas and Propagation*, Vol. AP–36, pp.1057–1065, 1988.

[43] X. H. Yang, L. Shafai, and A. Sebak, "A comparison study on wire–grid model and point matching technique with subdomain basis functions," *Proc. of Symposium on Antenna Technology and Applied Electromagnetics*, Winnipeg, 1992, pp.656–661.

[44] X. H. Yang, L. Shafai, and A. Sebak, "On the nature of wire grid modeling for numerical solutions of electromagnetic problems," Can. Jour. of Physics, Vol.71, Nov/Dec, 1993, pp.564–570.

[45] X. H. Yang, L. Shafai, and A. Sebak, "An efficient technique for the analysis of multi–object scattering," *Proc. of Symposium on Antenna Technology and Applied Electromagnetics*, Winnipeg, MB, 1992, pp.668–673.

[46] X. H. Yang, L. Shafai, and A. Sebak, "Efficient technique for analysis of multiobject scattering problems," *Electronics Letters*, Vol.28, No.15, pp.1442–1444, 1992.

[47] S. M. Rao, D. R. Wilton, and A. W. Glisson, "Electromagnetic scattering by surfaces of arbitrary shape," *IEEE Trans. Antennas and Propagation*, Vol. AP–30, pp.409–418, No.5, 1982.

[48] R. W. Jackson and D. M. Pozar, "Full–wave analysis of microstrip open–end and gap discontinuities," *IEEE Trans. Microwave Theory and Techniques*, Vol. MTT–33, pp.1036–1042, No.10, 1985.

[49] Sullivan and D. H. Schaubert, "Analysis of an aperture coupled microstrip antenna," *IEEE Trans. Antennas and Propagation*, Vol. AP–34, pp.977–984, No.8, 1986.

[50] D. M. Pozar, "A reciprocity method of analysis for printed slot and slot–coupled microstrip antennas," *IEEE Trans. Antennas and Propagation*, Vol. AP–34, pp.1439–1445, No.12, 1986.

[51] X. Gao and K. Chang, "Network modeling of an aperture coupling between microstrip line and patch antenna for active array applications," *IEEE Trans. Microwave Theory and Techniques*, Vol. MTT–36, pp.505–512, No.3, 1988.

[52] M. Himdi, J. P. Daniel, and C. Terret, "Analysis of aperture coupled microstrip antenna using cavity method," *Electronics Letters*, Vol.25, No.5, pp.391–392, 1989.

[53] M. I. Aksun, S. L. Chuang, and Y. T. Lo, "On slot–coupled microstrip antennas and their applications to CP operation—theory and experiment," *IEEE Trans. Antennas and Propagation*, Vol. AP–38, pp.1224–1230, No.8, 1990.

[54] A. Ittipiboon, R. Oostlander, Y. M. M. Antar, and M. Cuhaci, "A modal expansion method of analysis and measurement on aperture–coupled microstrip antenna," *IEEE Trans. Antennas and Propagation*, Vol. AP–39, pp.1567–1573, No.11, 1991.

[55] A. K. Bhattacharyya, Y. M. M. Antar, and A. Ittipiboon, "Spectral domain analysis of aperture–coupled microstrip antennas," *IEE Proceedings–H*, Vol.139, pp.459–464, Oct., 1992.

[56] X. Yang and L. Shafai, "A full wave approach for the analysis of aperture coupled microstrip antennas," *Proc. of the 3rd International Symposium on Antennas and EM Theory*, Nanjing, China, 1993, pp.483–486.

[57] X. H. Yang and L. Shafai, "Aperture coupled printed wire antennas of arbitrary shape and finite wire width," *IEEE Antennas and Propagation Symposium Digest*, Ann Arbor, Michigan, 1993, pp.642–645.

[58] H. Legay and L. Shafai, "Parametric analysis of an EMC patch surrounded by parasitic elements," *Proc. of Symposium on Antenna Technology and Applied Electromagnetics*, Winnipeg, MB, 1992, pp.385–390.

[59] L. Shafai, X. H. Yang, and H. Legay, "Aperture coupled microstrip subarray composed of coplanar parasitic elements," *Proc. of the 3rd International Symposium on Antennas and EM Theory*, Nanjing, China, 1993, pp.659–662.

[60] F. Croq and D. M. Pozar, "Multifrequency operation of microstrip antennas using aperture coupled parallel resonators," *IEEE Trans. Antennas and Propagation*, Vol. AP–40, pp.1367–1374, No.11, 1992.

[61] A. Ittipiboon, B. Clarke and M. Cuhaci, "Slot–coupled stacked microstrip antennas," *IEEE Antennas and Propagation Symposium Digest*, 1990, pp.1108–1111.

[62] F. Croq and D. M. Pozar, "Millimeter wave design of wide band aperture coupled stacked microstrip antennas," *IEEE Trans. Antennas and Propagation*, Vol. AP–39, pp.1770–1776, No.12, 1991.

[63] H. Legay and L. Shafai, "A new stacked microstrip antenna with large bandwidth and high gain," *IEEE Antennas and Propagation Symposium Digest*, Ann Arbor, Michigan, 1993, pp.948–951.

[64] L. Shafai and X. H. Yang, "Antenna performance enhancement by slotting microstrip patches," *Electronics Letters*, Vol.29, No.18, pp.1647–1649, 1993.

[65] X. H. Yang and L. Shafai, "Wideband techniques for the aperture coupled microstrip antennas," *IEEE Antennas and Propagation Symposium Digest*, Ann Arbor, Michigan, 1993, pp.952–955.